QUANTITATIVE CHARACTERIZATION OF CANCER MICROENVIRONMENT

Anju Mythreyi Raja

B.Eng (Hons.), BITS, Pilani

A THESIS SUBMITTED FOR THE DEGREE OF DOCTOR OF PHILOSOPHY

NUS Graduate Programme in Bioengineering

National University of Singapore

2009

Acknowledgements

I would like to thank my parents and brother who supported me through these four years and provide me with timely advice and motivation when I needed it. I would also like to thank Ashray for being supportive and encouraging during the times I felt I would give up. I joined Graduate Programme in Bioengineering with a group of enthusiastic colleagues Alberto, Chee Tiong, Darren, Vinayak, Kalyan, Lei Yang to mention a few. They were an amazing group of people to work and study with.

My two supervisors Dr. Hanry Yu and Dr. CS Chen were pillars of my scientific endeavour without whom I would not have achieved any of this. They were always there for me providing scientific guidance and inspiring me every step of the way. They encouraged me when I did well and were critical when I was going astray thus providing constant feedback to do my best. I here acknowledge members of both labs who treated me like one among their family and provided support, encouragement and companionship through these years. I would like to specially thank Dr. Sun Wanxin, Dr. Dean Tai Dr.Yi Chin, Danny Van Noort and Alvin Kang with whom I worked on the Second Harmonic Generation microscope.

I thank NUS, IBN, A-STAR and BMRC for the financial support as well as providing me a platform to do my scientific work for the last few years.

List of Published Work

- **Raja, A.M**., Tai, D.C.S., Xu, S., Sun, W., Zhou, J., Chen, C.S., Yu. H. (2009), "Pulse Modulated Second Harmonic Imaging Microscope (PM-SHIM) imaging quantitatively demonstrates marked increase of collagen in tumor stroma after chemotherapy" Manuscript in Preparation

- **Raja, A.M**., Xu, S., Tai, D.C.S., Sun, W., Chen, C.S., Yu, H. (2009), "Isolation of Cancer Initiating Cells from human breast cancer cell line MX-1 and imaging based characterization of CIC- microenvironment relationship" Manuscript in preparation

- Toh YC, **Raja AM**, Noort DV, Chen CS, Yu H. (2009), "Cancer Cell migration and invasion inside a 3D microfluidic model", Electrophoresis, Submitted

- Dean C. S. Tai, Nancy Tan, Shuoyu Xu, Chiang Huen Kang, Ser Mien Chia, Chee Leong Cheng, Aileen Wee, Chiang Li Wei, **Anju Mythreyi Raja**, Guangfa Xiao, Shi Chang, Jagath C. Rajapakse, Peter T. C. So, Hui-Huan Tang, Chien Shing Chen, and Hanry Yu, (Jul. 27, 2009), "Fibro-C-Index: comprehensive, morphology-based quantification of liver fibrosis using second harmonic generation and two-photon microscopy", J. Biomed. Opt. Vol. 14, 044013.

Table of Contents

Summary

Cancer Initiating Cells (CIC) have been shown to be present in various cancer types and characterised as highly tumorigenic, drug resistant and invasive sub-population. Identifying CIC in patient samples has been primarily done using flow cytometry with a few markers such as CD44, CD24 in breast cancer and CD38, CD34 in leukemia. Newer markers and signalling pathways are being identified as potential CIC markers and therapeutic targets but identifying CIC in tumors has been elusive.

We wanted to look at the CIC question in perspective of its environment and understand how cancer initiating cells interact with its environment in the micro and macro scale. We wanted to identify possible patterns of CIC interactions with ECM proteins such as collagen and fibronectin that can help us identify them in tumor samples. To enable us to answer these questions we established the CIC/non CIC model using a breast cancer cell line MX-1. We established in-vitro methodologies to study fibonectin fibres and collagen gel remodelling by CIC in bulk cultures and microfluidic channels. We established animal models to study the macro and micro interactions of CIC with its environment. We developed and improved Second Harmonic Generation (SHG) imaging tool to study collagen remodelling in tumor specimens without the need for staining and tedious sample preparation.

We have demonstrated that cancer initiating cells (CIC) are fundamentally different from the majority cancer population which we refer to as the non-CIC. We have isolated CIC from immortalized cancer cell lines such as MCF-7, MX-1, MDA-MB 231, HepG2 and Huh-7. We also demonstrate that the CIC isolated from MX-1 have higher proliferation potential, are drug resistant to mitoxantrone and doxorubicin and are phenotypically $CD44^{hi}$ and $CD24^{low}$.

We studied the CIC interacting with its environment in-vivo using a short term skin flap assay and a long term xenograft assay. In the skin flap technique we injected CIC in the blood vessel of an animal and observed the CIC forming colonies under the skin and extravasating into the surrounding tissue regions. The extent of colonisation and extravasation in CIC was significantly more than non-CIC. In the long term xenograft assay CIC and non CIC were injected subcutaneously in animals and CIC consistently formed tumors in all the animals injected with 100,000 of these cells while the non-CIC is able to form tumor only in one in five animals even though 10 million cells were injected.

We improved the SHG imaging microscope using a pulse compressor set up to reverse the problem of group velocity dispersion and hence enhance the signal to noise ratio. We achieved a 6x higher SBR using our pulse compressor. The tumors formed by CIC and non-CIC were harvested and studied using our improved SHG imaging system to visualise the collagen patterns in the tumors. The CIC tumors consistently had less collagen area percentage and distinct collagen remodelling patterns that can be used to identify CIC in-vivo.

List of Tables

List of Figures

List of Abbreviations

2PE	2-Photon excitation
3D	Three dimensions/ Three dimensional
ABC	ATP Binding Cassette
AI	Angle Index
AML	Acute Myeloid Leukemia
AOM	Acousto Optic Modulator
ATP	Adenosine Tri- Phosphate
BCIC	Breast Cancer Initiating Cells
BMP	Bone Morphogenetic Protein
BP	Band Pass
BRCA1/2	Breast Cancer Associated Gene 1/2
CD24	Cluster of Differentiation 24
CD44	Cluster of Differentiation 44
CIC	Cancer Initiating Cells
CK-19	Cytokeratin – 19
CT	Computerized Tomography
DNA	Deoxy Ribonucleic Acid
ECM	Extra Cellular Matrix
EDTA	Ethylene diamine tetraacetic acid
EGF	Epidermal Growth Factor
EM	Expectation Maximisation
ER	Estrogen Receptor
FACS	Fluorescence Activated Cell Sorting
FCS	Fetal Calf Serum
FROG	Frequency Resolved Optical Gating
fs	Femtosecond
GFP	Green Fluorescent Protein

GTP ases	Guanosine Triphosphate hydrolases
GVD	Group Velocity Dispersion
H&E	Hematoxylin and Eosin
HBSS	Hanks Balanced Salt Solution
Her-2	Human Epidermal Growth Factor Receptor-2
IACUC	Institutional Animal Care and Use Committee
MDR	Multiple Drug Resistance
MMP	Matrix Metallo Proteinases
MRI	Magnetic Resonance Imaging
mRNA	messenger Ribo Nucleic Acid
NFκB	Nuclear factor kappa-light-chain-enhancer of activated B cells
NI	Neighbor Index
Non-CIC	Non Cancer Initiating Cells
OCT	Optimum Cutting Temperature
PBS	Phosphate Buffered Saline
PFA	Paraformaldehyde
PI3	Phosphotidyl Inositol -3
PM-SHIM	Pulse Modulated - SHIM
PMT	Photo multiplier tube
RFP	Red Fluorescent Protein
RGB	Red Green Blue
Ras	RAt Sarcoma
ROS	Reactive Oxygen Species
RPMI	Rosewell Park Memorial Institute medium
SBR	Signal to Background Ratio
Sca-1	Stem cell antigen -1
SCID	Severe Combined Immuno Deficient
SHG	Second Harmonic Generation
SHIM	Second Harmonic Generation Imaging Microscope

Smad	A combination of C Elegans SMA protein and mothers against decapentaplegic (MAD) protein
SNP	Single Nucleotide Polymorphisms
SNR	Signal to Noise Ratio
SP	Short Pass
SP	Side Population
TGF-β	Transforming Growth Factor-β
TIMP	Tissue inhibitor of Matrix metalloproteinases
TPEF	Two photon excited fluorescence
TS	Tile Scan
UV	Ultra Violet
VEGF	Vascular Endothelial Growth Factor

Introduction

Cancer is one of the greatest medical challenges in Singapore with the number of cancer patients increasing every year [1]. Breast cancer is one of the leading killers of women in Singapore. Breast cancer is relatively easier to detect and treat compared to other cancers of the internal organs[2]. Nonetheless the treatment success remains low and the recurrence rate of the disease is quite high. Recent works have attributed this lower success and higher recurrence to a rare population of cells present in the bulk of the tumor called cancer initiating cells (CIC). The CIC population has drug resistance enabling them to escape treatment and feeds tumor growth lowering treatment success. And when the treatment regimen is good enough to kill the bulk of the tumor these rare cells remain dormant in the host body and leads to disease recurrence later on [3-5].

There are two hypotheses on how these cells could arise. Firstly the hierarchical model suggests that cancer is a monoclonal disease that has its origin from a deregulated stem cell [6]. A stem cell that accumulates enough mutations could become a cancer stem cell and thus generate a hierarchy of cancer cells from the primary to more differentiated cells [7-8]. As the cancer stem cell arises from a stem cell they have inherent chemo-protective mechanisms such as molecular pumps enabling them to survive harsh environments. The second hypothesis is the stochastic model where a cell in the body accumulates mutations over time and these random mutations trigger molecular processes that makes it a stem like cell. This hypothesis supports the fact that the cancer stem cells isolated from patient samples do not have all stem cell properties but only a few that enables them to survive and multiply indefinitely [9].

Whatever is the source of these cancer stem cells or cancer initiating cells it has been shown in literature that these cells can be isolated from patient samples and cancer cell lines. The cancer cells can be separated into a minority cancer stem cell or initiating cell population and a majority non stem or non-initiating population based on several properties such as their marker profiles [10-14], their drug effluxing properties [15-16] their ability to grow as spheroids independent of the culture substrate [17] or their protease activity levels [18-19].

The CIC that were isolated were shown to have several stem cell properties such as over-expression of c-kit, oct-4 and Sca-1 in certain cancer types [17, 20], capacity to differentiate into different lineages of that particular tissue type and chemo-protective properties [16, 21]. These CIC have the capacity to generate a tumor only when about a 100 of these cells were injected into the animal, while more than 10 million non-CIC were required to generate a tumor and in certain other cases non-CIC could not generate a tumor at all [15, 22]. The properties of the CIC point to the fact that if identified and characterized in vivo, we will be able to better diagnose the disease as well design new treatment methods to target these cells.

All the aforementioned literature has been focusing on the properties of CIC either in in-vitro or in-vivo systems as a stand-alone group of cells. But we know that all cancer cells take cues from their neighbors and the microenvironment to survive, divide, invade and sometimes to die [23-25]. Extra cellular matrix molecules such as collagen, fibronectin and other soluble molecules in the microenvironment niche and host derived cells such as endothelial cells and vascular progenitor cells have been shown to control how the cancer cells forms tumors, expand the tumor mass, develop blood vessels and metastasize [26-27]. The cancer cells have complex methods of ECM creation and degradation that enables in maintaining the structure of the tumor

as well as provide for the nutrition and oxygen supply through the blood vessel system [28].

We have approached this problem of cancer initiating cells with the microenvironment in perspective. We chose collagen as the extra cellular molecule that we could visualize in the CIC and non-CIC tumors to see how different the ECM remodeling is in the two systems. There are three main reasons to choose collagen as our molecule of interest. 1. Collagen is ubiquitously present in all tissue types and they are one of the main ECM molecules that provide both structural support and molecular signalling. 2. We have developed Second Harmonic Generation Imaging microscope (SHIM) in the lab that can visualize collagen without any staining and sectioning thus providing an easy to use clinical tool. 3. If we do find differentiating ECM remodeling patterns between the CIC and non-CIC groups we can further this study to clinical samples to find unique signatures that might predict the severity, stage and presence or absence of CIC.

SHIM works on the principle of Second Harmonic Generation (SHG) where the light interacts with materials with second order susceptibility and generate transmitted or reflected beam with half the wavelength or twice the frequency of the original light [29]. Most materials have very low second order susceptibility and hence the SHG signals generated by these materials cannot be detected. But non-centrosymmetric materials such as collagen on the other hand have high second order susceptibility, thus making collagen a suitable biomolecule for SHG imaging [30].

All microscopes have the problem of group velocity dispersion (GVD). When the beam passes through optical components like lenses and beam splitters the lower wavelength component of light will travel slower than the higher wavelength component leading to a temporal stretch in the beam. This is called negative GVD.

The GVD is an issue of concern in SHG microscopes as the laser beam used to excite the samples are femto-second pulses and a 50fs laser pulse after GVD could be stretched to a 200 fs pulse. This reduces peak power delivered to the sample, reducing the efficiency of SHG.

GVD can be reversed using pulse modulation. With the use of chirped mirrors, grating or prism pairs, the velocity of the higher and lower wavelength components of the beams can be altered to restore the beam to the native temporal width. In our work we have used the prism pair pulse compressor set up to reverse negative GVD. We would like to demonstrate that pulse compression improves the efficiency of second harmonic generation and thus enable us to detect even the smaller collagen fibrils that remain undetected with GVD.

Along with the CIC – ECM remodeling hypotheses, another venue we were interested to use the SHG system was to visualize collagen remodeling in drug treated tumors. It has been shown that the collagen fibers in the tumor limit the drug diffusion into the tumor and the use of relaxin and collagen degrading enzymes can improve drug penetration in the tumor and hence result in higher drug efficacy [31]. On the other hand it also has been shown that collagen fibers are in reduced numbers in tumor tissues compared to normal tissues [32]. We wanted to assess if the cancer cells modulated their collagen production in the presence of chemotherapeutic agents. We will also assess the maturity of the collagen fibers in the tumor samples after drug treatment to quantify the collagen remodeling in drug treated tumors.

In summary, the final objective of this project is to test the hypothesis that the CIC have different ECM remodeling properties in vivo compared to non-CIC. We would like to prove that CIC is unique in a quantitative manner in vitro and in vivo. In order to achieve that, we devise appropriate method to isolate CIC (aim 1), develop

and validate imaging method to visualize ECM in vivo (aim 2, 3) and use the tool to visualize CIC-ECM interactions (aim 4). The ECM remodeling capacity of this sub population can be used as a signature to identify this population in animal models for drug development studies. In the future CIC can be detected in patient samples to tailor therapies to target and eliminate CIC. To aid us in this validation we use the improved SHG microscope. We also explore the collagen remodeling properties of drug treated tumor samples to understand ECM in the context of chemotherapy regimens as well as to validate the improvement conferred to the SHG system with pulse compression.

The uniqueness of our approach lies in the focus on spatial and temporal analysis of cancer cell-matrix interaction in animal models. Our primary focus is the comparative study of the growth rate and vascularization and their relationship to ECM remodeling utilizing advanced imaging methods. The four specific aims are designed to achieve the aforementioned objectives.

Specific Aim 1: To isolate and characterize a highly tumorigenic sub-population in cancer cell lines using side Population analysis

Hypothesis 1: The cancer cell line population can be sorted into highly tumorigenic and less tumorigenic sub populations based on certain markers and/or their dye effluxing capabilities due to the multiple drug resistance (MDR) proteins.

Supporting Evidence:

Firstly, Cancer initiating cells (CIC) cells have been isolated using various methods in different types of cancer. Side population (SP) method is one such technique used to isolate CIC. Its application has been demonstrated in the cancers of the blood, brain,

breast, liver and ovaries [16]. The side population is named so due to the distinct tail like pattern that is formed during the flow cytometric analysis of these cells. Secondly these isolated sub population can asymmetrically divide to generate both the side and non-side population enabling faster growth of tumors. The SP express higher levels of VEGF; hence the tumors have better vasculature [33]. Thirdly this sub population is drug resistant (expressing higher levels of Multi drug resistance (MDR) or ATP Binding Cassette (ABC) proteins) [16].

Experimental Approach:

- Side population isolation using fluorescence Activated Cell Sorting (FACS)
- Characterizing the CD44 and CD24 expression patterns of the side population
- Cell proliferation comparison of the CIC and non CIC
- Drug resistance studies before sorting
- Drug resistance studies after sorting

Specific Aim 2: Developing tools and methods to visualize collagen and to correlate collagen remodeling by cancer cells to growth and vascularisation in conventional animal models.

Hypothesis 2: Extra cellular matrix (ECM) remodeling by cancer cells can be correlated to its tumor growth and vascularisation.

Supporting Evidence:

During the various phases of cancer, proteolytic ECM remodeling by the cancer cells and cell - ECM interaction play a decisive role [34]. Cancer cells needs to interact and remodel surrounding ECM for it to escape and metastasize [35]. Matrix

metalloproteinase (MMPs) are crucial proteases, which break down ECM for tumor progression and angiogenesis. Over expression of MMP1 due to Single nucleotide polymorphism (SNP) has been often found in cancer cell line and certain ovarian cancer patients [36].

Experimental Approach:

- Development of the Second Harmonic Generation (SHG) system for ECM visualization
- Improvement of the SHG system with pulse compressor
- Tumor growth and metastasis visualization using OV100
- Developing image processing algorithms to quantify and correlate spatial and temporal growth patterns and vascularization to ECM distribution

Specific Aim 3: To visualize collagen remodeling in drug treated tumor samples utilizing the improved SHG system and use this data to validate the improvement.

Hypothesis 3: Collagen remodeling is altered in tumors upon drug administration and the changes collagen patterns can only be visualized with the improved SHG system

Supporting evidence:

Collagen fibers in tumors have shown to hinder drug diffusion in animal models and cancer cells grown in 3D show higher mRNA expression of collagen upon drug treatment. It also has been shown that the tumor interior has lesser collagen than normal tissues using SHG. Thus we believe that the improved SHG will be able

to visualize even the small collagen fibers in the tumor interior and a difference between drug treated and control samples can be quantitatively determined.

Experimental approach:

- Develop drug treated and control xenograft models
- Visualize collagen using SHG microscope to obtain forward and backward SHG signal with and without pulse compression .
- Using the developed image processing algorithms to quantify collagen fiber length, width, number and area percentage in the drug treated group and control group tumor with and without pulse compression to validate improvement using pulse compression

Specific Aim 4: To utilize the above developed imaging tool to compare the spatial and temporal dynamics of the side population and non - side population of cancer cells in animal models.

Hypothesis 4: The side population has different ECM remodeling capabilities compared to the non- side population.

Supporting evidence:

This sub population has been proven to have superior tumor formation properties in animal models [15, 17] and have better vascularization [4]. The metastatic potential, ECM remodeling capabilities and the inter relationship between these properties of this subpopulation has not been explored to our knowledge.

Experimental Approach:

- Develop animal models for CIC and non-CIC cells
- Imaging to visualize growth rate, metastasis, angiogenesis and ECM remodeling using OV100 and the SHG microscope.
- Using the developed image processing algorithms to correlate and compare tumor growth, ECM remodeling and vasculature for the two sub populations.

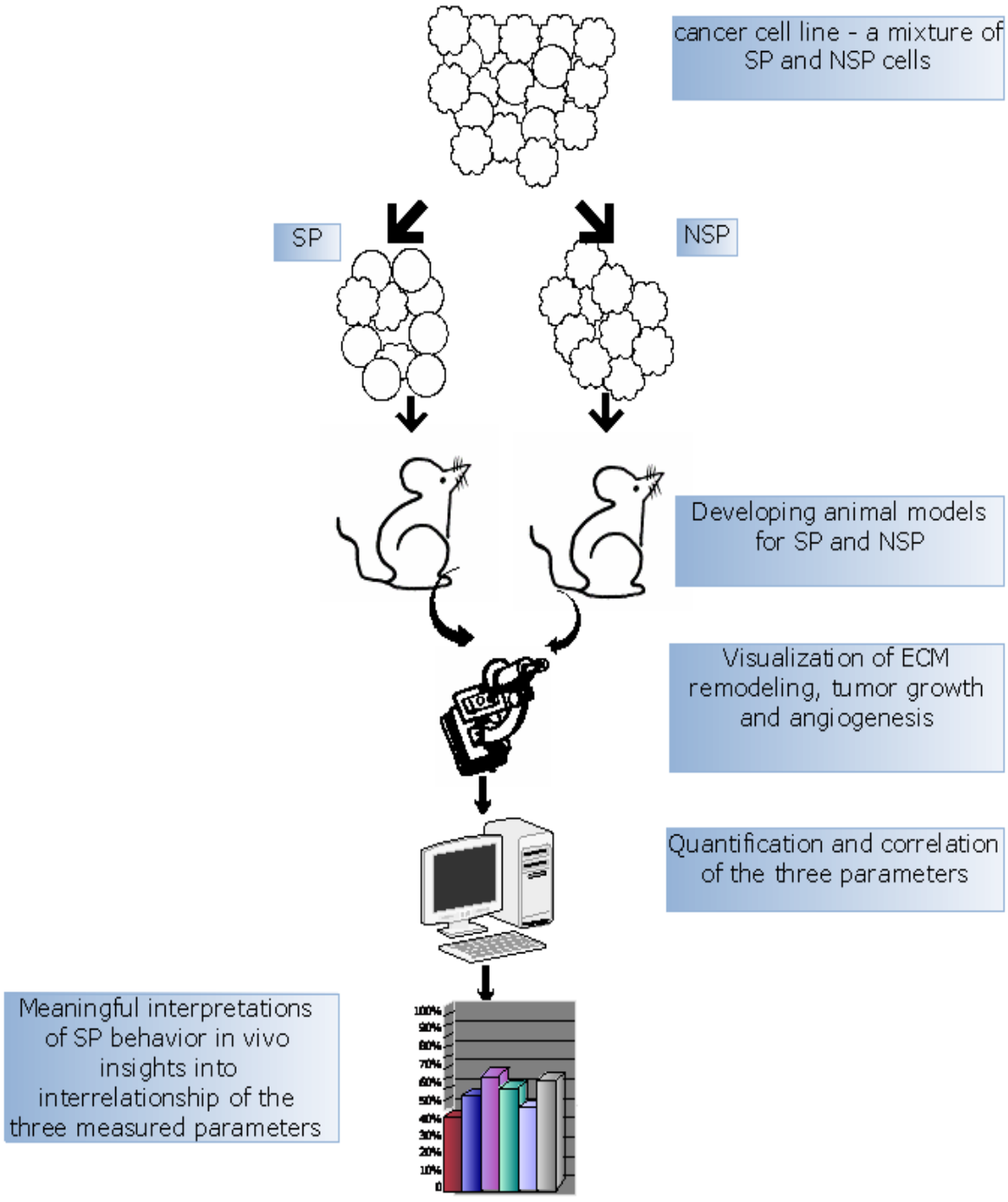

Figure 1: Schematic representation of the overall flow of the project.
The development of animal models, the appropriate tools such as SHG microscope with pulse compressor improvement and the software quantification algorithm development to assess the ECM remodelling property of CIC in vivo are shown here.

II Background and Significance

This chapter provides the background information that defines the rationale for this

thesis work. The chapter is divided into (1) background information on cancer initiating cells with a focus on breast cancer - this section provides information on breast cancer with the strategies of isolating and characterizing initiating cells and clinical translation of the CIC concept, (2) cancer and its microenvironment and the available tools to study cancer-microenvironment interactions – this section discusses the interdependence of cancer and its microenvironment with the limitations of tools in characterizing the microenvironment, and (3) an introduction to Second Harmonic Generation (SHG) imaging and how this tool is useful to study cancer - ECM interactions - current limitation and improvement of the SHG microscope are discussed.

2.1 Breast Cancer Initiating Cells

2.1.1 Origins of Breast Cancer

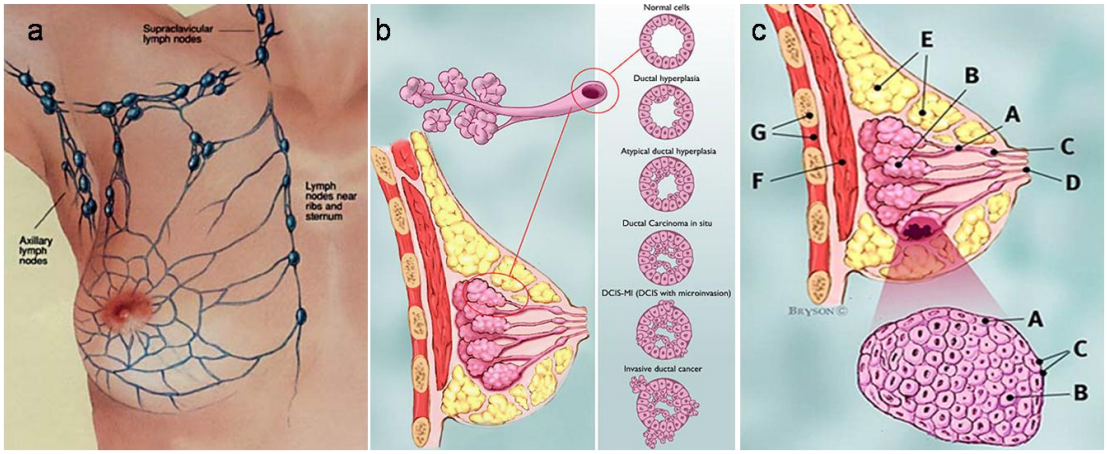

Figure 2: Structure of the female breast and carcinoma development in the breast (www.breastcancer.org)

Breast is a highly vascularised organ with extensive blood and lymph vessel network. 2a shows the lymphatic network of a female breast. Cancers in the breast develop with accumulated mutations in the ductal or lobular epithelia giving rise to ductal (2b) or lobular (2c) carcinoma, where the cancer progresses in several stages from hyperplasia to invasive carcinoma. Labels in 2c – A ducts B lobules C dilated section of duct to hold milk D nipple E fat F pectoralis major muscle G chest wall/rib cage Enlargement: A normal lobular cells B lobular cancer cells C basement membrane.

The most common causes of breast cancer are hereditary or acquired genetic mutations (BRCA1, BRCA2) [Brody], late or no pregnancies [Kelsey 1993], no breast feeding, hormone replacement therapies [Kelsey 1988] exposure to radiation [37]. There could be several known risk factors but cancer starts with a cell acquiring mutations and resist cell death or apoptosis. The acquired mutations will result in a group of cancer cells that can divide rapidly, resist drug administrations, invade local organs and metastasize to other organs of the body [38]. In breast cancer the cells acquiring such mutations can be of different epithelial lineages such as the lobular epithelium or the ductal epithelium [39]. When these normal cells acquire mutation there is increase in cell mass which is called hyperplasia [40]. If the cell proliferation is extensive but the cells have not invaded the basement membrane it is called carcinoma in-situ [41]. But when the cancer cells escape the single duct or gland and starts spreading to the other ducts and glands it is called invasive carcinoma [42]. Breast is a well vascularised organ with extensive blood and lymphatic vessel network. So when the invasive carcinoma cells reach the blood or lymph vessels they might metastasize to other organs such as the lungs and the bones where they form secondary tumors. This topic of invasion, migration and metastasis has been under intense research as most patient deaths are due to metastasis of malignant tumors [38, 43-44].

2.1.2 Breast Cancer as a stem cell disease

In normal stem cell hierarchy, there is a group of stem cells that divide asymmetrically to generate transit amplifying clusters of progenitor cells. The progenitor cells divide and differentiate further to become specialised cells with unique characteristics and functions. As we go down the hierarchy from stem cells to the differentiated cells, the replication potential of the cells is reduced [Fig 3A].

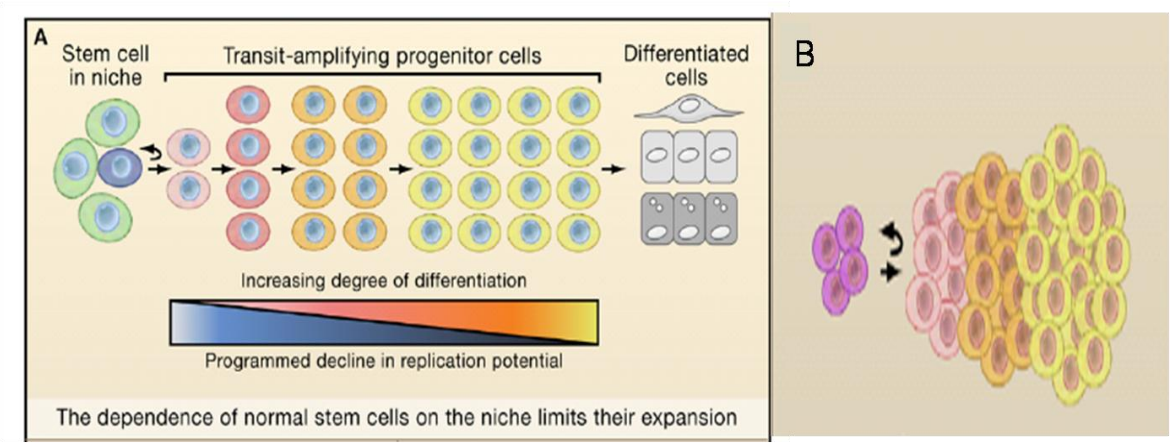

Figure 3: Differentiation of normal stem cells maintaining asymmetric division vs. Cancer stem cells [6]
Stem cells in their niche divide asymmetrically to generate transit amplifying progenitor cells as well as stem cells, thus ensuring its own maintenance. The progenitor cells go on to divide and differentiate until they become terminally differentiated cells, which have little or no replication potential(A). on the other hand CIC loose the context of niche control and divide uncontrollably to form tumors, generating progenitor or differentiated cells with little control of replication potential (B).

Many predict that the cancer causing mutations occur to less differentiated progenitor cells in the stem cell hierarchy, rather than the terminally differentiated cells, giving rise to cancer stem cell or cancer initiating cells (CIC). Or if the mutation happens to be a random phenomenon, the cells that acquire a unique set of mutations become partially stem cell like regaining their potential to replicate and maintain the small stem cell like population even without a unique niche. These are the cells that can survive and divide many folds to generate the tumor mass [Fig 3B]. The presence of

CIC – whether generated from stem cells or from differentiated cells – has been demonstrated in several cancers, several cell lines and various clinical samples.

2.1.3 Isolation and Characterization of Cancer Stem Cells or Cancer Initiating Cells

It has been hypothesized and demonstrated that the minority CIC population contributes to tumorigenesis and tumor growth where CIC cells can form tumors when only 100 CIC are implanted in an animal while atleast a million non-CIC cells are needed to form a tumor [17]. It has also been shown the CIC gives rise to the majority non-CIC population demonstrating asymmetric division [16]. In other words CIC is the fountain head of tumorigenesis, tumor growth and development. This minority CIC population is highly tumorigenic, invasive, metastatic, and it can effectively efflux the drugs administered to treat the cancer[45]. Various research groups have identified CIC using various techniques and they have named them differently. A few accepted terminologies are cancer stem cell, cancer initiating cells and also the side population due to its profile on flow analysis when stained with the Hoechst dye. When stained at 5 µg/ml, these cells can efflux the dye effectively because of which they appear as a "side population" distinctly separated from the majority of the cells. These cells are found to express certain stem cell markers like the C-Kit, Oct4 etc [17]. There have been striking similarities between this subpopulation and normal stem cells in properties like self renewal, migration, drug resistance, and immortality/longevity [46]. Hence the deduction that cancer originates from a deregulated stem cell. The following tables highlight the initiating cell populations identified in different types of cancers and the technique of isolation.

Table 1

Progenitor cell properties ($CD44^+/CD24^-$) of various breast cancer cell lines

Cell line	$CD44^+/CD24^-$	$CD44^+/CD24^+$	$CD44^-/CD24^+$	$CD44^-/CD24^-$	Tumor type[a] [24,50-52]	Tissue source[b] [24,50-52]	Cell type classification [25-27]
MDA-MB-231, TMD-231	85 ± 5	2	0	13 ± 5	AC	Pleural effusion	Mesenchymal
TMD-436	72 ± 5	27 ± 5	0	7	AC	Pleural effusion	Myoepithelial
Hs578T	86 ± 5	10 ± 5	0	2 ± 2	CS	Primary	Mesenchymal
SUM1315	97 ± 3	0	0	3 ± 3	IDAC	Metastatic nodule	Basal
HBL-100	37 ± 5	8	2	52 ± 6	Immortal	Milk	Myoepithelial
MDA-MB-468	3 ± 1	90 ± 6	7 ± 3	0	IAC	Pleural effusion	Basal
MCF-7	0	8 ± 3	87 ± 2	6 ± 2	IDAC	Pleural effusion	Luminal
T47-D	0	0	63 ± 3	37 ± 2	IDAC	Pleural effusion	Luminal
ZR-75-1	0	0	64 ± 1	36 ± 1	IDAC	Ascites	Luminal
BT-474	0	0	78 ± 7	22 ± 7	IDC	Primary	Luminal/$ErbB2^+$
SK-BR-3	0	0	84 ± 1	16 ± 1	AC	Pleural effusion	Luminal/$ErbB2^+$
DU4475	0	0	6 ± 1	94 ± 1	IDC	Cutaneous nodule	ND
MCF-10A[a]	17 ± 4	5 ± 3	20 ± 10	58 ± 20	Immortal	Fibrocyst	Basal

[a]Percentage of MCF10A cell progenitor and other subpopulation was influenced by species and batch of serum in culture media. AC, adenocarcinoma; CS, carcinosarcoma; IDAC, infiltrating ductal adenocarcinoma; IAC, Invasive adenocarcinoma; IDC, Invasive ductal carcinoma; ND, not determined.

Table 1: Various breast cancer cell lines have been characterized based on their expression of CD44 and CD24 to analyze for the presence of cancer initiating cells and progenitor properties of these CIC [47]

Cancer Initiating Cells isolated using molecular markers

Source	Type	CIC marker	References
Blood	Acute myeloid leukemia	$CD34^+$ $CD38^-$ $Thy1^-$ Lin^-	[48-49]
Breast	Primary tumor, metastatic pleural effusion	$CD44^+$ $CD24^{-/low}$ ESA^+ Lin^-	[11]
Brain	Medulloblastomas, glioblastomas, primary brain tumor	$CD133^+$	[50-52]
Lung	Non–small cell lung cancers	$Sca\text{-}1^+$ $CD34^+$ Lin^-	[53-54]
Skin	Metastatic melanoma	$CD20^+$	[55]
Prostate	Prostate cancer	$CD44^+$ $a2b1^{hi}$ $CD133^+$	[56]
Colon	Colon adenocarcinoma	$CD133^+$	[57]
Pancreas	Pancreatic adenocarcinoma	$CD44^+$ $CD24^+$ ESA^+	[58]
Head&neck	Head and neck squamous cell carcinoma	$CD44^+$	[59]

Table 3

Cancer Initiating Cells isolated using SP method

Source	Type	Sample	References
Blood	AML Blast cells	Primary	[60]
Brain	Neuroblastoma	Primary	[16]
	Neuroblastoma	B104	[61]
	Glioblastoma, astrocytoma	U87MG	[16]

	Brain glioma	HS683	[16]
	Glioma	D54, U87, U251, U373	[62]
Breast	Adenocarcinoma	SK-BR-3, MCF-7	[16, 61]
Cervix, Ovary and Prostate	Ovarian ascite cells	Primary	[63]
	Ovarian Cancer cell lines	IGROV-1, OVCAR-8	[63]
	Ovarian adenocarcinoma	SKOV3	[16]
Liver		Huh7, Hep3B, HepG2	[64]
Colorectal Cancer		WiDr, CCK81, Colo201	[64]
		Colo205, SW480, HSC15	
Pancreatic Cancer		PK9, PK45H	[64]

Table 2: List of various types of cancers in which cancer initiating cells are isolated using marker profiles

Table 3: List of various cancer cell lines and primary samples in which cancer initiating cells are isolated using side population method

2.1.3.1. Previous studies on Breast cancer initiating cells

CIC have been isolated based on various strategies. R.B. Clarke and his group have demonstrated that the sub population can be isolated using the side population analysis. This population is enriched in cells expressing putative stem cell markers p21, CK19 and musashi-1 along with ER alpha and Progesterone receptor. They are also proven to be undifferentiated since they lack myoepithelial and luminal specific cell antigen. Moreover these cells have superior colony formation capacity compared to the non-side population [65]. Other groups have cultured single cell suspension in medium supporting undifferentiated cells. They obtained clusters of cells, which are capable of growth in suspension. Moreover when these cells are dissociated, they were able to form clusters again. This elicits the fact that these cells have self-renewal properties. These clusters of cells were called mammospheres since they resemble neurospheres (neural stem cells) that are cultured in suspension [66]. In breast cancer this sub population is found to over express CD44 and have low or no expression of

CD24. Thus various groups have isolated it using $CD44^{+}/CD24^{-/low}$ strategy [22, 66]. Animal models of this SP and non-SP have demonstrated that SP induces tumor formation in as low numbers as 10^3 while the non-SP requires at least 10^6 cells or more to induce cancer [17].

2.1.3.2. Studies on CIC in other cancers

Cancer initiating cells were initially isolated from blood related cancers and hence one of the most well studied model systems in the cancer stem cell domain [67-68], In case of blood cancer there are various stages in which the Hematopoetic stem cell can be deregulated to generate cancer stem cells [69]. In case of acute myeloid leukemia, animal studies have shown that the deregulated stem cell possesses the differentiative and proliferative capacities and the potential for self-renewal expected as a leukemic stem cell, suggesting that normal primitive cells rather than committed progenitor cells are the target for leukemic transformation [70].Some of the other cancers in which CIC's have been isolated and characterized are in the cancers of the breast, brain, liver and lung. In case of neuroblastoma, the SP has been proven to have higher expression of ATP binding cassette proteins like ABCG2 and ABCC3. These ABC proteins are molecular pumps that endow the cancer cells the potential to efflux the drugs administered to them. The CIC survive better and can form colonies in the presence of the drug mitoxantrone [16]. Recently CIC have been isolated in ovarian cancer patient samples [63], colorectal cancer [71], and melanomas [55] as well. The above studies on these different cancer initiating cell populations provide hints on the unique properties of this population which might be the fountainhead of tumor development as the cells responsible for the initiation, maintenance and growth of tumors [6, 72-73].

2.1.4 Characterizing SP in vivo and its implication in pre clinical and clinical studies

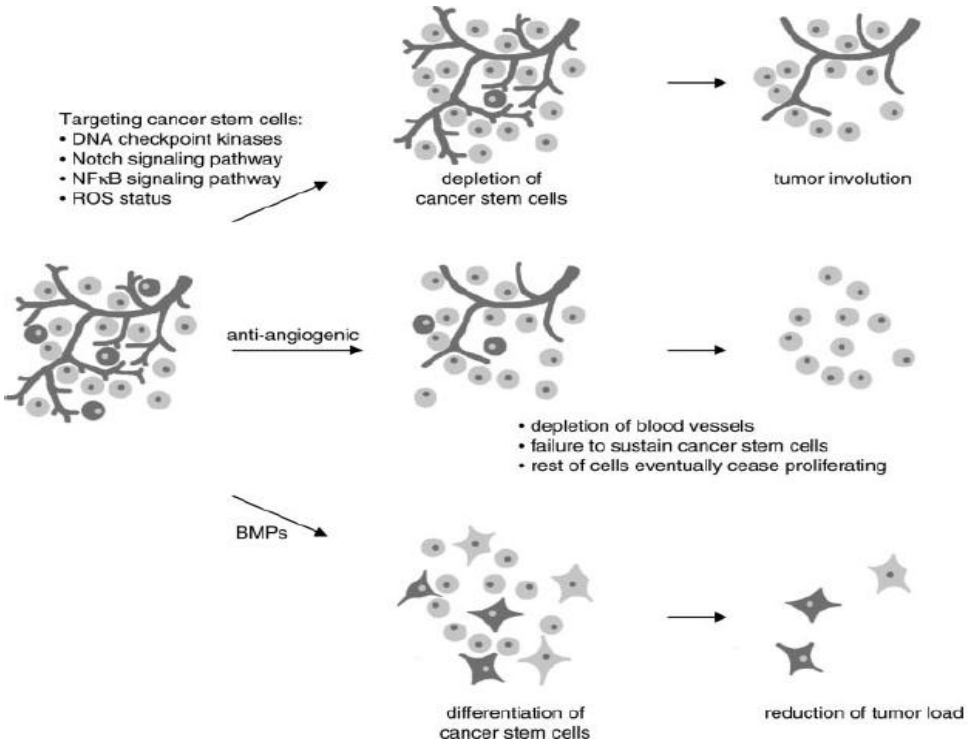

Figure 4: Strategies to target and eradicate CIC and the whole tumor [74]

On ascertaining the presence of CIC in a tumor mass, the tumors can be eliminated in a multi-pronged approach. The CIC can be killed targeting the signaling molecules that are involved with CIC. The reactive oxygen species (ROS) status of the CIC can be exploited to target them. The nutrition and oxygen supply to the tumors can be cut off using anti-angiogenic compounds choking the tumors The CIC can be forced to differentiate using factors such as bone morphogenetic proteins (BMPs) and lose its stem like phenotype giving a better chance for chemotherapy to kill the cells.

Prior works have mainly focused on various strategies of isolating the side population and in in-vitro characterization techniques of CIC (Table 3). The published animal studies assess only the tumorigenicity of CIC and the minimum number of CIC required to grow tumors. Further characterization of the tumor formed by CIC is lacking. There are several proposed ways of targeting cancer stem cells in the tumor. The CIC have been shown to be associated with several signaling pathways such as the NF-Kappa-B [Liu]. Wnt [Lindvall] , Notch [Farnie] signalling pathways in vitro. But the inter-relationships of these proteins and CIC in-vivo have not been established. Identifying CIC in-vivo is a challenge due to their small numbers. But if we do develop a technique to identify the presence of CIC in-vivo we can utilize a multi-pronged approach to either target these cells directly or by driving them towards differentiation and then killing them using traditional methods (Fig 4) [Carol Tang]. As identifying this small population in a tumor by traditional immunochemistry techniques is very difficult, and also with limited availability of tumor tissue from patient biopsies, we devised an alternate strategy.

There has been a growing body of evidence that cancer cells need a suitable microenvironment to establish and maintain a tumor and cancer cells suitably remodel their environment and establish a niche for sustenance. Thus we set out to study the interaction of the CIC with the stroma. We used animal models to gain valuable information on ECM remodeling by cancer initiating cells and identify if there are any hallmarks of ECM remodeling by CIC in tumors that can be translated to clinical studies. If we can demonstrate that CIC remodel the matrix significantly differently compared to the non-CIC, we can identify such features from clinical patient samples proving the presence of CIC. Therapies can then be designed to appropriately

eradicate the tumor.

2.2 Breast Cancer and its microenvironment

2.2.1 Changes in microenvironment with Cancer Progression

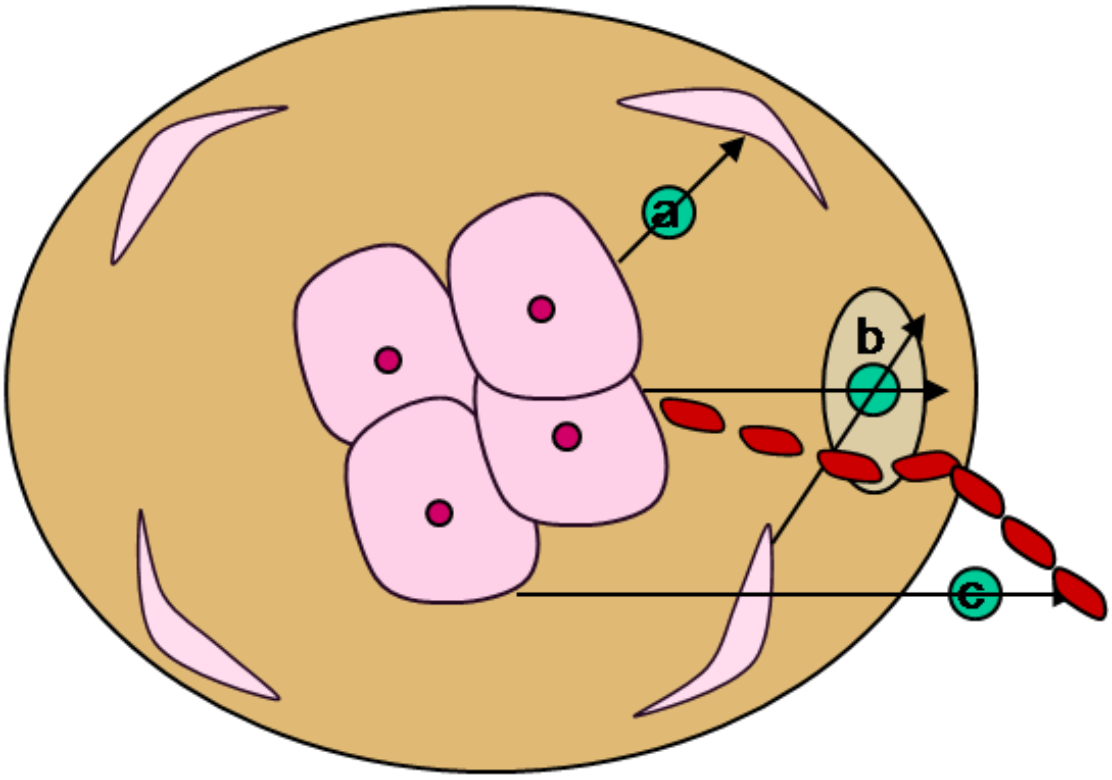

Figure 5: A schematic to show the host –tumor relationship
The cancer cells remodel the matrix environment to establish a tumour niche. (a) The cancer cells signal the non-cancerous neighbouring cells such as fibroblasts and endothelial cell. (b) The cancer cells and the stimulated neighbours secrete matrix metalloproteinase and other enzymes to degrade the matrix and facilitate tumor growth. (c) The cells secrete factors such as Vascular Endothelial Growth Factor (VEGF) to attract endothelial cells and precursors for angiogenesis and vascularisation of the tumor to supply the cells with nutrients and oxygen. The cancer cells also secrete new matrix components at other regions to provide mechanical support required for the cancer cells

The three defining characteristics of tumors are its proliferation rate and tumor size, lymph node involvement and metastatic potential, using which medical practitioners grade the tumor [75]. There are some theories that vascularization and metastasis are closely related, stating that formation of vessels can aid in the escape of cancer cells to invade distant organs [76]. An overlying factor that affects all stages of tumorigenesis, vascularization and tumor metastasis is the microenvironment. It is a

proven fact that cancer cells need a suitable environment to form a tumor [77]. The extracellular matrix (ECM) was believed to be just a scaffold providing physical support [78]. But it has been unraveled that there are mechanical and chemical cues that transact between cells and the ECM they reside in. In several organ systems it has been shown that cues from ECM are required for systematic development of the organ. But in case of cancers, the ECM – tumor relationship is altered compared to that of a normal organ. Whether the cues are aberrant or whether the aberrant cancer cells interpret the cues differently is not clearly understood. Whether the unique nature of a cancer microenvironment is a cause or an effect of tumorigenesis is yet to be explored.

The cancer cells establish this niche by recruiting host derived cells and altering the matrix components such as collagen, fibronectin, laminin etc. while these ECM molecules provide signalling to the cancer cells through cell transmembrane glycoproteins – integrins. The signalling from the ECM affects an array of cellular processes anything from cell shape, attachment, motility, transcription, synthesis and secretion. Remodeling the matrix surrounding the cancer cells principally creates a niche for the tumor to grow as well as help to generate new vessels [79]. Matrixmetalloproteinases and other proteases are the key players in this remodeling process. MMPs are both released by the cancer cell (e.g. MMP7) as well as the host derived cells like the endothelial cells, inflammatory cells, and myofibroblasts. The fibroblasts in the cancer niche are activated and they have a wound healing phenotype [80]. These peritumoral fibroblasts or Tumor activated fibroblasts help tumor progression by secreting MMPs [81-82]. Cancer cells and the surrounding ECM provide angiogenic cues to the host derived cells. The cancer cells directly attract host-derived cells by releasing chemokines and cytokines. The cancer cells also

remodel the surrounding ECM and secrete ECM components that attract host derived cells. These cues reach the host derived cells through various signaling pathways including tyrosine kinase, Smad, Ras, PI3K [83-84]

The cues provided by the microenvironment plays a crucial role for the tumors to establish vasculature as well as to establish metastatic sites [85-87]. Studies have shown that cancer cells specifically recruit mesenchymal stem cells from the bone marrow. These cells signal the cancer cells in a paracrine fashion making them more metastatic [88]. The cells that acquire the metastatic phenotype escape to form transit-amplifying clusters. These clusters can further go on to metastasize at specific sites. The importance of microenvironment is clearly elucidated by the fact that cancers can metastasize to specific organs attracted by ligands produced by the metastatic site ECM (e.g. osteonectin released by bone marrow ECM attracts breast cancer cells to specifically metastasize to the bone) [68]. The bone is rich in cytokines and chemokines released for the interaction amongst the osteoblasts and osteoclasts. The developing bone is also rich in vasculature allowing easy passage of metastatic cells [89].

Hence it is evident that the tumor cells, host derived cells and the tumor microenvironment work together in complex coordination to ensure the survival, proliferation and spreading of tumor. A quantitative observation and characterization of this ECM remodeling especially in the case of side population will give us useful insights into the process of tumor progression.

2.2.2 Current Techniques and its limitations in extra cellular matrix (ECM) Characterization

2.2.2.1 In vitro Studies of the components of cancer microenvironment

The interplay of cancer cells, host derived cells and the ECM has been studied using several in vitro approaches in the gene and protein levels [90-91]. Recently proteomic and genome wide studies have resulted in uncovering several interactions between chemokines, cytokines and their receptors on cell surfaces. Proteomic and Genomic array studies, imaging and histochemical methods are some of the techniques employed to uncover the interplay between these molecules [92-94]. Other than these assays to understand the chemical relationships between the cancer and its microenvironment, there are mechanical factors that come into play which has also been attributed to the establishment of the tumor niche [95].

The following table illustrates a few model molecules implicated in cancer, ECM and host cell interaction. These are representative studies that provide us insights into the complicated tumor – host interaction. We will be able to study the molecular interactions and signaling pathways using these in vitro models.

Biomolecule	Role in Cancer Development
1. Heparanase [96]	Over expressed in certain cancers Involved in ECM degradation and remodeling Involved in endothelial cell migration
2. Prolidase [97]	Catalyze the final stages of Collagen degradation Observed in breast cancer patients
3. Matrixmetalloproteinases (MMP) Tissue inhibitor of MMP (TIMP) [85, 98]	ECM remodeling surrounding the tumor Released by cancer cells and host derived cells Observed in various cancers
4. TGF- β [99]	Promote cancer metastasis by Effect on the tumor microenvironment Enhances cancer cell invasive properties Inhibit immune cell function
5. Cathepsins [100]	Affects immune response Affects migration of cancer cells
6. EGF [101]	Indicates poor prognosis Involved in cancer cell migration and
7. Rho GTPases [102]	Adhesion of cancer cells to ECM Over expressed in certain malignancies Implicated in metastasis
8. VEGF [103]	Implicated in tumor invasion, growth and vascularisation

Table 4: A list of extracellular matrix factors with distinct roles in tumor initiation, progression and invasion

2.2.2.2 In vivo Studies of the components of cancer microenvironment

For a macroscopic view of the ECM remodeling process, we need to turn to 3 dimensional models and animal models. Cancer animal models have been used for preclinical therapeutics studies and in understanding the effect of certain molecules on overall tumor development. Traditionally the tumor size changes are monitored over a period of time and the animals are sacrificed for histopathology studies. H&E stains and micro vessel count are performed. The tissue samples are sometimes further processed to study protein and mRNA expression. Most of these studies do not provide spatial information of host- tumor interaction. With the advent of fluorescently labeled cancer cells, skin flap models and dorsal skin fold chamber models; whole animal imaging has taken a lead role in answering critical questions in cancer progression. This method provides us with spatial information not obtainable in biochemical studies.

Whole animal Imaging

On comparing several existing methods of imaging, optical imaging has the following advantages

1. Long term labeling: the cancer cells can be transfected with fluorescent proteins, which are expressed as long as the cell survives
2. Resolution: using skin flap models and non-linear optics, features like cells and ECM can be distinguished clearly
3. Real time: The duration of imaging is very short compared to MRI and CT, which enable us to observe cellular events

Several fluorescent proteins are available for transfection. One among them is the Red fluorescent protein (RFP). The advantages of RFP over other fluorescent protein are that they have longer wavelength excitation (558nm) and emission (583 nm). This improves the penetration depth of the signal and enables deep tissue

imaging. Secondly their excitation and emission are well away from the auto fluorescence signals from the animal body, which are usually in the shorter wavelength range.

2.3 SHG as a tool to study cancer microenvironment

2.3.1 The theory and advantages of SHG

Recent work has demonstrated the application of imaging for studying ECM changes in in-vitro and in vivo models [34, 104]. We are employing Second Harmonic Generation (SHG) imaging to visualize ECM distribution from tissue samples. SHG can be used to visualize many biological structures that do not have central symmetry (surface materials, chiral materials). Collagen type 1 present in ECM is one such molecule that has noncentrosymmetry and hence generate second harmonic signals [105-106].

SHG imaging is usually performed along with two – photon excited fluorescence (TPEF) imaging, since both of them share the same laser source. TPEF can be used to visualize tissue and cellular architecture without extraneous staining just by making use of the auto florescence generated by certain biological molecules [107]. The excitation wavelength range for SHG is usually 700-900nm. Since the excitation wavelength is near infrared, the scattering is reduced and hence the increased depth of imaging. Moreover since the excitation energy is delivered to the sample in short pulses the average energy transferred to the sample is low. Hence tissue damage or photo bleaching is greatly reduced.

This technique can be used to study molecular adsorption, aggregation and orientation [105]. Prior work using SHG has been helpful in providing information of oral malignancy using non-invasive methods in hamster cheek pouch models [108].

The diffusion coefficient of drugs in tumors has been quantified using non-invasive means in SCID mice dorsal skin fold chamber models [31].

Figure 2a elucidates the concepts of TPEF and SHG. In two-photon fluorescence, when the fluorophore absorbs two photons simultaneously, the electrons in the fluorophore reach the excited state (Simultaneous absorption of two photons is a rare event and hence the source laser needs to generate high density of photons). The electron undergoes thermal relaxation and transits to ground state while emitting fluorescence. The probability of excitation is related to the square of the intensity of the excitation beam. Thus the excited fluorophore is confined to the focal volume. This reduces photo damage beyond the focal volume. In second harmonic generation, the excitation and emission signal has to be phase matched to obtain maximum output signal. In this process there is no absorption of the excitation photon to emit an output signal. Hence there is no excited state. Rather it is the property of the material to convert an excitation signal to an emission signal with double the energy.

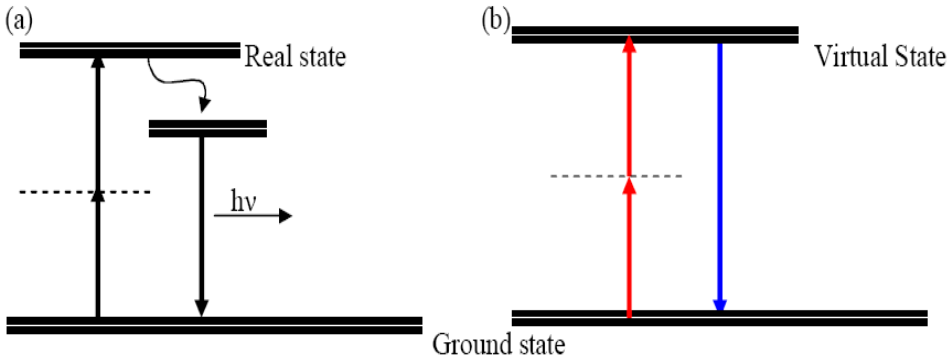

(c) (d)

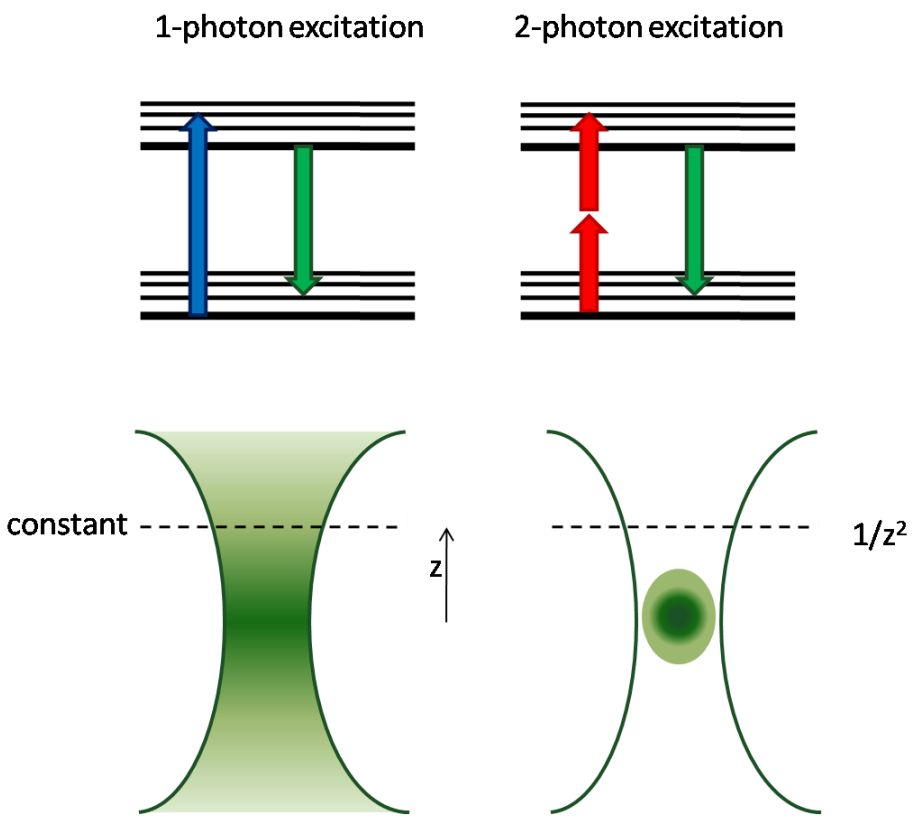

Figure 6: Energy level diagram for Two-photon excited fluorescence and Second Harmonic Generation.

(a) depicts two-photon fluorescence. The dotted line is the virtual state. (b) depicts SHG. (blue arrow) is half the wavelength as the excitation signal (red arrow). (c) depicts one photon excitation where there is no in-built confocality and all the fluorophores in the beam path is excited unless a pinhole is used. (d) shows two photon or SHG excitation where the excitation volume is restricted and thus reduces photobleaching and photo damage. The emitted SHG signal has certain directionality while the 2-photon emission (2PE) fluorescence is anisotropic

SHG has its unique advantages compared to other imaging modalities.

- SHG signals are generated due to the intrinsic structure and do not need any additional labeling such as dyes or fluorescent proteins.
- The incident signal is a very short, high energy pulse in the order of femto seconds impinging on the sample. This causes minimal damage to the sample.
- The signal to noise ratio is better in SHG compared to conventional systems such as florescence imaging.
- The known excitation and SHG emission spectral signatures, allows easy separation of signals from collagen and other fluorophores [31].
- SHG provides intrinsic confocality and deep tissue sectioning in complex tissue structures [109].

2.3.2 Limitations of SHG microscope – Group Velocity Dispersion

There are several advantages of using the SHG microscope to observe non-centro symmetric molecules as described above. But as with all ultra fast laser set-ups, the SHG microscope also suffers from Group Velocity Dispersion (GVD). As the term suggest, GVD is a dispersion of light on passing through dispersive optical components such as lenses, gratings and prisms, where the light is stretched temporally. Thus an ultra fast laser whose temporal profile is a Gaussian of 50fs will be stretched to a larger time profile. The dispersive components slow down the light with the higher frequency to a slower velocity.

;

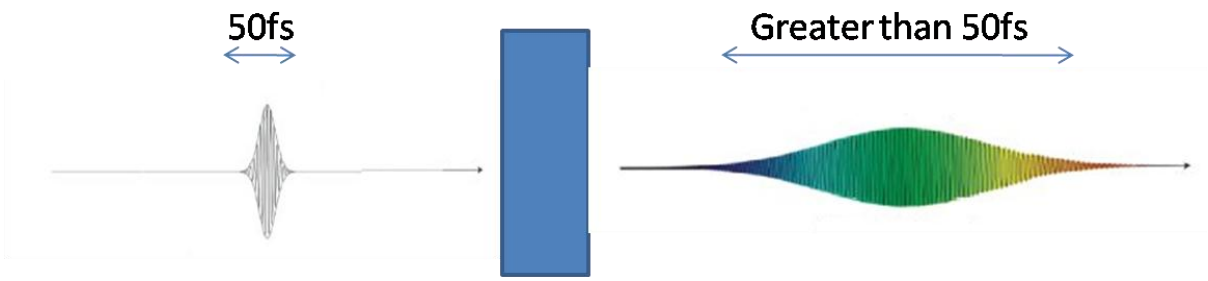

Figure 7: Group velocity dispersion of a femto-second pulse
Group Velocity dispersion: A 50 fs laser pulse passing through a dispersive optical component (depicted here as a blue rectangle) experiences a positive group velocity dispersion, where the longer wavelengths in the laser pulse travels faster than the shorter wavelengths, stretching the pulse temporally.

Group velocity is defined as the velocity at which the energy of the wave is carried. It is the derivative of the wave number with respect to angular frequency. It is related to phase velocity as follows,

$$V_g = C\left(n - \lambda \frac{dn}{d\lambda}\right)^{-1}$$

Where C is the velocity of light in free space 3 x 10^8 m/s, n is the refractive index of the traveling medium and λ is the wavelength of light in vacuum.

Group velocity dispersion can be compensated using GVD compensators. There are various dispersion compensators like the Chirped mirrors (Fig 10a), pulse compressors (Fig 10b) and negative dispersion gratings. Chirped mirrors in combination with photonic chirped crystal fibers have been used to generate sub 20 fs pulses [110]. These dispersion reversal tools are called pulse compressors or pulse modulators. The basic principle pulse modulation is to ensure that low frequency signals travel a longer path compared to the high frequency signal, such that all frequency components of the resultant wave reaches the sample in a narrow time

frame, usually in femtoseconds. To better enunciate this point, a Ti-Sapphire laser with a 700-900nm wavelength range and pulse duration of 70-100 fs, can be distorted to around 370 fs if the material dispersion is around 13,000 fs2. By placing a pulse compressor or compensator, the pulse duration can be readjusted to 100fs.

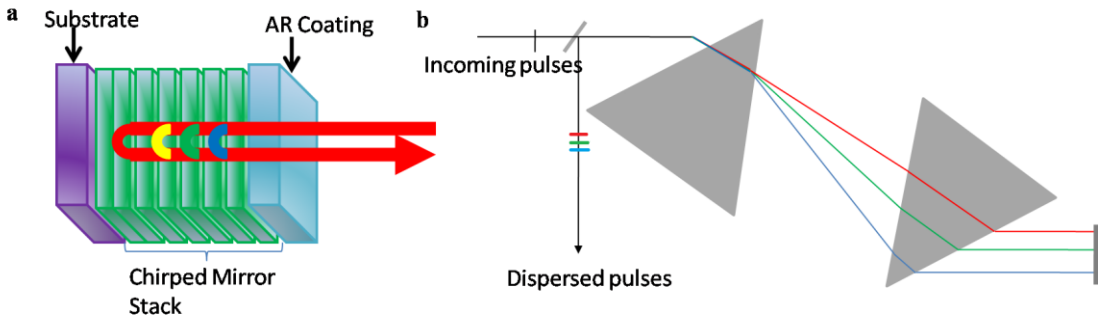

Figure 8: Reversing group velocity dispersion using pulse modulators such as chirped mirrors and paired prisms
(a) Chirped mirror – a stack of dielectric mirror in which the light of longer wavelength (red) travel deeper before it is reflected while the shorter wavelength (green, blue) light is reflected faster, hence compensating for the negative dispersion. (b) Prism based pulse compressor – a pair of prism spatially arranged in such a way that longer wavelength light (red) travels a longer path compared to the shorter wavelength (blue, green and yellow).

2.3.3 Advantages of using improved SHG to study basic biological processes

Clinicians and medical scientists are always looking for quantifiable information as it is easy to assess the severity of a condition as systematically as possible. SHG is an excellent tool for imaging collagen as the information obtained is immediately quantifiable. But to ensure the accuracy of the system, we need to ensure that the signal to noise ratio and sensitivity of the system is optimal to even pick up the smallest of collagen fibers. Pulse modulation ensures highest sensitivity and SNR achievable so that the information we obtain is quantifiable and accurate.

We have chosen collagen as our stroma molecule of interest to study cancer ECM interaction for the following two reasons. One – collagen is the most abundant biomolecule and cancer cells interact with collagen, remodeling it through matrix metalloproteinases. Two – we have an optimized imaging tool to quantify and study

collagen with no staining or tissue processing required.

2.4 Rationale for the proposed study

2.4.1. Studying the tumor microenvironment in relation to tumor progression and chemotherapy

Optical whole animal imaging and SHG imaging have been used to study tumor properties before, but to our knowledge we have not seen correlative studies of ECM remodeling with tumor progression. It is also not known if the ECM distribution varies with drug administration. In this work, with an improved SHG tool, we hope to monitor the collagen changes during tumor progression as well as during drug administration. The dynamics of ECM with tumor progression and drug administration can be used in pre-clinical drug studies to characterize the efficacy of the drug and quantify its effects both on the cancer as well as the host environment.

2.4.2. CIC's role in tumor development and its relationship to the microenvironment

Faster pace of drug discovery and drug testing has expedited the process of validating the drugs for human use. The five-year survival rate in case of breast cancer patients has improved to about 98% with the plethora of treatments. Nonetheless studies have demonstrated loco regional recurrences and distant metastases in 49% and 35% of the high risk breast cancer patients studied [111]. These information strongly point to the fact that current therapies might not be effective to target the CIC.

Current studies on CIC are more focused on its isolation and in vitro characterization. By isolating the CIC and establishing cancer animal models using

CIC and non-CIC we can compare growth rates, morphological differences, vasculature and metastatic characteristics. This information will enable us to elucidate CIC's role in tumor formation more clearly. The tissue samples obtained from the tumor can be used to study the tumor ECM interaction using SHG and TPEF. This information will help us compare the ECM remodeling capability of the CIC and non-CIC cells. Image analysis techniques can be used to identify collagen signatures unique to CIC which might help predict patient treatment regimen or prognosis

2.4.3. Improvement of current histopathological analysis

Histopathology studies are routinely done on patient tumor samples. The tumor sample is stained using Hematoxylin and Eosin usually to reveal cancer cells and surrounding cells. The information obtained from these studies is usually the type, grade, receptor status and prognosis of the patient. Along with the usual analysis, SHG microscopy of the sample will provide valuable information on ECM distribution in and around the tumor regions. We can identify unique collagen remodeling patterns in the biopsy samples indicating presence or absence of CIC. This information can help clinicians to decide on treatment regimens as well as used to predict the spatial and temporal growth patterns of the cancer.

III Isolation and Characterization of CIC in MX-1 GFP breast carcinoma cell line

3.1 Introduction

Breast cancer initiating cells (BCIC) has been isolated using several techniques and characterised quite extensively both in vitro and in vivo. In a study with the cell line MCF7, Ponti et al demonstrated that CIC can grow in suspension culture just like normal stem cells do. They called them mammospheres drawing parallels to neurospheres technique of neural stem cell culture. These cells escaped the process of Anoikis, which is cell death in the absence of adhesion. The mammospheres were shown to have differentiation potential and tumorigenicity in animal models. The tumors initiated by mammospheres had higher levels of VEGF expression [17].

Al Hajj and his colleagues utilised the differential expression levels of CD44 and CD24 on breast cancer cell lines and primary patient samples to isolate CIC, however the reason for choosing these two cell surface marker remains unexplained. The isolated $CD44^+$/ $CD24^-$ cells engrafted in animals in much smaller numbers compared to the bulk population. The histology also demonstrated that the tumors formed by $CD24^-$ had malignant cells, while the site of injection of $CD24^+$ cells resembled normal tissue showing no signs of engraftment [11]. In a later work the $CD44^+$/ $CD24^-$ were shown to be more invasive than the $CD44^+$/ $CD24^+$ population [47].

The side population method has been used to isolate stem cells from the hematopoietic system utilising the property of stem cells to efflux lipophilic dyes more than the differentiated cells. This technique has been successfully demonstrated in isolating CIC in several cancer studies [15, 54, 64, 112-113].

We wanted to demonstrate that side population method can be used to isolate the CIC from an invasive breast cancer cell line MX-1. We have performed in-vitro characterization of CIC vs. non CIC such as testing for its proliferative capacity, drug resistance and CD44/CD24 marker expression analysis, invasiveness and migration potential to ascertain that the side population we are isolating have the phenotypes of cancer initiating cells that are reported in prior literature. We have injected the isolated CIC and non-CIC in immune-compromised mice to study their tumorigenesis. After developing the animal models we have observed differential tumor growth and vascularization in the case of tumors formed by CIC compared to those of non CIC tumor. This implies that there are inherent differences between CIC and non CIC tumorigenicity, growth and invasion. All our experiments demonstrate that isolating CIC from GFP labelled MX-1 cells using the side Population technique is a suitable model to study CIC in-vitro and in-vivo. This model has been established for studying the ECM remodelling properties of CIC in-vivo which is discussed in chapter V.

3.2. Materials and Methods

3.2.1 Side Population Analysis, Cancer Initiating Cells Isolation and Cell Proliferation Assay

GFP labelled breast cancer cell line MX-1 was used for all the experiments. MX-1 cells were cultured in RPMI medium with 10% fetal calf serum (FCS), 1.5 g/L Sodium Pyruvate, Sodium Bicarbonate and Penicillin Streptomycin. Cells were split every 3 days when they were 80% confluent.

For side population analysis, cells were trypsinized, spun down and 1 million cells were resuspended in 1 mL RPMI medium with 2% FCS and 10 mM Hepes Buffer. 5ug/mL Hoechst 33342 dye was added and the cell suspension was placed in a 37 degrees water bath for 2 hrs. For blocking the cells from effluxing the dye the transporters can be deactivated using the drug verapamil (Sigma Cat No:V4629). 10 ug/mL of verapamil was added to the cell suspension during the 2 hr, 37 degrees incubation.

For the time profile analysis the cell suspension was incubated for 0.5, 1, 1.5, 2, 2.5 and 3hrs. The cell suspension was agitated to prevent the cells from settling down and to enable uniform dye distribution. After 2 hrs the cells were spun down in a centrifuge pre-cooled to 4 degrees. The cell pellet was resuspended in a chilled HBSS buffer with 2% FCS and 10 uM Hepes Buffer at a concentration of 3 million cells/mL. The temperature has to be maintained below 4 degrees at all times to prevent further dye leakage from the cells.

A BD fluorescence activated cell sorter (FACS) FACSAria was used to analyse for side population and sort for cancer initiating cells. A UV laser was used to excite the cells and emission at 450/20nm (blue) and 675 nm (red) were recorded. When the cells retain the dye in the cell interior a blue fluorescence can be detected. As time progresses the dye enters the nucleus where they bind to the DNA and produce red fluorescence. The side population or cancer initiating cells those are capable of pumping the Hoechst 33342 dye show up low on both blue and red fluorescence. Both the CIC and non CIC were collected in culture medium with antibiotics and antimycotic drugs added. For analysis data points from 100,000 cells were collected.

After sorting, 20,000 cells were plated in 24-well plate and monitored for contamination. After ensuring proper cell proliferation, light images were acquired using Olympus IX51 light microscope one week after sorting. The cells were cultured and maintained over five passages and cell numbers were counted. The experiment was performed twice in triplicates.

3.2.2 Flow cytometric Analysis for Chemotherapy drug efflux

To study the side population profile for short term drug treatment, the cells were incubated with Hoechst 33342 and 200 ng/mL doxorubicin or mitoxantrone for the first 1 hr of the 37 degrees incubation. The cells were spun down in a 37 degrees centrifuge and resuspended in RPMI medium containing the Hoechst dye alone and incubated for another hour. To study the side population profile for long term drug treated cells, MX-1 were cultured with 50 ng/mL doxorubicin or mitoxantrone for 7 days and then stained with Hoechst 33342 and analysed by flow cytometry. Doxorubicin can be excited at 488 nm and emitted fluorescence was detected at

565/50 nm. Mitoxantrone can be excited at 633 nm and emitted fluorescence detected at 670/40 nm.

3.2.3 Colony Formation Assay and imaging of drug treated cells

1000 CIC and non CIC were plated on 48 well plates and 50 ng/mL doxorubicin or Mitoxantrone was added to the culture medium. The cells were treated with the drugs for 7 days. The cells were cultured in medium alone for another 7 days before the colonies were counted. A colony was considered to at least have 10 cells.

After sorting CIC and non CIC, 10,000 cells were cultured in 8 well Labtek Chambers (Nunc, Cat No. 155411) for 3 days. 200 ng/mL doxorubicin or Mitoxantrone was added to the culture medium and incubated at 37 degrees for two hours. The cells were then washed with 1X PBS and fixed using 3.6% Paraformaldehyde and imaged using a Laser scanning confocal microscope. Doxorubicin was excited using a 488nm Argon laser and the emitted fluorescence detected using a 565-615 band pass filter.

3.2.4 Migration and Invasion Assay

50,000 isolated CIC and non-CIC cells were seeded on cell culture inserts (Cat No. 353097, Falcon, BD Biosciences, San Jose, CA) for migration assay and on cell culture inserts coated with Matrigel (Cat No.354277, BD Biosciences, San Jose, CA) for invasion assay. Cells were cultured with 1% Fetal Calf serum (FCS) containing media on the upper well and 20% FCS containing media in the lower well acted as the chemo-attractant. Cells were cultured in humidified 37ºC, 5% CO_2 incubator for 24 hrs. After which the cells or cells and Matrigel was removed using cotton swabs and the lower surface of the cell culture inserts was stained using crystal violet and the

number of migrated or invaded cells were counted using a light microscope (IX 51, Olympus Corporation, Japan) using a 20X objective. Cells in three fields of view per insert were counted and the average per insert was calculated. For each migration and invasion condition three replicates were performed.

3.2.5 CD44 and CD24 expression analysis of CIC and non-CIC

For CD44 and CD24 expression analysis, anti-human CD44 and CD24 antibodies tagged with PE (BD, Pharmingen Cat No: 550989, 555426) was added to the chilled cell suspension after Hoechst staining and allowed to stain for 15 mins. The cells were washed in 1X Phosphate buffered saline (PBS) thrice and resuspended in HBSS buffer. The cells were analyzed in a FACS machine (FACS Aria, BD). The cells were excited by UV (305 nm) as well as Argon (488 nm) lasers and the emission is collected using 450±50 nm and 585±20 nm band pass filters for the Hoechst and PE fluorescence respectively. 100,000 data points are collected and the percentage of CIC and non-CIC cells positive for CD44 or CD24 are analyzed using BD FACS Diva software.

3.2.6 Developing CIC animal models and in vivo imaging

Isolated CIC and non CIC were cultured for 2 days to allow them to recover from the stress of sorting before administration to animals. On the day of injection, 100,000 CIC and 1 million non CIC were trypsinised, counted, spun down and resuspended in 200 uL of chilled 1X PBS. The cell suspension was injected subcutaneously in the right flank of SCID mice. Sorting, cell culture and injection was done for consecutive four weeks to have four CIC and four non CIC SCID mouse model. Animals were anesthetised and shaved to image using the in vivo live imaging system (OV100,

Olympus Corporation). Images were taken once at 4 weeks after injection and then 8 weeks after injection.

3.2.7 Histology

Haematoxylin and Eosin (H&E) staining was carried out using standard protocol. Briefly tissue sections were fixed in ethanol and stained in Ham's Haematoxylin for two minutes, washed thoroughly, checked for good staining and stained in Eosin for a few seconds. The stained sections are dehydrated in ethanol and Xylene and mounted in Depex mounting medium.

3.3. Results

3.3.1 CIC can be isolated from the invasive breast cancer cell line MX-1

The side population analysis technique was established by Dr.Goodell's lab to study the stem cell populations in the hematopoietic system [114]. Stem cells possess the property to efflux administered dyes through molecular pumps and hence will appear to have low fluorescence when analysed in flow cytometry. Hoechst 33342 is a nuclear dye which emits blue fluorescence (Hoechst blue) as long as it is in the cytoplasm and red fluorescence (Hoechst red) when the dye binds to the DNA. Thus the stem cells will be low in both blue and red fluorescence and emerge as a tail like population in the lower quadrant of a flow cytometric experiment. The cells which lie along the x axis are the debris and dead cells. To ensure that the technique is suitable for isolating CIC from the MX-1 cell line, we tried out a time series of incubation of the cells with Hoechst 33342 (Fig 9a). After 0.5 hr and 1hr of staining, majority of the cells have taken up the dye but are still low in Hoechst blue fluorescence. After 1.5 hrs and 2hrs of staining the tail percentage drops to about 0.28%. This could be due to the beginning of effluxing action where the side population cells are getting stained and they are trying to pump the dye out, while the majority of the cells are unable to efflux the dye. At the 2.5 hr and 3hr time point the nucleus have been stained which can be seen by their elevated position along both x and y axis. The percentage of cells with low blue and red fluorescence has dropped to about 0.13%. These cells will be collected as the side population. The 2.5 hr long incubation was used for all experiments. The CIC percentage varied between 0.1% and 0.3% in our experiments. The 3 hr incubation period was not used as the number of dead cells increased (data not shown).

The CIC have been attributed to efflux the dye due to the enhanced function of drug efflux pumps such as the Multiple Drug Resistance (MDR) proteins, P-glycoprotein and ATP binding cassette (ABC) family transporters such as ABCG2 and ABCC1. These pumps can be ubiquitously blocked using drugs such as verapamil, cyclosporin and Fumitremorgin C. We used verapamil to block the drug transporters to ensure that the CIC population are low in dye concentration due to the effluxing functions of these pumps. On adding verapamil, the CIC population was almost abolished (less 15 folds), demonstrating that the cells are effluxing the dye through the transporters (Fig 9b, 9c).

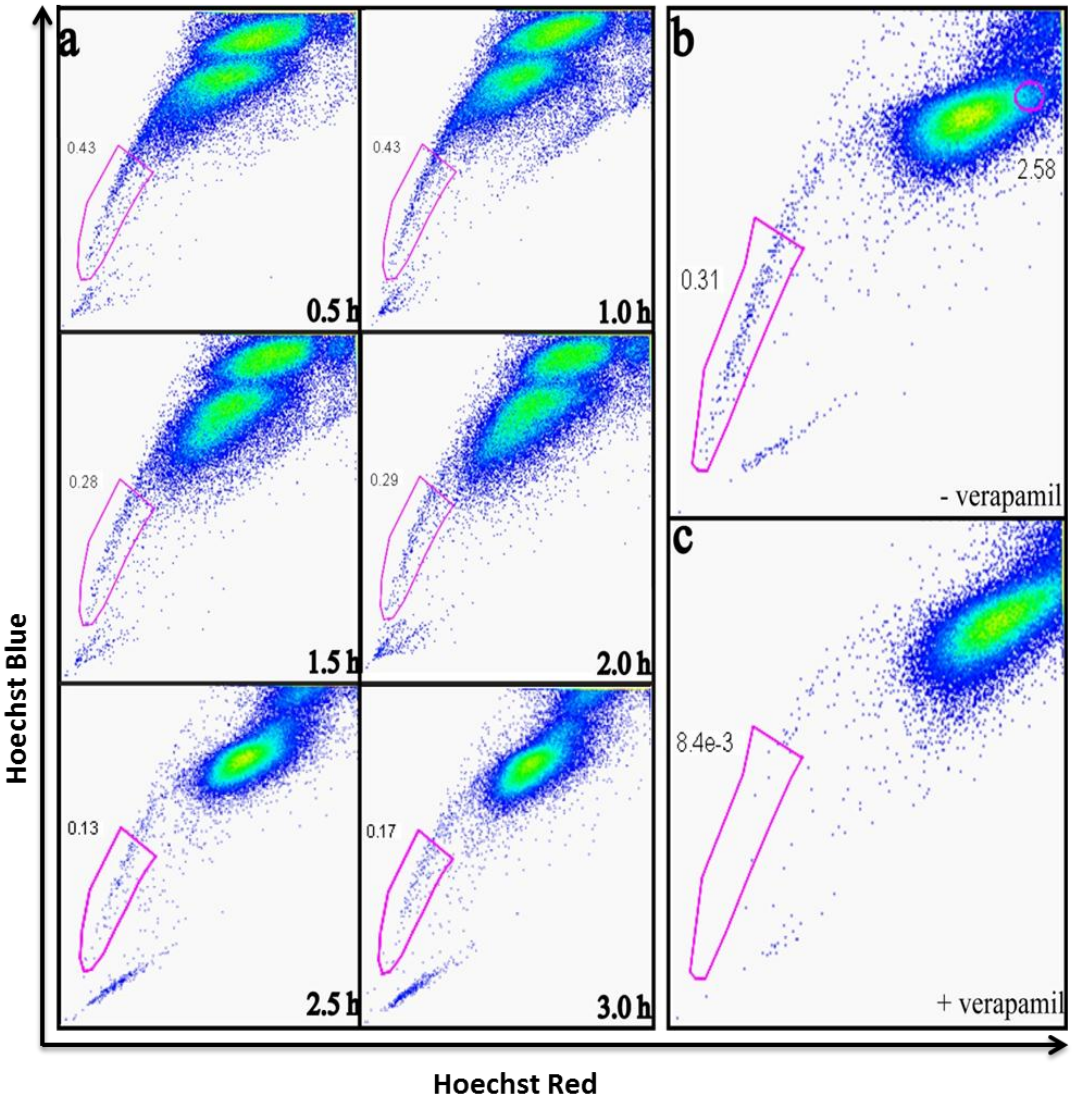

Figure 9: Cancer Initiating Cells can be isolated from MX-1 using side Population method
MX-1 cells stained with Hoechst 33342 were analyzed for the stain levels every half hour from 0.5 hr to 3hr time point. The cells equilibrated at 2.5hr time point where the majority G0-G1-S population was saturated with the dye. The 2.5 hr incubation was used for all cancer initiating cells isolation (a). Verampil a channel blocker is used to block the pumps on the cell surface preventing the cells from effluxing the dye, confirming that CIC is a population with dye effluxing properties (b, c).

3.3.2 CIC shows less differentiated morphology, better proliferative capacity and higher CD44 expression

As the Hoechst dye is toxic in high concentrations the cells do not proliferate as fast as pre-sorting. The plated cells take about a week to form colonies in the case of CIC (Fig 10a). The non CIC cells also proliferate but they do not have clone like appearance (Fig 10b). The less differentiated cells or precursor cells when seeded as single cells can repeatedly proliferate to form tight colonies while the more differentiated cells do proliferate but have a flat and spread out morphology. This could also indicate that the CIC are less attached to the substratum while the non CIC is well attached to the substratum.

To examine the proliferation capacity of these cells we tracked the cell count over several passages with an initial seeding count of 20,000 cells. The CIC were able to proliferate at a higher rate to yield 33 million cells in five passages, while the non CIC was able to yield 11.5 million cells (Fig 10c). The difference in proliferation in the first passage was more drastic where the CIC proliferated to produce 2 million cells compared to the 320,000 cells of non CIC.

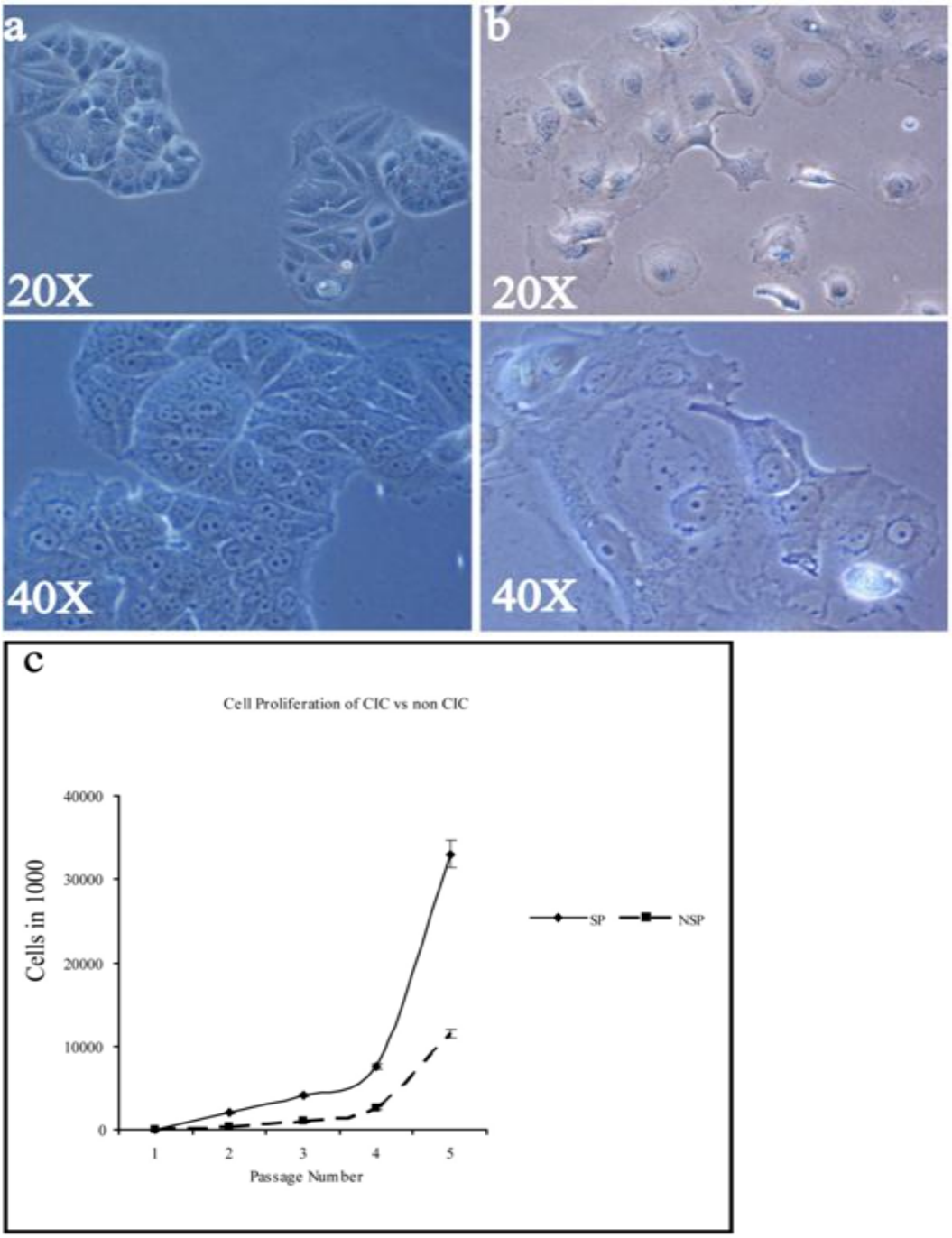

Figure 10: CIC morphology and their proliferation properties

Light micrographs of CIC and non CIC in culture, 7 days after isolation show that CIC forms colonies with more 3D appearance (a) while the non CIC are more spread out and well attached to the substratum (b). The top two panels show images taken with a 20X objective and the bottom two are magnified images with a 40X objective. CIC population generates both CIC and non CIC as it proliferates. The proliferation rate of this population is higher than that of non-CIC alone (c). Scale bars 20µm in (a) and (b)

3.3.3 CIC survives better under chemotherapeutic treatment regimens of doxorubicin and mitoxantrone due to their superior drug effluxing capability

We demonstrate the improved drug resistance of CIC using a short term 2 hr and long term 7 days drug exposure followed by staining and analysing for CIC. Due to the short term drug exposure the percentage of CIC does not change significantly while the non CIC population seems disrupted in the case of doxorubicin and mitoxantrone (Fig 11a, 12a). After 7 days of drug exposure, the non CIC population is virtually eliminated in case of doxorubicin and reduced considerably in the mitoxantrone treatment. The CIC population now constitutes about 26% of the sorted cells (Fig 11b, 12b). This increase may be due to the proliferation of CIC in culture or due to the sensitization of the drug transporters enabling them to efficiently pump out more dye.

As both the drugs emit fluorescence, the drug concentration in CIC and non CIC populations were recorded using appropriate filters. The CIC cells had lower mitoxantrone concentration than the non CIC cells (Fig 12d). We were unable to visualise any changes in doxorubicin concentration in the flow cytometry experiment.

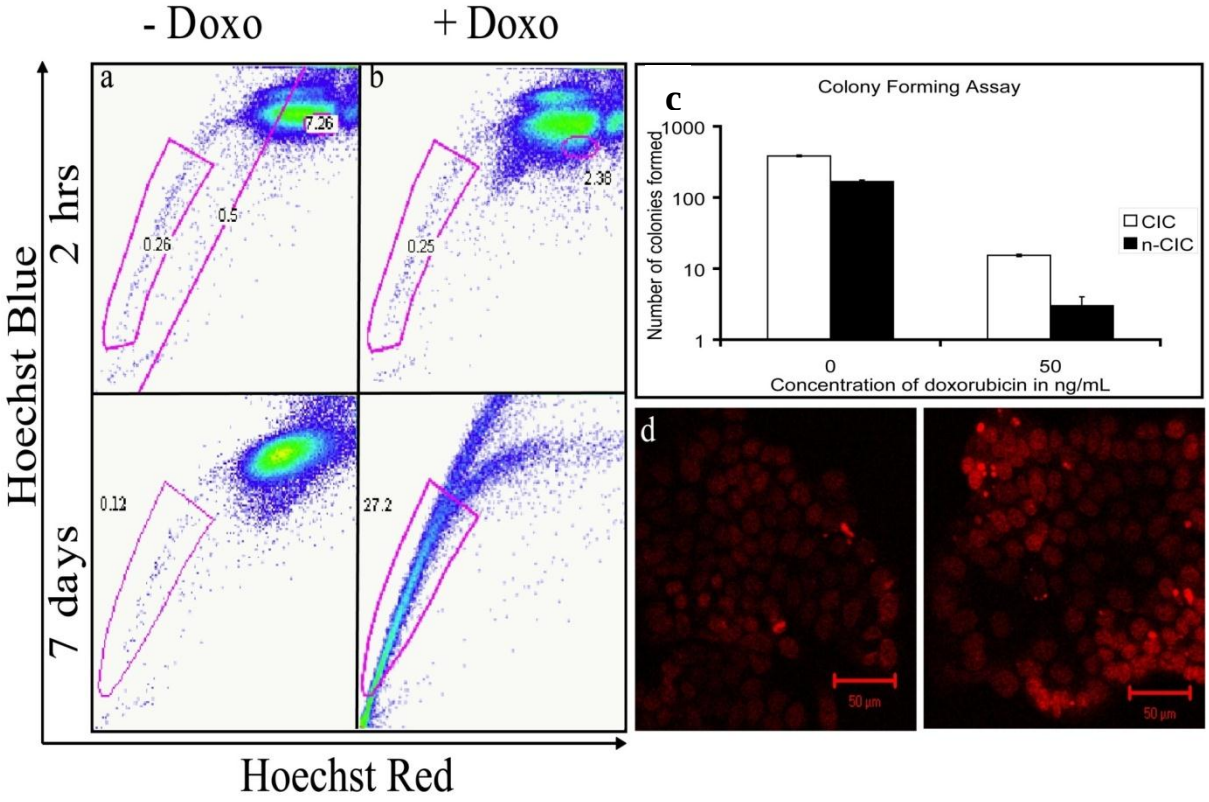

Figure 11: CIC is more resistant to Doxorubicin treatment

MX-1 cells were treated with doxorubicin either for 2 hrs or 7 days and stained with Hoechst and analyzed to observe the changes in the CIC and non CIC population.(a) The top two panels show that after short term treatment the CIC percentage remains constant while the non-CIC population is disrupted (a). The bottom two panels show that after long term treatment the non-CIC population is almost abolished (b). Colony formation assay was performed with sorted CIC and non CIC to observe that CIC forms four time more colonies than non-CIC in the presence of 50 ng/mL doxorubicin (c). Fluorescence confocal microscope images of CIC (left) and non-CIC (right) cells after two hours treatment with doxorubicin show that non-CIC distinctly accumulates the drugs (d). Scale bar 50µm in (c).

3.3.4 Isolated CIC forms more colonies in the presence of the drugs doxorubicin and mitoxantrone and show lower drug accumulation in fluorescence imaging

The sorted CIC when cultured in the presence of doxorubicin or mitoxantrone are able to form more colonies (Fig 11c, 12c). In the absence of drugs, CIC are able to form about 395 colonies for every 1000 cells seeded while non CIC forms 177 colonies. In the presence of 50 ng/mL doxorubicin the number of CIC colonies drops to 16 while the non CIC can form 3 colonies and in 50 ng/mL of mitoxantrone the CIC forms 18 colonies while the non CIC forms 3 colonies. 4% and 4.5% of the CIC colonies survive the doxorubicin and mitoxantrone treatment, while 1% of the non-CIC survives the treatments. In this experiment, colonies with at least three or more surviving cells were counted as surviving colonies. The single cells that were in the tissue culture plate were not counted. The colonies formed by CIC by dividing are not all CIC. Thus the number of surviving CIC could have been underestimated.

We observed the drug accumulation in CIC and non CIC colonies after two hours of doxorubicin treatment (Fig 11d) and mitoxantrone treatment (data not shown). Distinct spots of drug accumulation were observed in non CIC, compared to the background amount of doxorubicin in CIC.

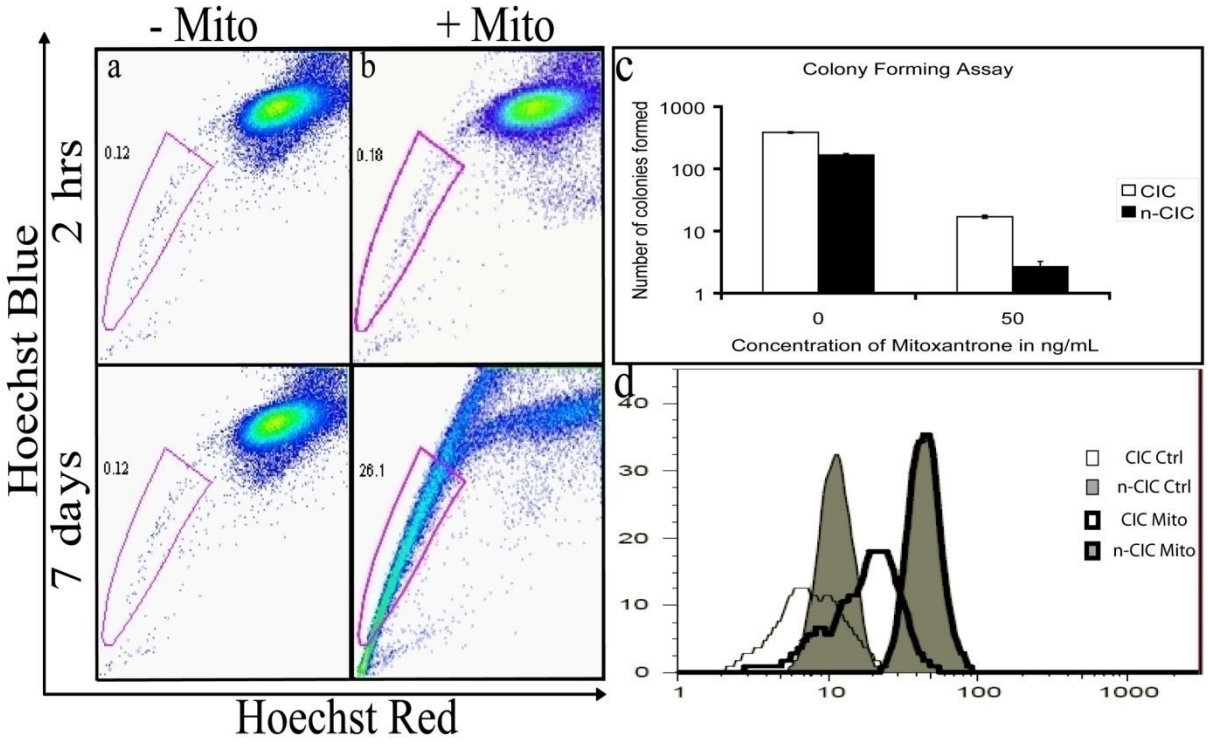

Figure 12: CIC is more resistant to Mitoxantrone treatment

MX-1 cells were treated with mitoxantrone (+Mito) either for 2 hrs or 7 days and stained with Hoechst and analyzed to observe the changes in the CIC and non CIC population compared to the untreated samples (-Mito) .(a) The top two panels show that after short term treatment the CIC percentage remains constant while the non-CIC population is disrupted (a). The bottom two panels show that after long term treatment the non-CIC population is almost abolished (b). Colony formation assay was performed with sorted CIC and non CIC allowed to reach about colonies of 10 cells and then treated with 50 ng/ml of mitoxantrone to observe the number of CIC colonies surviving compared to the non-CIC colonies. Six times more CIC colonies can survive in the presence of 50 ng/mL mitoxantrone than non-CIC colonies (c). MX-1 cells were incubated with Hoechst stain along with mitoxantrone and the fluorescence data at 633nm of mitoxantrone was collected from the CIC and non-CIC population during flow analysis to conclude that non-CIC (33.76±0.5AU) had higher fluorescence compared to CIC (10.9175±0.78 AU) (d).

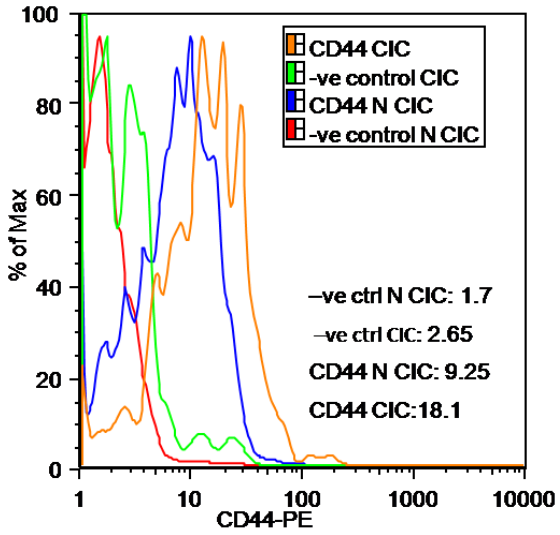

Figure 13: CD44 expression in CIC and non-CIC.
CD44 expression assessed on CIC and non-CIC revealed that CIC expresses two folds higher level of CD44 than non-CIC and both CIC and non-CIC had ten folds higher expression of CD44 than the negative control.

3.3.5 CIC have higher expression of CD44 and is more invasive and migratory compared to non-CIC

When the CD44 expression level of CIC and non-CIC was compared, it was found that CIC expressed two folds higher CD44 compared to non-CIC (Fig 13). The CD44 high phenotype of CIC isolated using side population method correlates with CIC isolated using marker expression.

In in-vitro assays, using transwell chambers, the CIC is found to be more migratory and more invasive than non-CIC. CIC had at least two fold higher migration potential across the membrane towards a chemoattractant. The number of CIC invading across an ECM matrix towards a chemoattractant was also found to be significantly higher than non-CIC cells (Fig 14a).

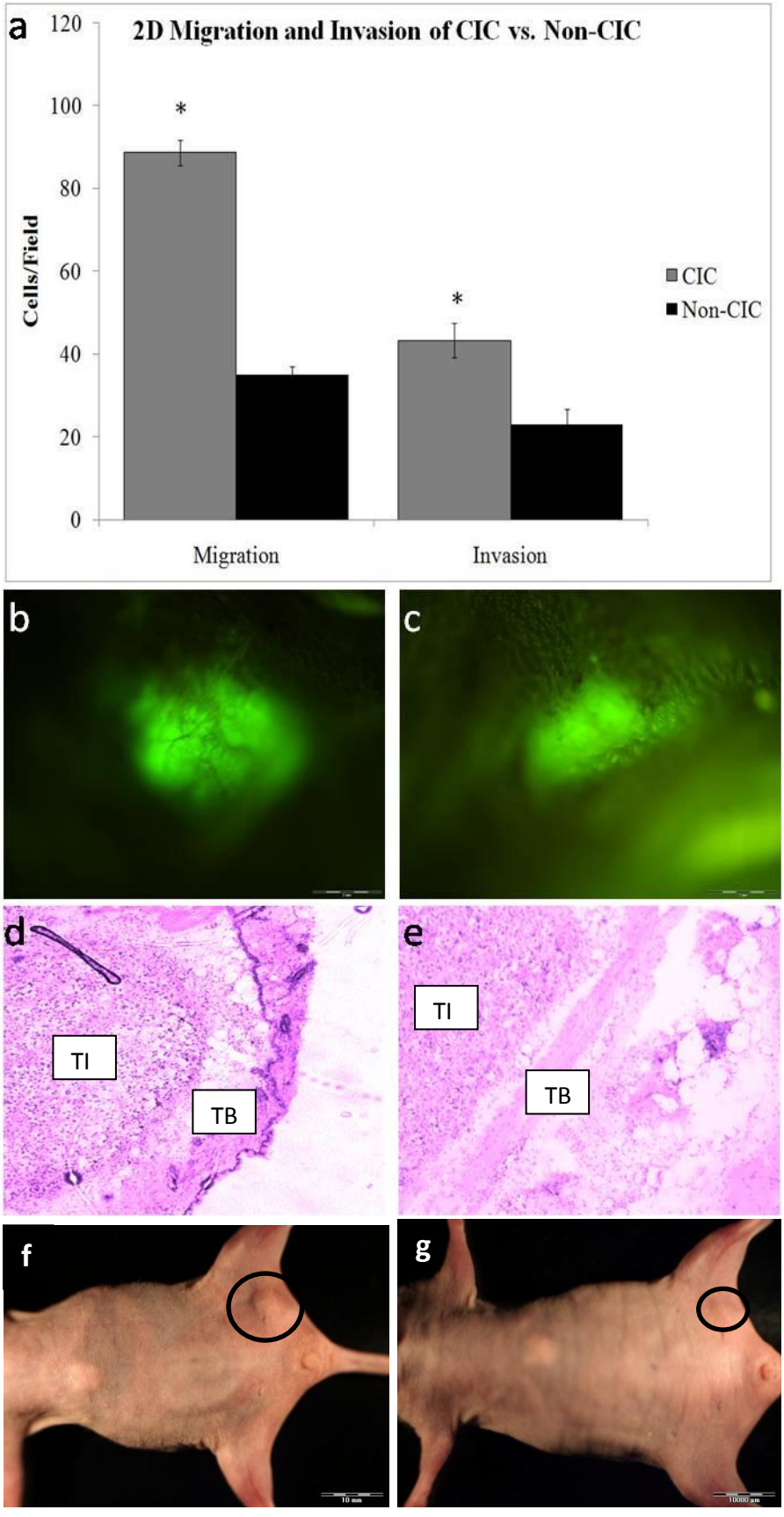
a
2D Migration and Invasion of CIC vs. Non-CIC
Cells/Field
120
100
80
60
40
20
0
*
*
CIC
Non-CIC
Migration
Invasion
b
c
d
TI
TB
e
TI
TB
f
g

Figure 14: CIC is more invasive and migratory *in vitro* and more tumorigenic *in vivo* than non-CIC

(a)Boyden chamber assay comparing the migratory and invasive potential of CIC and non-CIC showed that CIC was at least two folds more migratory and invasive than non-CIC (*: t test: $p<0.05$). The grey bars depict CIC while the black bars depict non-CIC. Whole animal imaging system was used to image the GFP labelled tumours in-vivo. After 8 weeks, visible tumours were observed in all the CIC injected animals of which one is shown here (b), and only one non-CIC injected animal (c). The CIC tumors were bigger than the non-CIC tumor. Blood vessels were visualised in the CIC tumor but not in the non-CIC tumor. The H&E images of CIC (d) and non-CIC (e) shown are acquired using a light microscope with a 10X objective. The tumor interior (TI) and tumor boundary (TB) are shown for both the CIC and non-CIC tumor. The bright light CIC (f) and non-CIC (g) tumor images are also shown. Scale bar 1mm in (b) and (c) and 50µm in (d) and (e), 10 mm in (f) and (g)

3.3.6 CIC is more tumorigenic in SCID mice models than non CIC

Tumorigenicity in animal models in small numbers has been considered hallmark of cancer initiating cells. In in-vivo experiments where 100,000 CIC and 10 million non-CIC were injected into animals, tumor growth was observed using a whole animal imaging system (OV100, Olympus Corporation, Japan). Despite injecting hundred folds more non-CIC than CIC, all five animals injected with CIC formed tumors while only one animal with non CIC formed a tumor in 8 weeks time. The representative fluorescence images of the CIC and non-CIC tumors are shown in Fig 14b and 14c. The fluorescence intensity and area has been quantified and it was found to be at least three times higher in CIC compared to non-CIC. H&E stains are shown in Fig 14d and 14e. The H&E stains showed well-developed tumor encapsulated by surrounding tissue in all five CIC tumors and one non-CIC tumor. Histological examination of the other four non-CIC tissues showed no tumor cell implantation.

3.4. Discussion

The side population analysis technique was established in Dr.Goodell's lab to study the stem cell populations in the hematopoietic system [114]. The CIC have been attributed to efflux the dye due to the enhanced function of drug efflux pumps such as the Multiple Drug Resistance (MDR) proteins, P-glycoprotein and ATP binding cassette (ABC) family transporters such as ABCG2 and ABCC1. These pumps can be ubiquitously blocked using drugs such as verapamil, cyclosporin and Fumitremorgin C. The mammosphere culture technique, in which the CIC's property to be able to sustain in suspension culture and overcome anoikis, has also been used to isolate CIC [17]. Certain markers for stemness and surface markers such as CD44, CD133 have also been used to isolate CIC [11]. In our study we have been able to isolate CIC from MX-1 cell line successfully using the side population technique and the drug verapamil abolished the population proving the role of the molecular pumps in side population. We also tried the suspension culture but were unable to create a mammosphere culture. Along with performing the side population analysis we also immunostained the cells for CD44 and found that the CIC was $CD44^{high}$.

We explored the difference in proliferation of the CIC and non-CIC after sorting. The difference in proliferation in the first passage was more drastic where the CIC proliferated to produce 2 million cells compared to the 320,000 cells of non CIC. This difference cannot be only attributed to the Hoechst retention by the non CIC as the drugs are cleared by the cells in 2 to 3 days and we do not observe proliferation of either CIC or non CIC 2-3 days post sorting. We believe that this higher proliferation of CIC is not because they generate more CIC, instead they divide to generate non CIC, because on reanalysis of the proliferated cells, they recapitulate the entire population consisting of both CIC and non-CIC cells. The ability of CIC cells to

proliferate to generate the entire population has also been demonstrated as the hallmark of CIC [15]. The non CIC cohort alone might not be able to sustain themselves in the absence of CIC and hence unable to proliferate as fast as the CIC cohort. The CIC are shown to proliferate more and form small tight colonies in ovarian cancers as well [63] while in nasopharangeal cancer the CIC lost its characteristic as differentiated squamous epithelial cell and appeared more like fibroblasts [115].

Drug resistance is one of the hallmarks of cancer relapse where a few cancer cells can evade the treatment and go on to establish tumors at the primary site or metastasize to other organs. CIC have shown that these cells are more radiation resistant and chemo-resistant than the bulk of the cells [116-118]. We used two commonly used chemotherapeutic drugs doxorubicin and mitoxantrone to determine the drug resistance profiles of CIC. Doxorubicin is an anthracycline antibiotic, DNA intercalating agent used for the treatment of leukaemia, lymphomas, several epithelial cancers, sarcomas and myelomas. Mitoxantrone is an anthracenedione, topoisomerase II inhibitor which prevents DNA synthesis and repair. It is used in the treatment of metastatic breast cancers, non Hodgkin's lymphoma and acute myeloid leukaemia (AML). There have been some studies to test the resistance of the CIC to chemotherapeutic agents such as paclitaxel, doxorubicin and mitoxantrone [63]. There is a marked inhibition of non-CIC cells by these chemotherapeutic agents compared to CIC. We studied both the short term and long term chemoresistance of these cells to doxorubicin and mitoxantrone. Within 24 hours the changes in CIC is not visible but the non-CIC population seems disrupted. In the long term study, there is a marked increase of CIC cells being able to survive 7 days of chemotherapy. This increase of CIC may be due to the proliferation of CIC in culture even in the presence of

doxorubicin or mitoxantrone, or due to the sensitization of the drug transporters enabling them to efficiently pump out more drugs. It is thus shown that these broad spectrum chemotherapeutic agents are unable to interfere with the DNA in the CIC population and prevent its proliferation. There has been an effort to show that recombinant erythropoietin and oncolytic adenoviruses can be used as an approach to target CIC [119-120]. Certain pathways including that of NF-Kappa-B [Liu]. Wnt [Lindvall] , Notch [Farnie] are being implicated in CIC progression. These pathways are involved in normal stem cell development as well. The challenge is to be able to identify unique features or pathways in CIC to target them to eradicate these cells [Zhou J 2008].

Tumorigenicity in animal models in small numbers has been considered hallmark of cancer initiating cells. This has been shown in several studies [Ponti, Hirschmann, szotek, chiba]. When we injected 100,000 CIC cells and 10 million non-CIC cells into the animals, all CIC injected animals developed tumors, but only one non-CIC injected animal formed a tumor. In an ovarian cancer study they demonstrated that the non-CIC population was able to form a tumor only because there was a contamination of the non-CIC with some CIC cells [63]. In our study we did not isolate live tumor tissue to perform this experiment. In our experimental set up we tried to inject fewer CIC cells such as 1000 cells and 10,000 cells into the animal. We were unable to visualize any pellet of cells after centrifugation of the sorted cells. Thus to ensure that the sorted cells were spun down properly to be in the 200 µl injection volume was not possible. Hence we decided to perform the final comparison experiment with 100,000 CIC and 10 million non-CIC. The tumors in the CIC cohort showed well developed structure with blood vessels seen in the whole animal imaging system. The only tumor

in the non-CIC cohort was poorly developed and it was barely visible under the animal's skin.

3.5. Conclusions

We have demonstrated that CIC can be isolated from an invasive breast cancer cell line MX-1. The CIC isolated from MX-1 have a higher proliferative capacity than the non-CIC. The CIC can proliferate and generate both CIC and non-CIC after a few passages. CIC is more resistant to chemotherapy administrations such as doxorubicin and mitoxantrone. They survive both short and long term exposure of the drugs, efflux the drug efficiently and are able to form more colonies in the presence of these drugs in culture. In xenograft models, the CIC established tumors in all five mice administered with 100,00 CIC while only one out of the five mice formed a tumor when injected with 10 million non-CIC. Thus CIC can form tumors with 10 fold less cells compared to non-CIC. Whole animal imaging revealed that tumors formed by CIC were larger and more vascularised compared to the one formed by non-CIC. Thus we have established a CIC isolation and characterization strategy for the breast cancer cell line MX-1 using side population analysis method. The CIC and non-CIC tumors obtained from these xenograft models will be used for studying the CIC-ECM interactions in-vivo using the SHG imaging system. As discussed in section 2.3, current SHG systems are limited by GVD. In chapter IV we describe how we improve the SHG system by reversing GVD. The CIC-ECM interactions will be studied using the improved SHG system in chapter V.

IV Development of SHG microscope with Pulse modulation (PM-SHIM) and validating the PM-SHIM using chemotherapy studies

1. Introduction

Cancer is a disease where a series of mutations accumulate in normal cells, with increased resistance to cell death or apoptosis followed by uncontrolled cell division. The cancer cells need the host-derived cells like the endothelial cells and fibroblasts for vascularization and support to form a tumor [121]. The host cells help the cancer cells by degrading or secreting component of the microenvironment to establish the tumor niche. Collagen is one such component that is an important component of this tumor niche. The cancer cells use the collagen fibers for physical support in the growing stages and the fibers are remodeled as the tumor mass requires expansion and invasion [122-123].

Second Harmonic Generation (SHG) imaging is suitable to visualize non centro symmetric biomolecules such as myosin, collagen type I and IV [124-125]. SHG imaging is especially suitable for tumor pathology studies as there are no staining process involved and thin tissue sections are not required, making sample preparation simple, providing 3D sectioning capability without using confocal pinhole, with deeper penetration depth [126-127] [128]. [129-130]. There has been a series of articles demonstrating collagen imaging in several tissue types and whole organs in in-vitro, animal and human studies [131-135]. SHG imaging of collagen in cancer models have been demonstrated in Melanoma, breast cancer, cervical and ovarian cancer in animal and human studies [31, 136-140]. But almost all of them have not been able to quantitatively visualize collagen patterns in the tumor interior.

The optical components introduce Group Velocity dispersion (GVD) where the longer wavelength light in the pulse travels faster than the shorter wavelength light

[141-142]. SHG depends directly on the peak power delivered to the sample. SHG and TPEF signals generated from the sample are inversely proportional to the pulse duration of the excitation light. Thus GVD increases the pulse duration, reduces the peak power of the incident light on the sample affecting the second harmonic and TPEF signals generated. Pulse modulators can be introduced in the optical path of the microscope to introduce negative chirp that counteracts the positive chirp introduced by dispersive optical components [143]. There are a few articles that show the improvement in SHG after pulse modulation using biological samples such as human skin and mouse kidney [144-145].

We demonstrate that by using pulse modulated second harmonic imaging microscope (PM-SHIM) collagen fibers of all dimensions can be detected and quantified. We validate the functionality of this improved system in muscle tissue, liver tissue and collagen gels, thereby demonstrating the wide array of applications of the PM-SHIM in connective tissue related studies. A key validation of the PM-SHIM is done using the ex-vivo tumor samples from xenograft models after chemotherapy.

There are several studies to demonstrate that collagen acts as a hindrance to drug diffusion both in in vivo [31] and in vitro models [146], and by breaking down the barrier there can be an improvement in drug delivery [147-148]. On the other hand, the tumor stroma has lower collagen content than normal tissue [32]. In that case the drug should be able to reach the tumors better. But in solid tumors chemotherapy can be initially effective and became ineffective later [149-151]. Gene expression studies show that chemotherapy stimulates wound-healing responses in tissues upregulating collagen [152-155]. We hypothesize that quantifying the spatial distribution of collagen inside tumors will yield a highly sensitive means to directly monitor the drug-induced barriers to further efficacy, and become a powerful tool to aid in the

development of drug combinations or regimens that remain efficacious to achieve complete tumor cell elimination. Understanding the process of collagen remodeling inside tumors will require more sophisticated tools for quantification. We have demonstrated that the increased sensitivity of PM-SHIM to quantify collagen in tumor allowed us to directly test the hypothesis that chemotherapy can increase collagen fibers inside tumors to impede further therapeutic efficacy of chemotherapeutic agents.

2. Materials and Methods

2.1 The Imaging System

The light source used is an ultra-fast laser operating at 900 nm with 100 fs pulse duration (Mai Tai Titanium Sapphire Laser, Spectraphysics). The imaging was done using a confocal microscope (LSM 510 Meta, Carl Zeiss GmbH). Source laser passes through the prism based pulse compressor (Femto Control, APE GmbH, Germany) followed by the Acousto Optic Modulator (AOM) and is then focused on the sample with a 20x objective lens, numerical aperture (NA) =0.5. The SHG signal was measured at the other side of the sample, filtered through a 450 nm band pass (BP) filter (full-width half-maximum = 10nm) before reaching the photomultiplier tube (PMT) (R6357, Hamamatsu Photonics). The schematic of the microscope set up is shown in Fig 1a.

A chirp analyzer (GRating-Eliminated No-nonsense Observation of Ultrafast Incident Laser Light E-fields, Swamp Optics) was used for measuring the dispersion profile of the laser resulted from pulse compression. The Frequency Resolved Optical Gating (FROG) based chirp analyzer measures the spectrum of the laser pulse by using a Fresnel Biprism and a thick SHG crystal {Akturk, 2004 #101}. The beam profile was measured at three locations: A) before the AOM, B) after the AOM, and C) at the sample stage (see Fig 15a). In positions A and B, measurements were made by direct interception and feeding the laser to chirp analyzer. In position C, a mirror was placed on the microscope stage and a beam splitter was used such that the measurement was taken after laser enters and leaves the microscope under identical paths (see Fig 15b). For all positions, pulse duration was optimized by systematically adjusting the prism 1 and prism 2 positions inside the pulse compressor. The prism

positions were controlled using a stepper motor whose angular positions can be varied using a remote control.

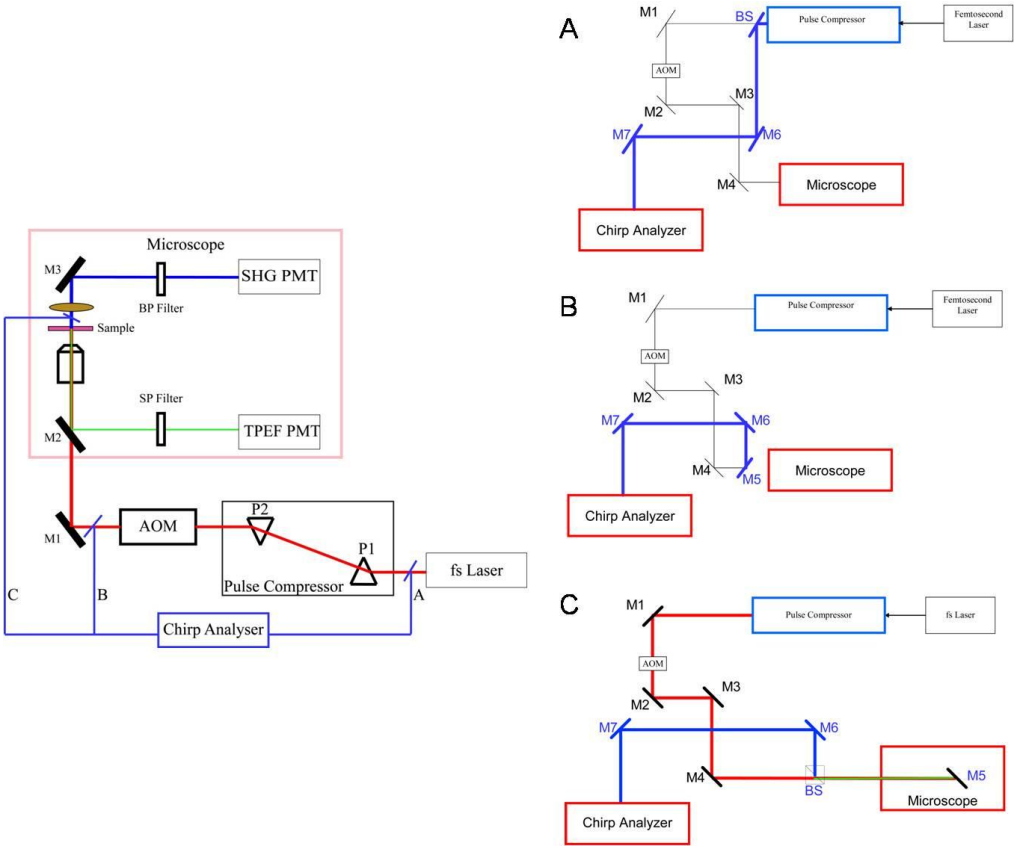

Figure 14: Schematic of the PM-SHIM set up.

The set up of the PM-SHIM is shown in the left and the alignment configurations for chirp analysis is shown in the right. The PM-SHIM consists of a femtosecond (fs) laser followed by the pulse compressor, AOM and the confocal microscope set up. The AOM is used to modulate the power delivered to the sample using a diffraction grating. The laser beam reaches the sample and the SHG and TPEF signals from the samples pass through a band pass (BP) and short pass (SP) filter in the transmission and reflection mode respectively and the signals are collected using a photomultiplier tube (PMT). A, B and C are three positions at which the laser beam is characterized using the Chirp analyzer. The laser beam from the femtosecond laser, before the AOM (A), after the AOM (B) and at the sample stage (C) are guided to the chirp analyzer using mirrors (M1 –M6) and a beam splitter. The beam splitter (BS) is used to reduce the laser power by 50% in A and to split the beams orthogonally in C and then guide using mirrors to the chirp analyzer.

2.2 Xenograft Model, Tissue Isolation and Collagen hydrogel preparation

Cell Culture: MV4-11 cells were cultured with RPMI1640 (Invitrogen, Carlsbad, CA, USA) supplemented with the addition of 10% fetal bovine serum (FBS; JRH Bioscience Inc., Lenexa, KS, USA) at a density of 2–10 × 10^5 cells ml^{-1} in a humid incubator with 5% CO_2 at 37 ºC.

Animals: Female severe combined immunodeficiency mice (17–20 g, 4–6 weeks old) were purchased from Animal Resources Centre (Canning Vale, WA, Australia). Exponentially growing MV4-11 cells (5×10^6) were subcutaneously injected into loose skin between the shoulder blades and left front leg of recipient mice. All treatment was started 25 days after the cell injection; when the mice had palpable tumor of 300–400mm^3 average size, ABT-869 was administrated at 15mg $kg^{-1}day^{-1}$ by oral gavage daily. ABT-869 was provided by Abbott Laboratories (Chicago, IL, USA). For in vivo experiments, ABT-869 was prepared as published previously [156]. The protocol was reviewed and approved by Institutional Animal Care and Use Committee in compliance with the guidelines on the care and use of animals for scientific purpose (IACUC Protocol No.050118).After completion of treatment, animals were anesthetized using 90mg Ketamine and 9 mg Xylazine mixture. The skin flap was opened; chest cavity was exposed to perform a cardiac perfusion of saline to flush out blood and then 4% Paraformaldehyde (PFA) to fix the tissues. The tumors were isolated and frozen immediately in liquid nitrogen. Liver and muscle tissues were also isolated from other animals. Tissues are sectioned at 40μm, 20μm and 10μm for imaging.

Collagen hydrogel was prepared by mixing 0.49ml rat tail type I collagen (BD Biosciences, San Jose, CA), 100µl Phosphate buffered saline (PBS) and 0.41 ml 0.025 M Sodium hydroxide to obtain a 4 $mgml^{-1}$, pH 7.4 neutralized collagen solution. 100µl of the solution was pipetted onto 0.17mm thick coverslip and dried at room temperature for 48hrs before imaging.

2.3 Image Acquisition and Signal to Noise Ratio Analysis

Conventional SHG images were taken without pulse compression, in which laser by-passes the pulse compressor prisms and routed directly to the microscope. PM-SHIM images were taken when the pulse duration was minimized with optimized pulse compression. All samples, including muscle, liver, and collagen hydrogels were imaged with both conventional SHIM and PM-SHIM. In all cases, we recorded a background image using plain glasses as dark background levels for signal processing. We used the 20X objective to obtain 460 µm x 460 µm, 512x512 pixels images. Nine such images were stitched to obtain the tile scan image of 1382 µm x 1382 µm, 1536x1536 pixels images. The tile scan images were used for analysis purposes. Signal to background ratio (SBR) was defined as the average pixel intensity value of SHG signal to the background intensity acquired earlier from the plain glass. SBR of conventional SHIM and PM-SHIM was compared directly by dividing one SBR with the other.

2.4 Image acquisition and quantification of collagen remodeling in tumor samples

PM-SHIM and conventional SHIM images of the tumor sample were acquired as per previous settings. An image segmentation algorithm based on mixture Gaussian model was performed to remove background and noise. It is assumed that the

intensity of pixels in the image can be modeled as the mixture of two Gaussian distributions, one representing collagen area with strong SHG signals and the other representing the background. Using the Expectation-Maximization (EM) algorithm {Dempster, 1977 #229}, the parameters of the Gaussian distributions which model the intensity of pixels in the image best could be found. A binary image was generated by applying value 1 to all the pixels having intensity which belongs to the Gaussian distribution representing collagen area and value 0 to the rest of the pixels.

We quantified four parameters namely collagen area percentage, fiber number, fiber length and fiber width. The percentage of collagen area was determined as the number of pixels which are segmented as collagen divided by total number of pixels in the same image. The connected component labeling algorithm {Gonzales, #338} was performed on the binary image which groups the connected pixels with value 1 into one object, while each object represents a collagen fiber or fiber bundle. The fiber number was determined as the number of objects in each image. The fiber length was calculated as the average length of the long axis of each object in the image, and the fiber width was quantified as the average length of the short axis of each object in the image. All image processing and algorithm execution were carried out using MATLAB (The Math Works, Inc, Natick). Image processing algorithm code is available for readers upon request.

3. Results and Discussion

Here we systematically optimized the PM-SHIM by using a chirp analyzer to characterize both the spatial and temporal profiles in order to determine the optimal pulse compression. With the optimized PM-SHIM, we observed a significant improvement in SBR, as high as 3.2 times, in many biological samples. In addition, we were able to visualize and differentiate the collagen fibers in treated and control tumor samples. We have observed that collagen quantity has increased significantly in the treated group comparing to the control group and found a distinct difference in morphological features from both groups. These findings are being reported for the first time, to the extent of our knowledge, because of the superior excitation and detection sensitivity in PM-SHIM that we have developed over conventional SHIM.

3.1 Pulse Compressor Optimization

In figure 16, the optimization of prism positions in the pulse compressor to obtain the best pulse modulation is shown. The left column shows the pulse duration plots and the right column shows the pulse spectral width plots at various prism positions. The "Before AOM P1 out", "After AOM P1 out" are the plots when prism 1 is pulled out of the beam path bypassing the pulse compressor. The "Before AOM P2", "After AOM P2" and "At sample stage P2" are the plots at various positions of prism 2 at an optimized prism 1 position. The optimized prism 1 position was found to be 1100 and the optimized prism 2 position was 2100. The prism positions are controlled by rotary motors. 1100 and 2100 indicate the motor control positions.

3.2 Group Velocity Dispersion analysis

The spectral and temporal profiles of the beam measured at 3 different locations are shown in Fig. 16, in which beam profile in the PM-SHIM and the conventional SHIM are shown in dotted and solid lines respectively. Amongst the three positions where measurements were taken, the most significant improvement is seen at location B, after AOM, where the pulse spectral width reduced from 14 nm to 13.18 nm in the PM-SHIM and the pulse duration improved from 215 fs (conventional SHIM) to 96 fs (PM-SHIM). From Fig 17 we can also see that dispersion introduced by the optical components affects mostly the pulse duration instead of the pulse spectral width. GVD affects the velocity of different frequencies and not the wavelength of the light. Also, we can see that the most dispersive component in the beam path is the AOM, and it has increased the pulse duration to 215 fs. By applying the pulse compression in the PM-SHIM system, the pulse spectral width can be reduced to 96 fs.

The pulse duration measurement at the sample stage was taken from the reflection of the signal from the sample stage. The components in the microscope path could have introduced asymmetry to the pulse shape at the sample stage. In effect the light is travelling through the microscope components twice and the pulse duration measured at the end point was 115 fs. Thus the pulse duration of the beam reaching the sample is estimated to be lesser than 115 fs and more than 96 fs (pulse duration measured before entering the microscope).

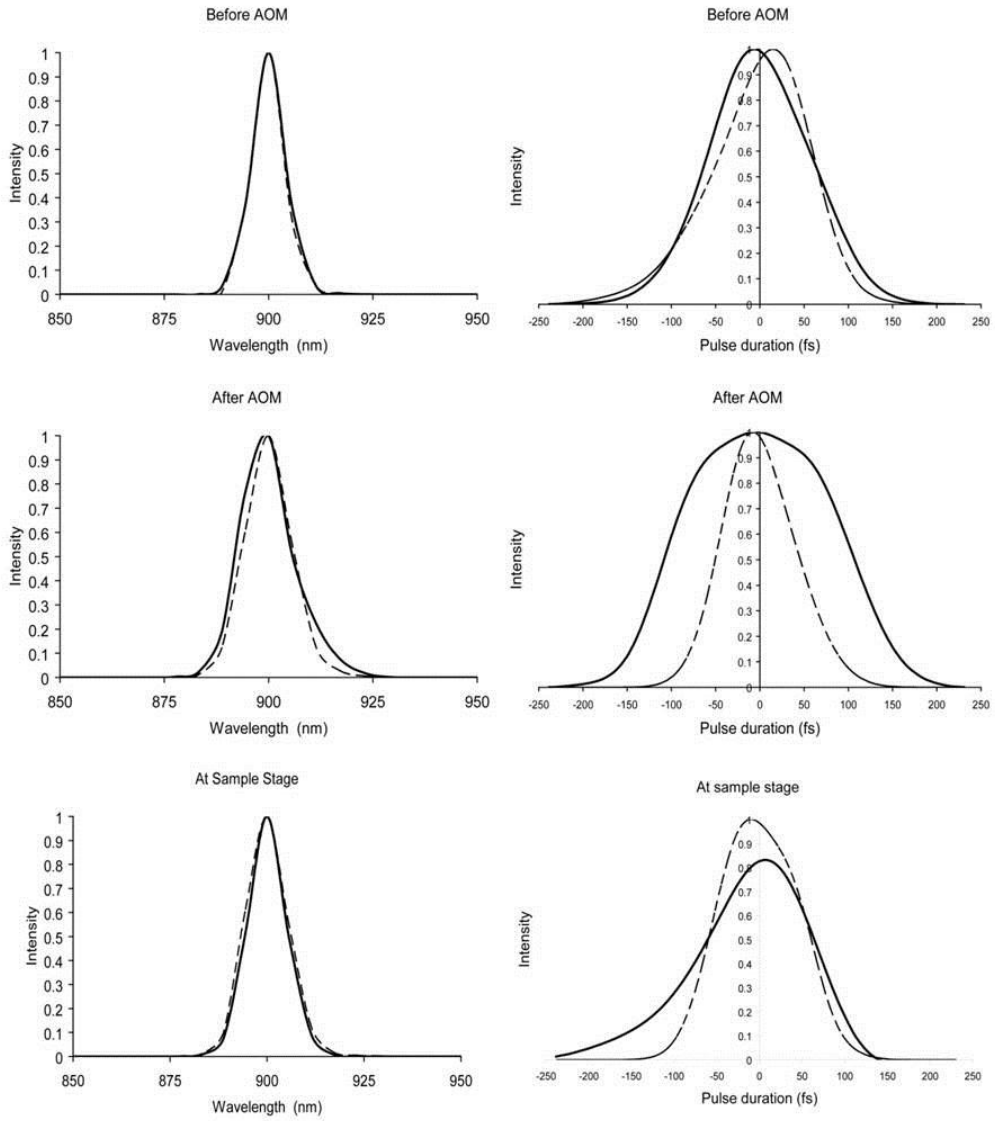

Figure 15: Chirp analyses of laser beam of the PM-SHIM shows a distinct temporal profile improvement after AOM.

Spatial profile – pulse spectral width in nm (left column) and temporal profile – pulse duration in fs (right column) of the laser beam before AOM, after AOM and at the sample stage are shown. The dotted line represents PM-SHIM and the solid line represents conventional SHIM. The dispersion affects the pulse duration rather than the pulse spectral width. The pulse duration profile is symmetric and centered after pulse modulation. The improvement in the PM-SHIM can be distinctly seen in the temporal profile after AOM which introduces the maximum dispersion. At the sample stage the intensity of the beam is improved from 0.8 to 1.0 with pulse modulation.

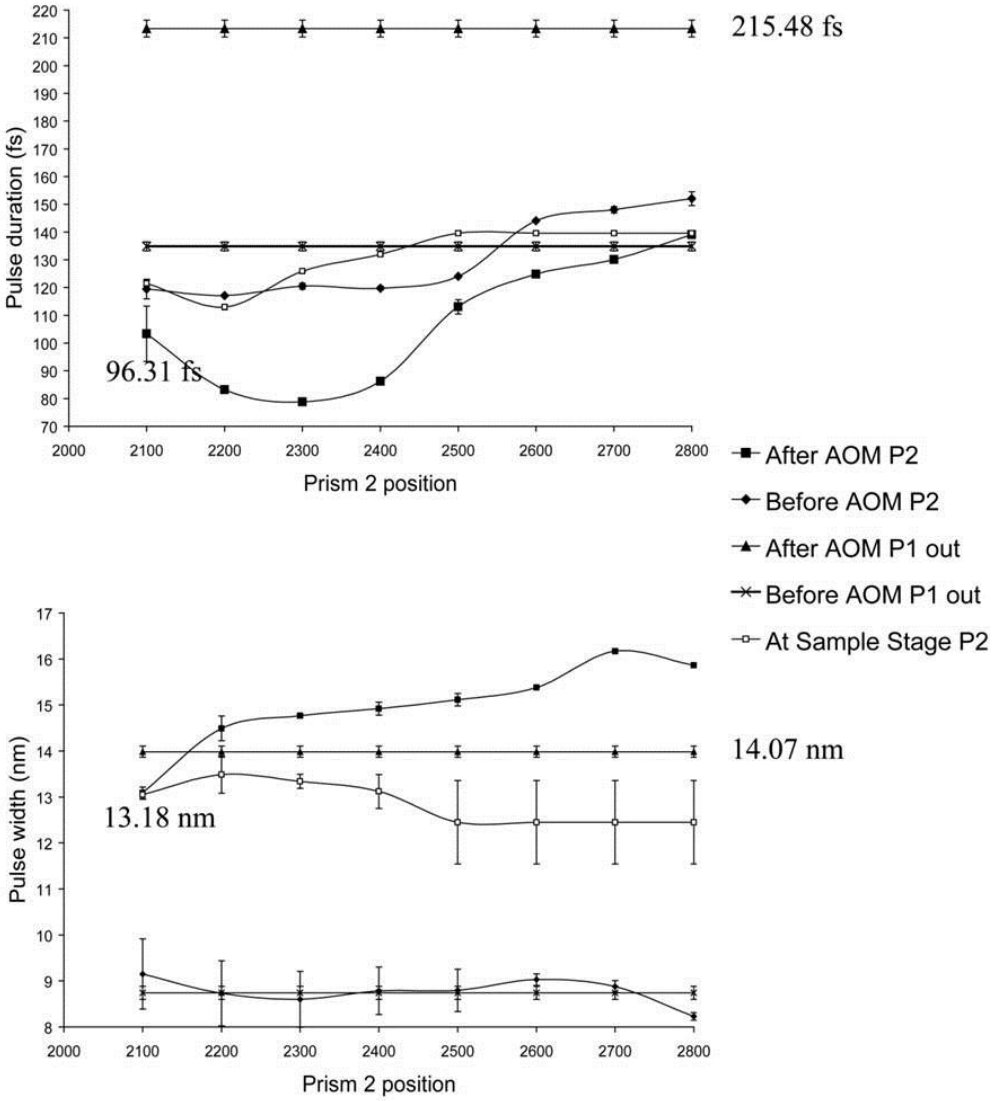

Figure 16: Chirp analyses of the laser beam of the PM-SHIM for optimization of prism positions in the Pulse compressor.

Pulse duration in femtosecond (fs) and pulse spectral width in nm for different prism positions in the pulse compressor are obtained before AOM, after AOM and at the sample stage. The "Before AOM P1 out", "After AOM P1 out" are the plots when prism 1 is pulled out of the beam path bypassing the pulse compressor. The "Before AOM P2", "After AOM P2" and "At sample stage P2" are the plots at various positions of prism 2 at an optimized prism 1 position. The maximum pulse duration after dispersion is 215.48 fs and the minimum pulse duration after modulation is 96.31 fs. The optimized prism positions are 1100 for prism 1 and 2100 for prism 2. The prism positions are controlled by rotary motors. 1100 and 2100 indicate the motor control positions.

3.3 Signal to Noise Ratio improvement in the PM-SHIM

SHG images from collagen gels, liver, and muscle sections in the conventional SHIM and PM-SHIM are shown in Fig 18. The SHG image obtained from the collagen fibers in the gel construct using the conventional SHIM (Fig 18a) are not clear while those obtained using PM-SHIM are brighter and sharper (Fig 18d). Fig 18b and 18e shows the bile canaliculi in liver, imaged with conventional SHIM and PM-SHIM. The SHG signal generated by collagen is shown in the green channel and the two photon excited fluorescence (TPEF) in the hepatocytes is shown in the red channel. The smaller collagen fibers surrounding the bile canaliculi are clearly visualized with PM-SHIM but not with SHIM. Similarly, with mouse thigh muscle, the individual muscle fibers and the collagen fibrils surrounding the muscle fibers cannot be visualized with conventional SHIM (Fig 18c) but only can be seen with PM-SHIM (Fig 18f).The ratio of SBR from PM-SHIM and SHIM is shown in the lower right corner of the images. On average, there is a 3.3±0.9 fold improvement for collagen gels, 2.5±0.7 fold increase for liver tissue and 2.1±0.4 fold SBR improvement in muscle samples.

We have demonstrated a marked improvement for collagen visualization with more than two fold improvement in SBR. As SHG is a stain-free imaging system, the SHG signal intensity observed correlates directly to the collagen amount present in the sample rather than the quantity of dye present in the sample. It also helps in faster sample preparation making it a quick and easy technique for imaging biopsy samples, where the tissue can be imaged using PM-SHIM and then taken for other routine histology techniques.

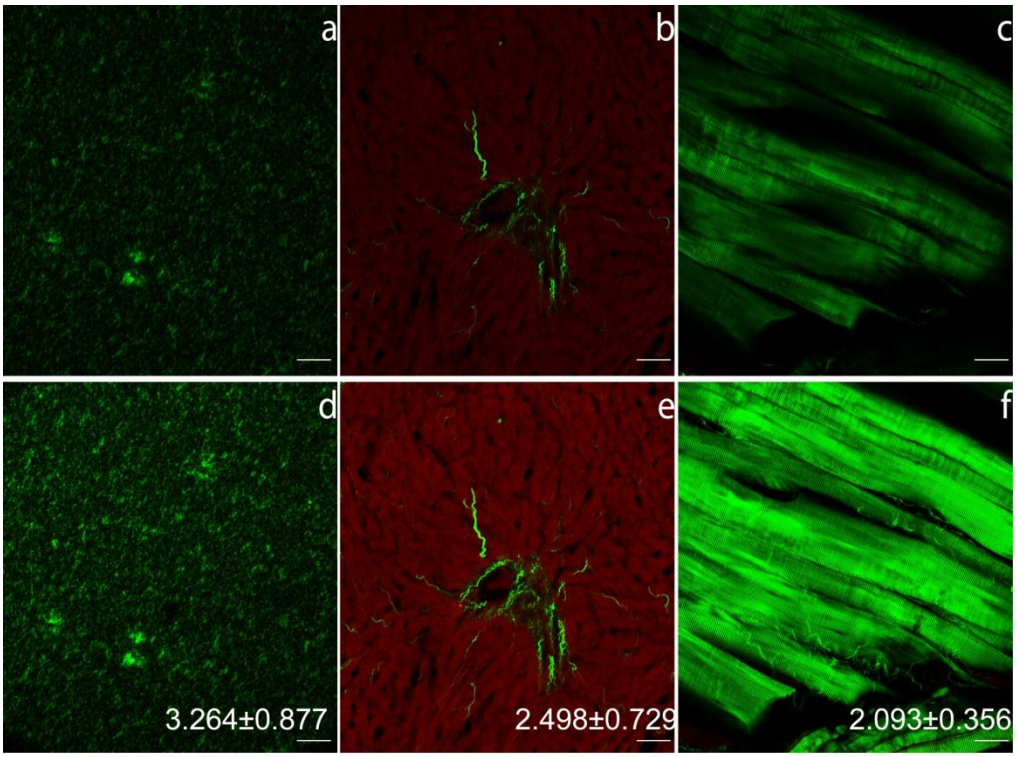

Figure 17: Collagen gels, liver sample and muscle sample demonstrates improvement of SBR with PM-SHIM.
Samples demonstrating the improvement of SHG and TPEF signals in collagen gels (a, d) liver tissue slice (b, e) and mouse thigh muscle (c, f). The improvement in Signal to Noise Ratio is mentioned on the improved images in the right bottom corner. The visualization of small collagen fibres in the liver sample (e) and the collagen fibrils in the muscle sample (f) is made possible with pulse modulation. Scale bar: 50µm.

3.3 Collagen modulation upon drug administration visualized with PM-SHIM

The in-vivo activity of ABT-869 on MV4-11 xenograft tumors have been published in Zhou et al [157]. The tumors were reduced to unpalpable size but the tumors were not completely eliminated by the drug treatment. In the conventional SHIM, not all collagen fibers can be visualized even with maximized laser power and detector sensitivity (Fig 19a and 19b). When looking at the same region with PM-SHIM, after optimizing the system (both laser power and detector sensitivity was not maximized), collagen fibers can be visualized clearly (Fig 19c and 19d). Only by using PM-SHIM, the collagen fiber content between control and the treated groups can be clearly differentiated.

Collagen fiber contents in the tumors were quantitatively analyzed. The collagen fiber number and collagen area percentage of the treated and control tumors are shown in Fig 20. The drug-treated group is shown in white bar and the control group in black bar, for both PM-SHIM and conventional SHIM systems. We have found that, using PM-SHIM, the number of collagen fibers is much higher in the drug-treated group (Fig 20a , 3470.8±1092 fibers /mm^2) than the control group (Fig 20a, 1131.7±315 fibers /mm^2) with $p< 0.0002$. In the conventional SHIM, the fiber numbers were 1208.6±107.3 fibers/mm^2 for the treated group and 386.9±104 fibers/mm^2 for the control group with $p< 0.079$. As shown in Fig 20b, using PM-SHIM, the collagen area percentage of the drug-treated group was 7.9±3% while that of the control group was 2.0±0.2%. In the conventional SHIM, the percentages were 2.1±0.7 % and 0.8±0.3% for the treated and control group respectively. On comparing the treated and control samples using a Student's t-test, the percentage calculated from the PM-SHIM images showed a statistical significance of $p< 0.0004$ and for the conventional SHIM it was $p< 0.094$.

On quantifying the collagen fiber lengths and widths, we found that we were able to detect longer and wider fibers in the treated group using PM-SHIM. The longest fiber we detected in the treated group using PM-SHIM was 155.2 μm, while that of the fibers visualized using conventional SHIM was 48.8 μm. The longest fiber for the control group visualized using PM-SHIM was 55.7 μm and that using conventional SHIM was 32.9 μm. Similarly the widest fiber we detected in the treated group using PM-SHIM was 77 μm, while that of the fibers visualized using conventional SHIM was 17 μm only. The longest fiber for the control group visualized using PM-SHIM was 12.6 μm and that using conventional SHIM was 11.7 μm. This shows that there were several disconnects in the fibers visualized using conventional SHIM, hence

segmenting the same fiber into smaller, thinner fibers. Even though the fibers were segmented the overall number of fibers detected was not elevated in the conventional SHIM, as many of the fiber signals were too weak to be detected.

The frequency distribution of the length and width of the fibers for the treated group and control group imaged with PM-SHIM (solid squares and triangles) and conventional SHIM (empty squares and triangles) in Fig 21 I and 21 II respectively. Regions of the plot are enlarged to show clearly the length and width distribution of the fibers as Fig 21a-21d. It can be seen from the enlarged graphs that only the length and width distribution of PM-SHIM is distinguishable between the treated and control group.

The fibers observed in the control group include thick and long fibers, representing more mature fibers, and some scattered, small, and thin fibers which appeared as speckles, representing less mature fibers or degrading fibers. In the treated group, we observe branched and shorter fibers along with the long mature fibers, and the fibers appeared to be brighter in general. Not many speckled collagen structures were observed in the drug-treated group. The reduced speckle content in the drug-treated sample could indicate lower degradation of the collagen fiber. The brighter short fibers could indicate more collagen production and the long thick fibers represent fiber maturation in the drug-treated group. ABT-869 is a multi-targeted receptor tyrosine kinase inhibitor targeting mainly the Vascular Endothelial Growth Factor Receptors (VEGFR) and Platelet Derived Growth Factor Receptors (PDGFR). PDGFRs have been shown to activate collagen production in sclerosis models [158]. Thus ABT-869 blocking PDGFRs should theoretically down-regulate collagen production, which cannot explain the observed up-regulation of collagen production in the tumors. Thus it is more likely that the chemotherapy triggers a wound-healing

response resulting in the production of new collagen fibers and reduced degradation of the existing fibers.

One of the hallmarks of tumor progression is reduced expression of extra cellular matrix especially collagen type I [159]. The collagen in the tumor interior is reduced, while at the tumor boundary the area of collagen (collagen cap) is increased. The increase in collagen in the cap has been attributed to the pushing of the pres-existing collagen bundles by the cancer cells onto the surrounding normal tissue [160]. The collagen cap is further bolstered by collagen production by activated fibroblasts. The collagen cap acts as a barrier to drugs [31], but when needed the barrier is broken down by metastasizing cancer cells [161]. In the tumor interior, the collagen fibers are thin and sparse as they are all newly synthesized by activated fibroblasts and cancer cells but not part of existing collagen bundles.

Upon chemotherapy, when the drug diffuses beyond the collagen cap and reaches the tumor interior, several genes in the fibroblasts and cancer cells can be activated to release factors that might render the cancer cells resistant to chemotherapy. There are studies pointing to this effect of chemotherapy on activated stromal cells releasing factors, such as hyaluronic acid [162], integrins and fibronectins [163-164], that are often associated with local wound healing processes. A study by Farmer et al [155] showed that a distinct increase in the expression of stromal signature genes predicts resistance to chemotherapy in biopsy samples. However, none of these hypotheses have been directly tested by investigating the tumor responses to chemotherapy. In our study, we have quantified an increase in collagen fibers in the tumor interior after chemotherapy, which might be due to the activated stromal cells involved in local wound healing.

Furthermore, this increased collagen in the tumor interior can activate TGF- β, a master cytokine which in turn affects Fibroblast Growth Factor (FGF), Platelet Derived Growth Factor (PDGF) [165], Insulin like Growth Factor (IGF) and Interleukin-6 [166]. These factors exert compounding effects on the proliferation, activation and transformation of stromal and cancer cells. The collagen increase in the tumor interior can also increase the mechanical stiffness of the tissue microenvironment which favors cancer cell proliferation [167]. Finally, the additional collagen fibers can bind to pro-angiogenic factors preventing new vessel formation [168] thus further limiting the access of chemotherapeutic agents to the remaining cancer cells. Therefore, the observed increase in collagen in the tumor interior could impede sustained efficacy of chemotherapy through more complex mechanisms than previously postulated based purely on the ECM modulation observed in the tumor boundary [31]. PM-SHIM will provide us with a quantitative tool to further investigate these mechanisms. PM-SHIM can also enable us to design new regimens of drug treatment including collagen modulating components introduced at the appropriate time to reduce collagen hindrance and promote drug penetration.

The mature fibers in the tumor interior can be visualized with the conventional SHIM albeit with reduced signal intensity but the small immature fibers that contribute to a considerable amount of collagen area are only visible in the PM-SHIM images. Thus using the PM-SHIM we obtained accurate quantification of collagen area percentage, fiber number, collagen fiber length and width, allowing us to draw statistically significant conclusions about the drug effects on tumor.

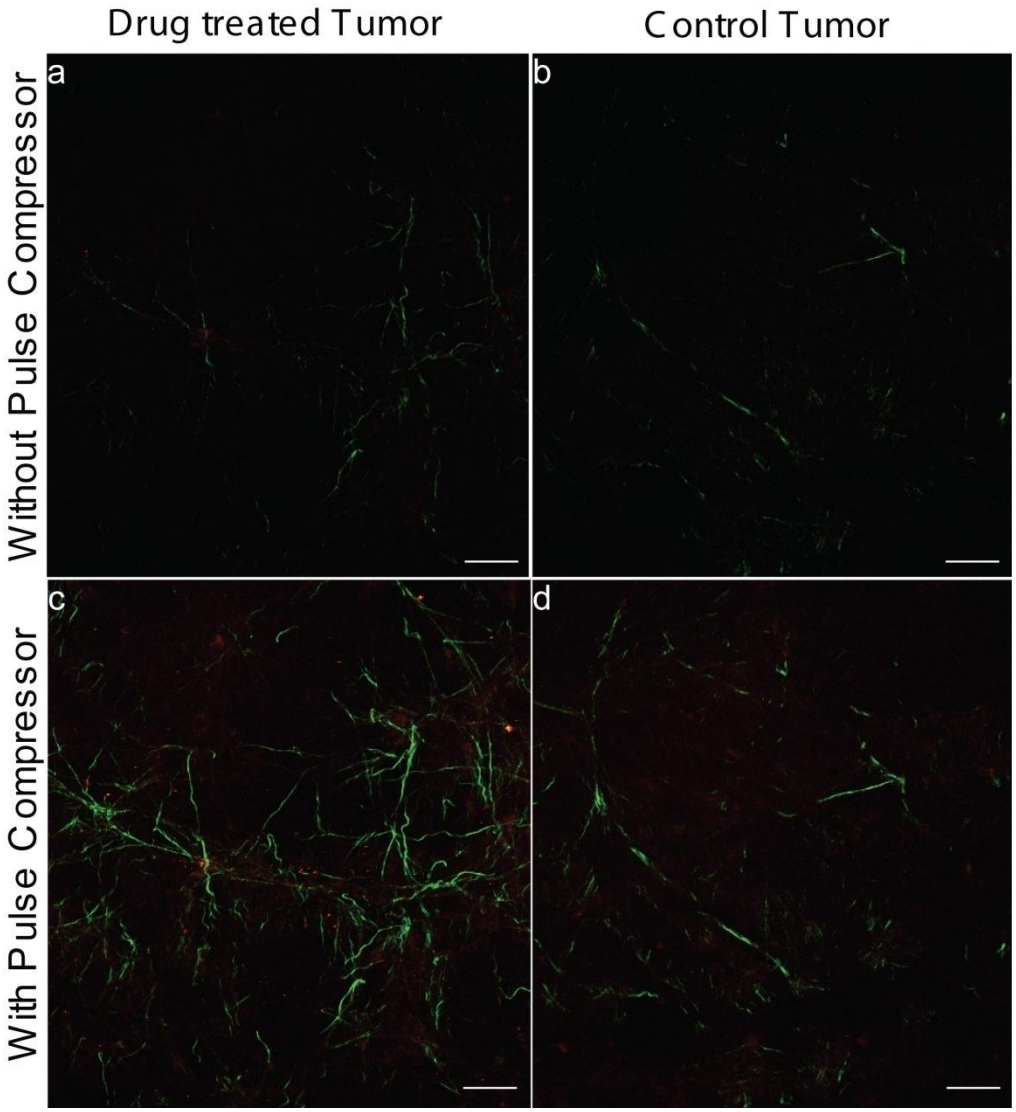

Figure 18: Collagen fibers in chemotherapy treated samples can be clearly visualized using the PM-SHIM.

Representative images of tumor samples before and after chemotherapy are shown. The top panels (a, b) show images taken with conventional SHIM and the bottom panels (c, d) show images taken with PM-SHIM. The laser power used to excite the samples with conventional SHIM was 10% higher than with PM-SHIM. The smaller fibers are visualized by the PM-SHIM which are not excited with conventional SHIM. Scale bar: 50µm

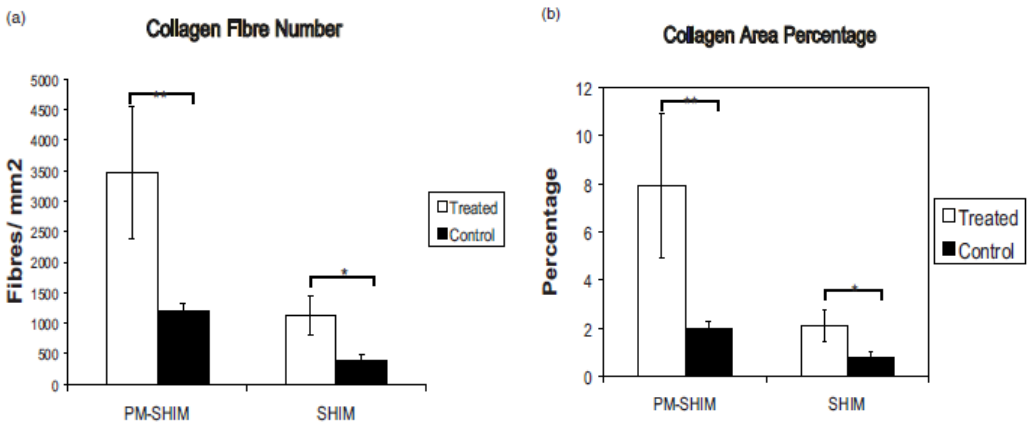

Figure 20: Quantification of collagen properties in chemotherapy treated samples shows improved fiber number and collagen area percentage with PM-SHIM.
The collagen fiber number and area percentage are shown in (a) and (b). The two parameters are plotted for the drug-treated (white bars) and control (black bars) samples with PM-SHIM and with conventional SHIM. Statistical significance was tested with a Student's t-test, $p<0.0002$ for collagen fiber number and $p<0.0004$** for collagen area percentage with PM-SHIM, and $p<0.079$* and $p<0.094$*, respectively, for conventional SHIM.**

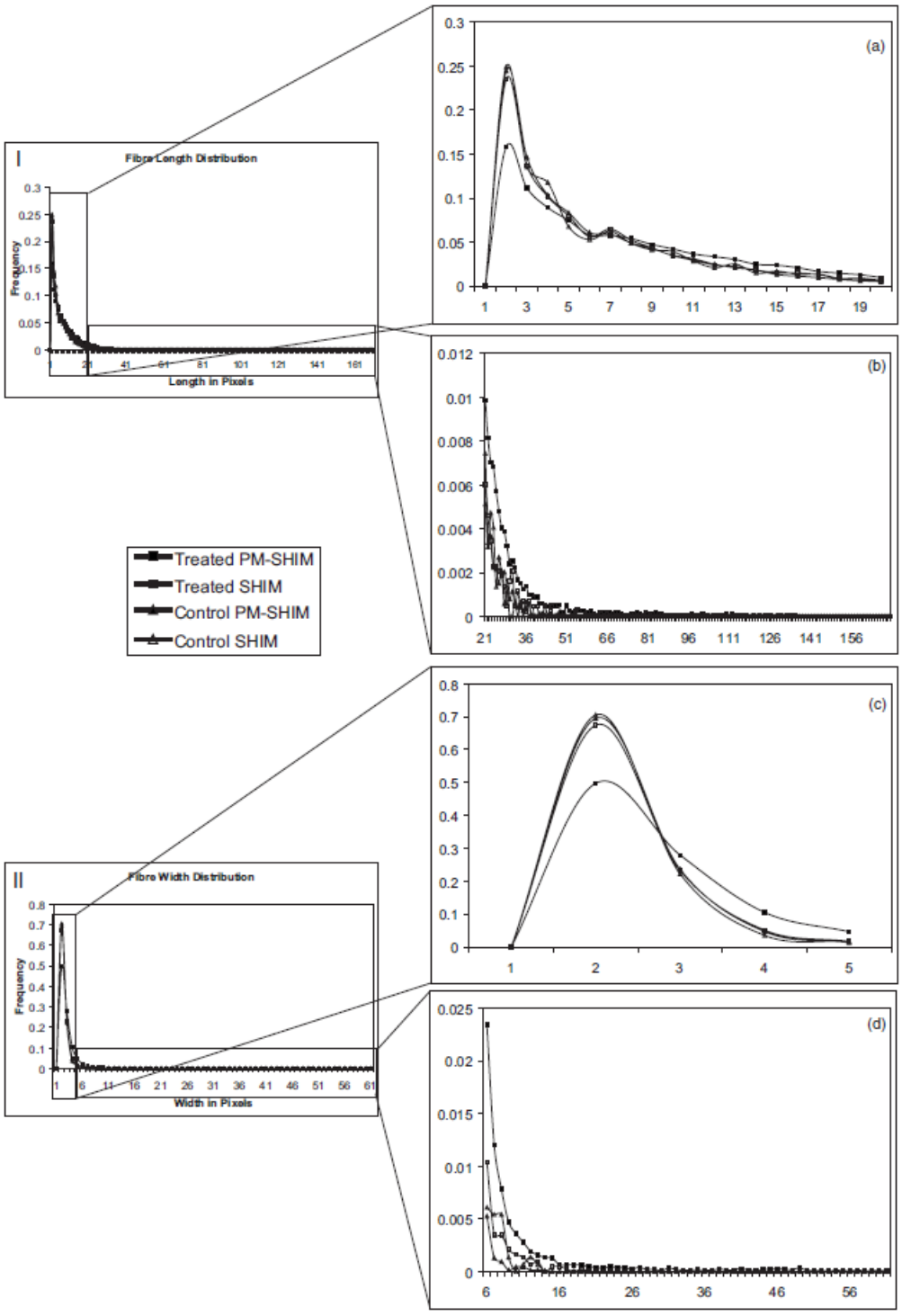

Figure 21: Quantification of collagen fiber length and width shows distinction between the treated and control samples with PM-SHIM.
Graphs 1 and 2 depict the length and width frequency distribution of the treated and control group visualized using the PM-SHIM (solid squares and triangles) and the conventional SHIM (empty squares and triangles). The enlarged view of collagen fiber length distribution is shown in (a)and (b) and the collagen fiber width in (c) and (d).

4. Conclusion

In conclusion, we have successfully incorporated the pulse compressor in our SHG imaging system and validated the pulse characteristics improvement using a chirp analyzer as well as with biological samples like muscle, liver and collagen gel samples. In the drug treatment study, we were able to map out the collagen profile in terms of fiber length, width and numbers with and without drug administration. This stain free imaging method can help us quantify drug efficacy in terms of collagen remodeling. Due to hassle free tissue preparation technique, it can be used as a quick check method for faster preclinical trials and lesser drug turnaround time. Such a technique will be helpful in preclinical drug studies with animal models. When translated to clinical application, PM-SHIM can be used to study collagen modulation in drug treated patient samples to design better chemotherapeutic regimens that might include matrix modulating components. We have also validated that PM-SHIM can be used for studying collagen changes in fine detail and thus it is a fitting tool to study CIC-ECM interactions.

Chapter V Characterization of the MX-1 CIC and non-CIC tumor models using PM-SHIM

5.1 Introduction

In chapter III and IV of this thesis we developed xenograft model for CIC and non-CIC and also validated the PM-SHIM to be able to visualize and quantify small changes in quantity and spatial distribution of collagen. In this chapter we utilize the PM-SHIM to monitor the collagen changes during tumor progression and study the CIC-ECM interaction quantitatively.

Our objective was to approach the CIC not just as a standalone group of cells but in relation to its microenvironment. At every stage of tumor progression – initiation, vascularization and growth the cancer cells interact with their microenvironment. The cancer niche is created due to the inter relationship of the extra cellular matrix (ECM) components, the cancer cells and the host derived cells such as the fibroblasts and endothelial cells. There have been several studies of cancer microenvironment either in vitro or in vivo with cancer cells, cell lines or bulk tumors but never with cancer initiating cells [169-170]. CIC have been shown to be highly tumorigenic, with higher expression of VEGF and more invasive than the non-CIC in various studies [15, 17, 47]. This enhanced capacity to form and sustain tumor should be linked to how they interact with the matrix. The link between cancer initiating cells and the microenvironment in relation to metastasis was explored in a review by Sleeman and Cremers [171]. So far CIC properties have been studied ex-vivo where they are taken out of the host environment. Identifying this small group of cells in tumor tissue is not possible with current histology techniques. Thus instead of looking for the cells itself, we hope to visualize the effects of these cells on the ECM. Thus we aim to visualize and quantify the cell-matrix interaction of CIC in a xenograft model.

With the PM-SHIM system we quantify the collagen area percentage in breast cancer tissues isolated at 8, 12 and 16 week time points. The results provide us with an idea as to how collagen changes during the course of tumor development. We then image the relationship of cancer initiating cells with collagen in the microenvironment using the PM-SHIM system. We develop certain indices to compare the CIC and non-CIC interactions with collagen. This imaging and quantification technique can be further developed to define tumor boundaries in clinical settings and prospectively identify CIC in patient samples.

5.2 Materials and Methods

5.2.1 MX-1 Breast Cancer and CIC xenograft model

Cell Culture and CIC isolation: GFP labelled breast cancer cell line MX-1 was routinely cultured in T-75 culture flasks in RPMI-1640 culture medium with added 10% Fetal Calf Serum, Sodium bicarbonate, Sodium Pyruvate and Penicillin – Streptomycin mixture. Cells were harvested using a Trypsin – EDTA solution, viability was checked with Trypan Blue and 10 million cells were prepared for injection.

CIC and non-CIC were isolated using the side population method and cultured for 2 days to allow them to recover from the stress of sorting before administration to animals.

Animals: All animal work was approved by the IACUC of National University of Singapore and Biological Resource Centre. 3-4 weeks old Female severe combined immunodeficiency mice (17–20 g, 4–6 weeks old) were purchased from Animal Resources Centre (Canning Vale, WA, Australia) and checked for any illnesses. It was ensured that they were healthy before the injection of the cancer cells.

On the day of injection, 100,000 CIC, 10 million non CIC and 10 million unsorted cells were trypsinized, counted, spun down and resuspended in 200 μL of chilled 1X PBS. The cell suspension was injected subcutaneously in the right flank of the mice. Sorting, cell culture and injection was done for consecutive four weeks to have four CIC and four non CIC SCID mouse model. 12 animals were injected for the unsorted group. Tumour growth and animal weight and health were monitored regularly.

5.2.2 Tissue isolation, sectioning and Staining

3 animals in the unsorted group were sacrificed each at 8, 12 and 16 weeks. All the CIC and non-CIC animals were sacrificed at the 8 week time point. The animals were anesthetised using 90mg Ketamine and 9 mg Xylazine mixture. The skin flap was opened; chest cavity was exposed to perform a cardiac perfusion of saline to flush out blood and then 4% Paraformaldehyde (PFA) to fix the tissues. The fixed tumour was stored in 4% PFA in room temperature overnight and then transferred to 30% sucrose solution for 48 hours.

The tumour was cut to manageable sizes and mounted on a cryostat chuck using Tissue Freezing medium. A standard cryosectioning tool is used to cut tissue slices of 40 um, 20 um and 10 um for imaging and staining purposes.

Statistical analysis

We performed student t-test for two group comparisons.

5.2.3 Image Acquisition, Processing and Quantification

The 40 um tissue section was fixed in ethanol for 10 mins and washed in 1X PBS and de-ionized water for 10 mins each to remove the remnant OCT solution. A 0.22 mm coverslip is mounted on the glass slide over the tissue section and it is imaged using the Non linear Optics incorporated confocal microscope (Carl Zeiss LSM 510 Meta NLO). The excitation Ti Sapphire laser (Mai Tai, Spectra Physics, Mountain View, CA) wavelength is 900nm and the SHG signal from the collagen in the tissue passes through a 450 nm band pass filter and collected using a photomultiplier tube (PMT) (Hamamatsu, R6357). The two photon excited fluorescence (TPEF) from the GFP labelled cells and the adipose tissue are collected using another PMT after it passes a 685 nm short pass filter in reflection mode. Images were acquired using a 0.45 NA, 10 x Objective.

For the unsorted group, we obtained 4 image stacks per animal, 3 animals per time point at 8, 12 and 16 weeks. Tile scan images were acquired of both the tumor boundary as well as the tumor interior. Tumor boundary was assessed based on the H&E staining. The collagen signals (SHG) were quantified using Matlab. The RGB images were separated into three channels. The collagen channel data was thresholded and converted to a binary file. Then it was filtered using a 3x3 median filter, eroded and dilated. The pixels were counted and an area percentage of collagen with respect to the entire image was calculated.

Images were obtained from the four CIC tumor samples, one non CIC tumor sample and four non-CIC sites of injection. Individual color channels (SHG-Green, TPEF-Red) were extracted from the images and the background was removed by

thresholding. The SHG channel images were then converted to binary format and the collagen signal was counted as the number of pixels in the image. The collagen area percentage was calculated as the ratio of the collagen pixels to the total number of pixels in the image. The calculations were performed for 30 images from each tumor sample and the average was calculated.

An image segmentation algorithm based on mixture Gaussian model was performed to remove background and noise. It is assumed that the intensity of pixels in the image can be modeled as the mixture of two Gaussian distributions, one representing collagen area with strong SHG signals and the other representing the background. Using the Expectation-Maximization (EM) algorithm [172] the parameters of the Gaussian distributions which model the intensity of pixels in the image best could be found. A binary image was generated by applying value 1 to all the pixels having intensity which belongs to the Gaussian distribution representing collagen area and value 0 to the rest pixels.

The binary image was then divided into small blocks and the overall collagen fiber orientation in each block was calculated using the Fourier transform (converting the orientation of individual fibers into a frequency distribution of number of fibers at each orientation) as in [173]. The collagen fiber was characterized using angle index (AI) and neighbor index (NI) similar as in [174]. The angle index is quantified as the sum of the differences in the orientation of the index block and that of each of its neighbor blocks normalized to n, the number of neighbors used in the computation. The neighbor index refers to the number of nonparallel neighbor blocks, while a neighbor block is defined as nonparallel if the difference between its orientation angle and that of the index block is greater than a threshold. The angle index and the neighbor index were calculated for the entire tumor as well as the regions near the

boundary. Different sizes of the block were evaluated, and it was found that the block size will not affect the quantification results of AI and NI when it is smaller than 100 pixels by 100 pixels.

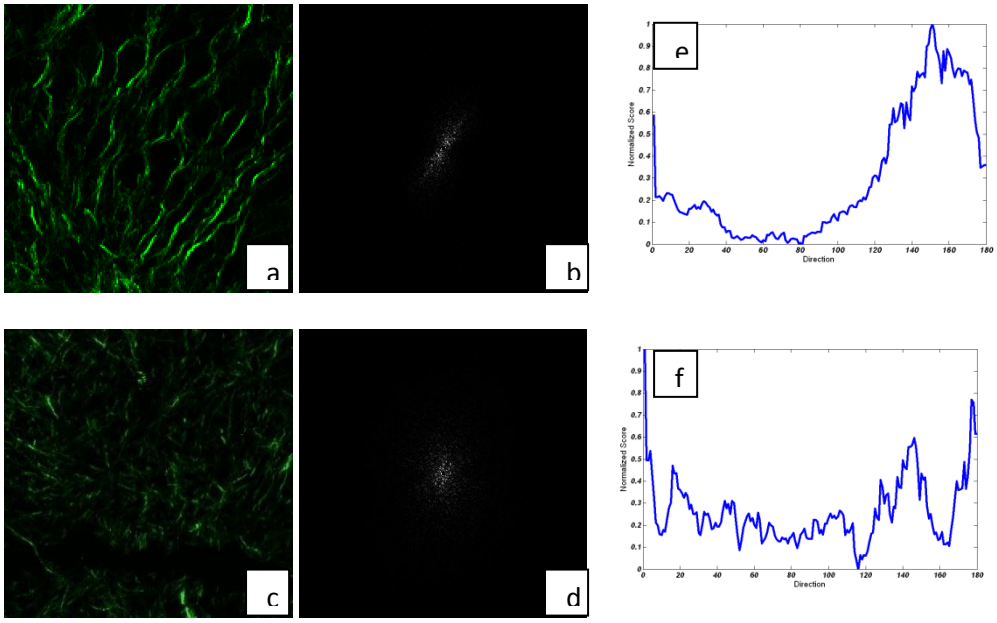

Figure 22: An example to demonstrate the quantification of Angle index and neighbor index. a and c are the SHG images. The fiber orientation is Fourier transformed and a resultant orientation for every 100×100 pixel is computed as in b and d. The plots in e and f show the distribution of fiber angles in the 100×100 pixel area. In the top panel almost all of the fibers have similar orientation, while in the bottom panel the fibers are not aligned in any particular direction.

The boundary regions of the tumor were divided into small block with 100 pixels deep from tumor surface and 100 pixels in width. In each block, the collagen fiber network was extracted using the algorithm in [175]. The angle between each collagen fiber and tumor surface was calculated and a histogram was generated.

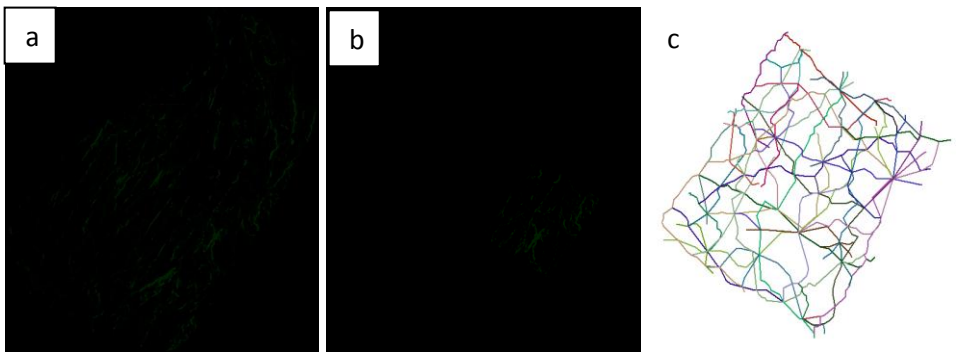

Figure 23: An example to demonstrate the fiber orientation quantification along the tumor boundary.
a shows an image of the tumor boundary. b shows the 100 pixel long by 100 pixel wide area extracted from the tumor boundary. c is the quantified individual fibers in the area b. Each fiber is shown in a unique color. The fiber orientation with respect to the boundary angle is calculated.

5. 3 Results

5.3.1 Monitoring tumour progression using PM-SHIM

Breast tissue samples were imaged using the conventional SHIM and the PM-SHIM. Both the tumor interior and the boundary were imaged. The tumor cell mass and collagen showed enhanced TPEF and SHG signal after with PM-SHIM. Fig 23a –c, 23d -f shows tile scan images of the tumor at three different time points 8, 12 and 16 weeks imaged with conventional and PM-SHIM respectively. The collagen fibre aggregates with tumor progression with an overall increase in collagen signal and reduction of small fibres in the tumor interior. The collagen area percentage was quantified and plotted as shown in Fig 23e. As the tumor progresses both the cell mass and collagen intensities increases. With PM-SHIM there is an increasing trend in the collagen area percentage while in the conventional SHIM the percentage seems to reach a plateau. There is a non-linear relationship between the amount of collagen and the signal generated. The laser beam in the conventional SHIM is not able to excite all the collagen fibres in the sample leading to a considerable reduction in the signal collected. The smaller collagen fibres were visualised clearly and in 3D imaging connected fibre network were seen which were not visualised in the conventional SHIM. In summary we were able to quantify the collagen and cell density in breast cancer tissue and capture the trend of these parameters accurately. This provides us insights into the collagen remodelling process as the cancer progresses.

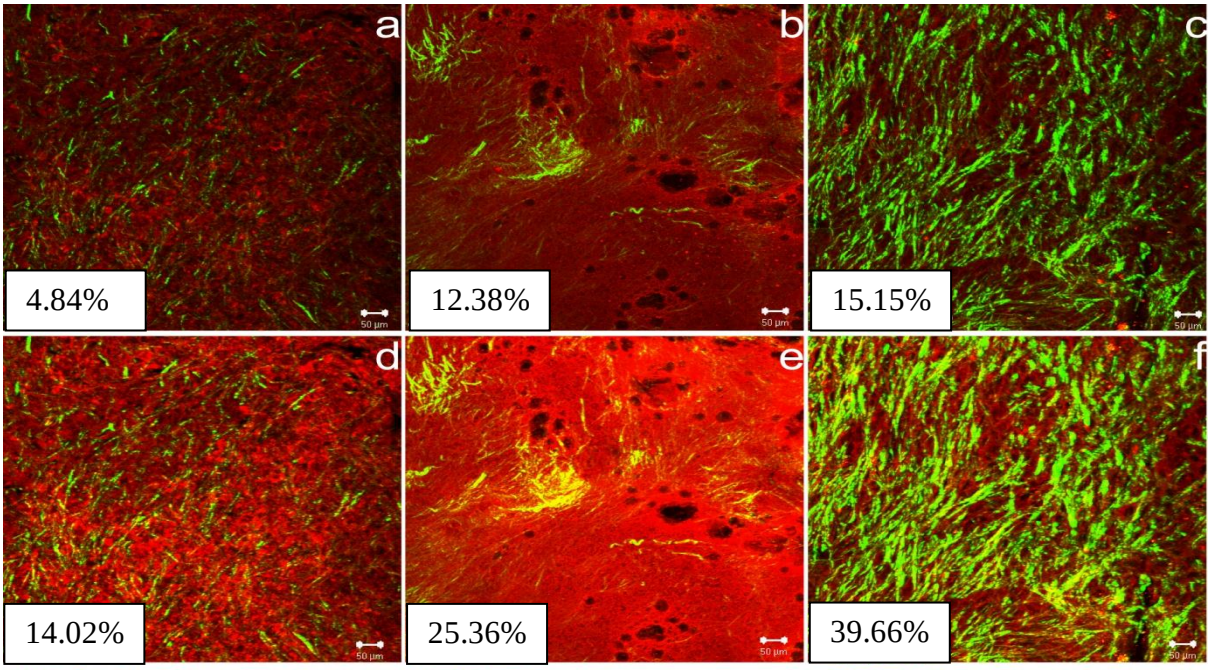

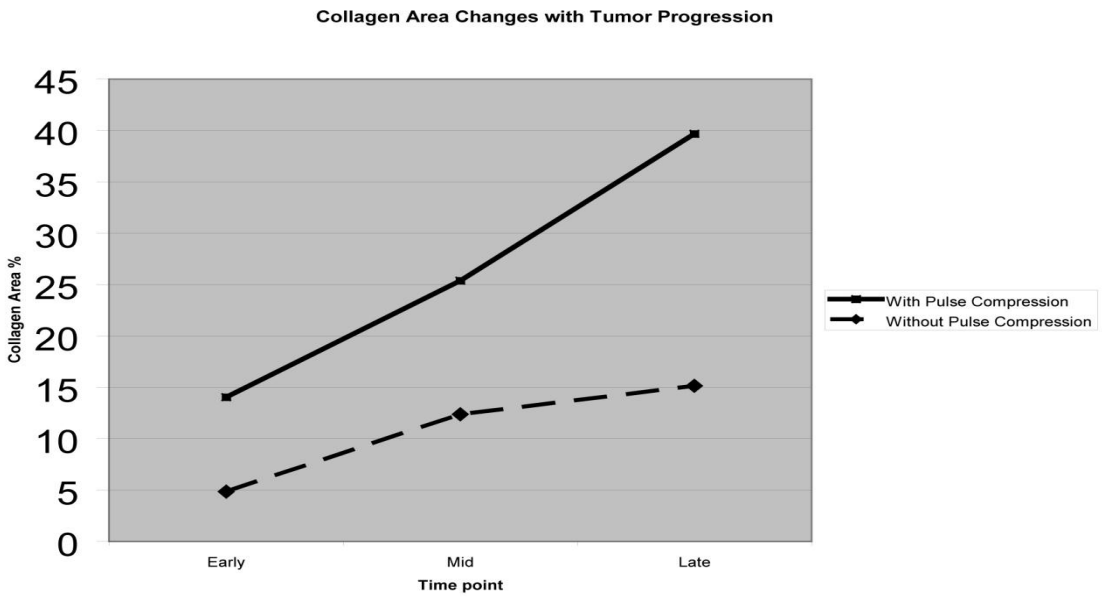

Figure 24: Representative images of tumor samples at the early, mid and late time points of 8, 12 and 16 weeks.

The top three panels (a-c) show images taken without pulse compression and the bottom three panels (d-f) show images taken with pulse compression. The collagen area percentage was quantified and it was plotted for the three time points. The trend in collagen area percentage with pulse compression shows a linear profile while without pulse compression it seems to plateau.

5.3.2 CIC formed tumors remodels collagen extensively in the tumor interior

The SHG tile scan (TS) images of non-CIC and CIC are shown in Fig 24a and 24c. The 10x images of non-CIC and CIC tumors are shown in Fig 24b and 24d. The collagen amount and distribution is distinct in case of CIC compared to non CIC. The collagen area percentage was found to be lower in CIC compared to non-CIC. In the CIC tumors collagen area percentage varied from a minimum of 1.5% in one tumor sample to a maximum of 14% in another tumor sample. The average collagen area percentage was 10.02%±0.4%, while in the case of the non-CIC tumor sample the collagen area percentage was 30%.

On collagen fiber orientation analysis, as shown in Table 25a and 25b, it was found that the average angle index and neighbor index for CIC tumor interior was 69.55 ± 0.55 and 3.12 ± 0.014 respectively and for non-CIC tumor the values were 62.42 ± 0.32 and 2.88 ± 0.006 respectively. The angle index and the neighbor index of the stroma near the tumor boundary for CIC was found to be 60.80 ± 0.69 and 2.22 ± 0.04 respectively and for non-CIC tumors the values were 55.30 ± 10.2 and 2.47 ± 0.58. The higher the angle and neighbor index the more misaligned the fibers are with respect to each other. Thus in the tumor interior, the fibers in CIC tumors look more misaligned than the non-CIC tumors. But when the region near the tumor boundary is quantified, the CIC collagen fibers are well aligned compared to the non-CIC tumors. Also the difference in alignment between CIC tumor interior and boundary is significantly different compared to the non-CIC tumor interior and boundary. The histogram in Figure 25c shows the distribution of fiber orientation in the tumor boundary with respect to the angle of the boundary. The number of fibers aligned perpendicular to the boundary was significantly higher in CIC tumors, while the

number of fibers aligned parallel to the boundary was significantly higher in the non-CIC tumor.

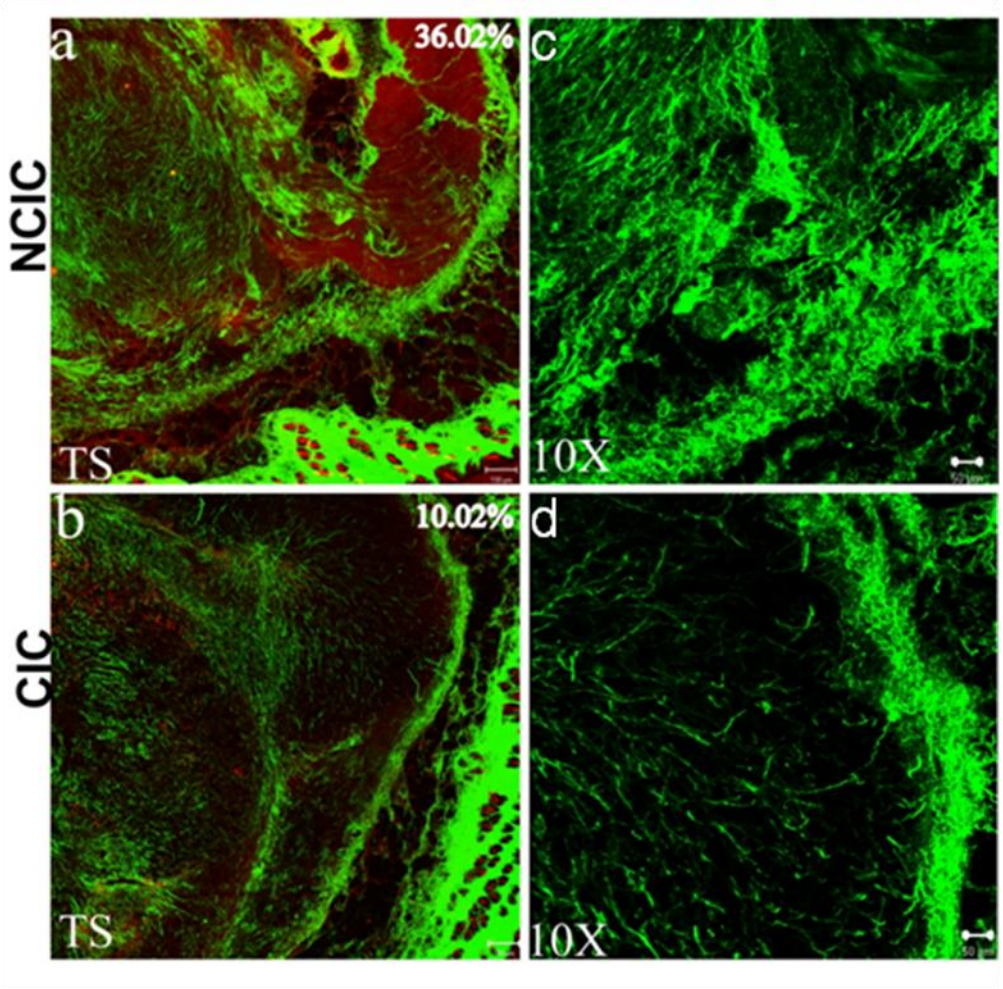

Figure 25: CIC remodels the collagen matrix more than non-CIC
Second Harmonic Generation (SHG) images of non-CIC cohort (a, b) and the CIC cohort (c, d) are representative images showing a tile scan (TS), projection of an image stack (10X). Tile scan images were acquired using 10X objective and stitched together as a single image. The red channel depicts the cells and the green channel the collagen. Image stacks were acquired of the 40 um thick sample and the projections of the green channel were reconstructed to show collagen structure in the tumor. Scale bar in the 200µm in (a) and (c) and 50µm in (b) and (d).

CIC	AI	NI
Interior	69.55 ± 0.55	3.12 ± 0.014
Boundary	60.80 ± 0.69*	2.22 ± 0.04*
P-Value	<0.05	<0.05

N-CIC	AI	NI
Interior	62.42 ± 0.32	2.88 ± 0.006
Boundary	55.36 ± 10.2	2.47 ± 0.58
P-Value	>0.2	>0.2

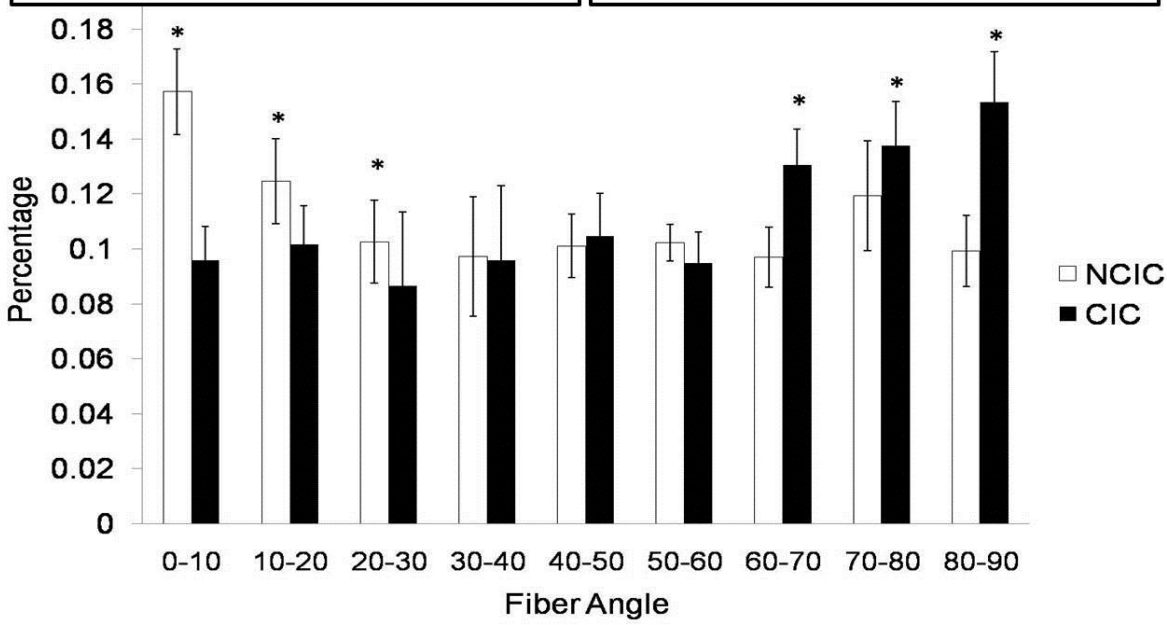

Figure 26: Collagen fibers in CIC tumors are aligned perpendicular to the boundary

Angle indices and Neighbor indices for CIC interior and boundary are given (panel a). the interior fiber orientation is significantly different from the boundary fiber orientation. In the non-CIC case (panel b), the AI and NI are not significantly different in the interior and boundary regions. The fiber orientation with respect to the boundary of the tumor is shown (c). The fibers in non-CIC are significantly oriented parallel to the tumor boundary while the CIC are oriented perpendicular to the tumor boundary. * indicate $p < 0.05$.

5.4. Discussion

Second Harmonic Generation (SHG) imaging is a powerful tool for observing collagen in tissue samples without the need for staining, with no problems of photo bleaching and with increased depth of imaging of up to 250 μm. SHG imaging revealed that the CIC tumor interior had well remodeled collagen fibers and the fibers were sparse in nature. The collagen distribution in the non-CIC tumor was dense with matted matrix.

In the initial phases of tumor development the matrix provides the much needed support and chemical cues for the cancer cells to establish a tumor but as the tumor development progresses the collagen molecules will be remodeled to support cell proliferation, expansion, angiogenesis and possibly metastasis. SHG imaging of collagen in cancer models have been qualitatively demonstrated in melanoma, breast cancer, cervical and ovarian cancer in animal and human studies [136-140]. In the case of melanoma [31] the skin is a relatively accessible organ with a rich supply of collagen and hence backward SHG of collagen fibers up to the depth of the melanoma capsule is possible; but within the actual tumor mass in melanoma the collagen fibers are reported to be sparse [176] . In case of solid tumors deep inside the host tissue, some studies focused on the stromal regions surrounding the tumor [177-178] , while the others who imaged the regions within the tumor qualitatively observed disruption in collagen fibers and loss of fine fibrils [139, 179-181]. Quantification of the fibers in the tumor interior have been reported to be difficult [32]. Using the pulse-modulated second harmonic imaging microscope (PM-SHIM), we were able to visualize collagen both within the tumor and the boundary of the tumor and quantify the collagen changes as the tumor grows. The collagen trend in the PM-SHIM images

show a linear increase in fiber content in the tumor while without pulse compression the fiber content seems to plateau.

Even though there are several studies where SHG imaging of cancer has been demonstrated, the in-depth quantitative comparison of collagen patterns is lacking. Wolf et al [Wolf K, 2009] describe three dimensional movements of cancer cells through in vitro 3D collagen matrices. The in vitro imaging of cancer cell invasion is useful to understand how cancer cells change themselves as well as their surroundings in the process. But several other factors come into play when the cancer cells are growing together in a solid tumor such as vascularization and other cell types in the tumor. One of the landmark article that performed a quantitative comparison of collagen signatures in breast cancer in vivo is by Provenzano et al [140] describing the tumor associated collagen signatures where the collagen density above and around the tumor is increased and the collagen in the non-invading areas of the tumor to be parallel to the boundary. Keely et al. defined tumor associated collagen signatures at tumor host tissue interface where fibers were perpendicular to the surrounding host tissue at invading regions in collagen overexpressing mouse models [182]. Few other groups working on SHG imaging of tumors have reported that very less collagen fibers can only be visualized in the tumor interior in their models and they mainly study the boundary where the implanted tumor meets the native tissue [Hompland, 2008][Kirkpatrick, 2007].

We quantified the collagen fiber orientation both in the tumor interior and tumor boundary using two parameters –angle index and neighbor index. The entire image was divided into 100 μm x 100 μm blocks. The angle index indicates how well the fibers are aligned in a block with respect to its surrounding 8 neighboring blocks and the neighbor index indicates the number of misaligned neighboring blocks. The higher

the indices the more misaligned the fibers are with their neighbors. When the AI/NI was compared in the tumor interior and boundary of CIC tumors, there was significant reduction of AI/NI from the tumor interior to the boundary, suggesting that the fibers are more aligned in the boundary compared to the interior. The fibers which were misaligned in the tumor interior assemble near the tumor boundary. In case of non-CIC tumors the fiber alignment changes from the interior to boundary but it was not significant.

We went on to quantify the alignment of all the fibers in the tumor boundary. We have seen that in CIC tumors, near the boundary about 40% of the collagen fibers are aligned perpendicular to the boundary. This could be a hallmark of an expanding tumor mass. The expanding phenotype of CIC might be related to their higher migratory and invasive potential. The possible lack of non-CIC's ability to migrate and invade and to perform efficient matrix remodeling could have resulted in not forming tumors in most of the animals and poor structural development. These CIC associated collagen signatures can be identified in more animal models and patient samples to ascertain the presence of CIC in a tumor mass.

5.5. Conclusions

In the breast cancer study, with the improved system we were able to acquire better quality signal with higher signal to noise ratio and also the capability to pick up signals from small collagen fibres. We were able to map out the collagen profile as the tumor progresses. Areas where the cancer cells have broken the collagen fibres where the boundary is considerably thin can be seen. These collagen reduced areas maybe the regions where the tumor expands and invades the surrounding tissue. With such improved system a grading system can be established from the various stages of cancer progression based on collagen status. The metastatic status can be assessed based on the collagen density in the tumor boundary. Such a technique will be helpful in preclinical drug studies with animal models. This stain free imaging method can help us quantify drug efficacy in terms of collagen remodelling and tumor staging. It can be used as a quick check method for faster preclinical trials and lesser drug turnaround time. With improved accuracy and repeatability we can extend the staging system for human samples. Biopsy samples can be imaged easily using the SHG/TPEF system and tumor stages can be determined reducing the need for tedious histopathological technique.

The SHG imaging technique is a quantitative imaging method with great potential for clinical applications. As Keely and her colleagues have shown that there could be tumor associated collagen signatures, there might be CIC associated collagen signatures that can be identified in animal models and patient samples. With such collagen signatures, clinicians might be able to assess the presence of CIC in patient samples and design treatment regimens to improve patient prognosis.

VI Conclusions

This thesis has documented the establishment of a cancer initiating cell isolation model, improvement of a conventional Second Harmonic Imaging Microscope (SHIM) with a pulse modulation system to develop the PM-SHIM and studying the CIC ECM relationship in a xenograft model. We used the side population technique to isolate CIC from a breast cancer cell line MX-1 and shown that the CIC had better survival, proliferation, drug resistance, migration and invasion. The CIC isolated through side population method has higher expression of CD44 and lower expression of CD24. Another well established technique to isolate CIC is to use the $CD44^{+}$/ $CD24^{-/low}$ profile. Our result indicates that the population we isolate using side population method is the same as the one isolated using the marker profile. CIC when injected in animals formed better tumors than non-CIC even when tenfold fewer cells were injected. Thus with a comprehensive *in-vitro* and *in-vivo* study we established a method to isolate CIC and develop xenograft models from the breast cancer cell line MX-1.

We intended to approach the problem of CIC in relation to its extra cellular matrix and decided SHIM as the most suitable tool to study the CIC-ECM relationship. We introduced pulse modulation to the conventional SHIM and optimized the pulse modulation using Chirp analysis. The improved system was called pulse modulated SHIM (PM-SHIM). We reduced the group velocity dispersion and delivered the maximum excitation to the sample thus obtaining a twofold improvement in the SBR in the PM-SHIM compared to the conventional SHIM. To demonstrate this improvement we used the collagen gels, liver tissue slice and muscle sample and in all the biological sample we demonstrated that finer details could be obtained using the PM-SHIM which were missed by the conventional SHIM.

We used a chemotherapy model to assess the effects of drug administration to collagen content in the tumor as well as compare the performance of PM-SHIM to the conventional SHIM. We identified clear quantitative differences between the treated and control tumor samples. The collagen content increased after treatment which might offer the tumor a protective barrier against further drug diffusion into the tumor. This collagen content increase was only visualised using the PM-SHIM. We can use this study to assess patient biopsy samples before and after treatment. We can develop new treatment regimens to administer matrix remodelling drugs to intervene collagen production at appropriate times to enable the effect of chemotherapy.

With the PM-SHIM, we studied the CIC-ECM relationship with collagen as our molecule of interest. We quantitatively determined that CIC tumors had much lesser collagen content compared to non-CIC tumor. We analyzed the images to identify the orientation of the collagen fibers in the tumor interior and tumor boundary. The collagen orientation information indicates that in CIC tumors the collagen fibers are aligned significantly perpendicular to the boundary, while in non-CIC tumor the fibers are aligned parallel to the tumor boundary. The fibers aligning perpendicular to the tumor boundary might indicate an expanding tumor boundary. This fiber orientation phenotype might indicate presence of CIC in tumor samples. In future studies the collagen fiber orientation in patient samples can be quantified to assess presence of CIC and help tailor therapies. In conclusion, we have established a tool to systematically study the cancer initiating cells and ECM relationship and identified unique collagen pattern and signatures specific to CIC in xenograft models. This imaging and image quantification tools can be used for pre-clinical and clinical studies to identify CIC and may be used to develop therapies targeting CIC.

VII Recommendations for future research

7.1 SHG imaging of pre-clinical trial samples and drug administered patient samples to evaluate collagen dynamics after drug treatment and derive meaningful relationships

The extracellular matrix has been shown to be a diffusive barrier to chemotherapy {Horning, 2008 #117}. The alteration of this barrier has resulted in improved drug penetration into the tumor {Brown, 2003 #103}. This in turn would result in better killing of cancer cells. We have demonstrated that upon drug administration, this ECM barrier to therapy increases. We have quantified this ECM change in terms of collagen fibers and have ascertained that the collagen area percentage increases four folds and there are significant increase in fiber number, fiber length and width.

We can use this imaging and image processing tool developed for animal models in pre clinical trials to ascertain the time frame in which the increase in collagen takes place by sampling at different time points of the treatment. Collagen dynamics with drug administration can give us insight into the chemo-protective response by the cancer cells. We will be able to identify drugs that elicit such a response and these drugs might work better in combination with matrix modifying components. The collagen dynamics will reveal the time point at which the cancer cells increase collagen content. The combination chemotherapy and matrix modifying components such as relaxin can be administered during the correct treatment window revealed by the collagen dynamics information. When administering the combination of chemotherapy and matrix modifying components, we can assess the collagen changes again and enquire if the treatment is more effective than the chemotherapy alone. We can build a database of the collagen dynamics of various chemotherapy molecule and identify the best combinations to deliver maximum drugs to the cancer cells and ensure eradication of the tumor mass.

We can translate the study to patient biopsy samples. The biopsy samples from the treated and control group can be obtained from the tissue repository. The collagen content change of these biopsy specimens under various drugs regimens can be identified. Also fresh biopsy samples from patients undergoing therapy can be imaged. As PM-SHIM technique is a non-invasive, stain-free imaging technique, the biopsy sample can be used for other histology techniques after PM-SHIM imaging. This way the collagen dynamics of individual patients can be tracked through the treatment as and when biopsies are taken. The increase in collagen content can indicate to the clinician that the cancer cells are eliciting a chemo-protective response and hence they need to change the treatment regimen.

We have developed specific image processing algorithms to quantify collagen fiber properties in animal models. These algorithms can be adapted and developed to suit patient samples and give accurate quantitative information for pre-clinical studies and clinicians to evaluate chemo-protective response by the cancer cells and tailor therapies accordingly.

7.2 SHG imaging of patient samples to identify cancer initiating cell niches in tumors to help design appropriate therapies

The ubiquitous presence of extra-cellular matrix and its chemical and mechanical role in tumors have been well documented {Ghajar, 2008 #336;Ingber, 2008 #337}. Several different ECM molecules roles have been studied in various tumor types. Collagen is one such ECM molecule which is found abundant in the microenvironment. The concept of CIC in patient samples and their implication in treatment failure is steadily gaining ground. We have identified that collagen is remodelled extensively in tumors initiated by CIC compared to tumor formed by non-CIC. The collagen percentage is significantly lower in CIC tumors and also the fiber orientation is distinctly different compared to that of non-CIC tumors. We have identified an unique collagen signature along the tumor boundary where the fibers are distinctly aligned perpendicular to the boundary. The fiber alignment might indicate an expanding or invading tumor mass compared to that of the non-CIC where the fibers are aligned more parallel to the tumor boundary.

We propose that such collagen signatures can be identified in patient samples. We can conduct preliminary studies from tumor explants. Some tissue sections can be used to do SHG imaging and we can obtain sufficient cell numbers from the tumor explants to ascertain the presence of CIC using techniques such as side population method or markers such as CD44/CD24. Thus the collagen patterns from tumor samples can be correlated with presence or absence of CIC. Based on the pilot studies we can develop CIC associated collagen signatures. Appropriate image processing algorithms can be developed to identify these signatures accurately and rapidly from SHG images of the tumor samples. The collagen pattern can also be correlated to the prognosis factors such as tumor size, lymph node involvement, estrogen receptor/ progesterone receptor status, Her2/ neu status. All these prognostic factors help clinicians to decide if the

disease would recur or not. Thus through the collagen signatures, CIC presence can be linked to the risk of recurrence of tumors.

Once the SHG imaging system and image processing techniques are set up, we can image biopsy samples obtained for histo-pathology. The tissue slices can be imaged and it later can be used for other staining purposes. The collagen signatures will be identified during image analysis. Based on the collagen signatures presence or absence of CIC can be determined. There are several new strategies being developed to stifle the CIC and prevent chemoresistance and tumor recurrence. The clinician can make an informed decision about the treatment strategy that will be adopted to target and eradicate the CIC.

With SHG imaging of tumor tissue obtained post operation, we can determine collagen signatures indicating presence of CIC and predicting the risk of recurrence of the disease. Based on the assessment, patients can be advised suitable follow-up strategies that will help them combat any such recurrences at an early stage.

VIII References

1. *Singapore Cancer Registry, Interim Report (Trends in Cancer Incidence in Singapore 2002-2006)*. 2006.
2. *Breast Cancer Epidemiology (1997 to 2006) and the Impact of the National Breast Cancer Screening Programme*. 2006.
3. Sell, S., *Potential gene therapy strategies for cancer stem cells.* Current Gene Therapy, 2006. **6**(5): p. 579-591.
4. Huff, C.A., et al., *Strategies to eliminate cancer stem cells: Clinical implications.* European Journal of Cancer, 2006. **42**(9): p. 1293-1297.
5. Finlan, L.E. and T.R. Hupp, *Epidermal stem cells and cancer stem cells: Insights into cancer and potential therapeutic strategies.* European Journal of Cancer, 2006. **42**(9): p. 1283-1292.
6. Clarke, M.F. and M. Fuller, *Stem cells and cancer: Two faces of eve.* Cell, 2006. **124**(6): p. 1111-1115.
7. Reya, T. *Imaging Asymmetric Division in Stem Cells and Cancer*. in *50th Annual Meeting of the American- Society-of-Hematology*. 2008. San Francisco, CA.
8. Reya, T., et al., *Stem cells, cancer, and cancer stem cells.* Nature, 2001. **414**(6859): p. 105-111.
9. Odoux, C., et al., *A Stochastic Model for Cancer Stem Cell Origin in Metastatic Colon Cancer.* Cancer Res, 2008. **68**(17): p. 6932-6941.
10. Neuzil, J., et al., *Tumour-initiating cells vs. cancer [`]stem' cells and CD133: What's in the name?* Biochemical and Biophysical Research Communications, 2007. **355**(4): p. 855-859.
11. Al-Hajj, M., et al., *Prospective identification of tumorigenic breast cancer cells (vol 100, pg 3983, 2003).* Proceedings of the National Academy of Sciences of the United States of America, 2003. **100**(11): p. 6890-6890.
12. Vassilopoulos, A., et al., *Identification and characterization of cancer initiating cells from BRCA1 related mammary tumors using markers for normal mammary stem cells.* International Journal of Biological Sciences, 2008. **4**(3): p. 133-142.
13. Clarke, R.B., et al., *A putative human breast stem cell population is enriched for steroid receptor-positive cells.* Developmental Biology, 2005. **277**(2): p. 443-456.
14. Read, T.A., et al., *Identification of CD15 as a Marker for Tumor-Propagating Cells in a Mouse Model of Medulloblastoma.* Cancer Cell, 2009. **15**(2): p. 135-147.
15. Chiba, T., et al., *Side population purified from hepatocellular carcinoma cells harbors cancer stem cell-like properties.* Hepatology, 2006. **44**(1): p. 240-251.
16. Hirschmann-Jax, C., et al., *A distinct "side population" of cells with high drug efflux capacity in human tumor cells.* Proceedings of the National Academy of Sciences of the United States of America, 2004. **101**(39): p. 14228-14233.
17. Ponti, D., et al., *Isolation and in vitro propagation of tumorigenic breast cancer cells with stem/progenitor cell properties.* Cancer Research, 2005. **65**(13): p. 5506-5511.
18. Vlashi, E., et al., *In Vivo Imaging, Tracking, and Targeting of Cancer Stem Cells.* Journal of the National Cancer Institute, 2009. **101**(5): p. 350-359.
19. Lagadec, C.H., et al. *Low proteasome activity as a means to track and target breast cancer stem cells in-vivo*. in *31st Annual San Antonio Breast Cancer Symposium*. 2008. San Antonio, TX.
20. Grange, C., et al., *SCA-1 Identifies the Tumor-Initiating Cells in Mammary Tumors of BALB-neuT Transgenic Mice.* Neoplasia, 2008. **10**(12): p. 1433-1443.
21. Locke, M., et al., *Retention of intrinsic stem cell hierarchies in carcinoma-derived cell lines.* Cancer Research, 2005. **65**(19): p. 8944-8950.

22. Al-Hajj, M., et al., *Prospective identification of tumorigenic breast cancer cells.* Proceedings of the National Academy of Sciences of the United States of America, 2003. **100**(7): p. 3983-3988.
23. Lee, J.T. and M. Herlyn, *Microenvironmental influences in melanoma progression.* Journal of Cellular Biochemistry, 2007. **101**(4): p. 862-872.
24. Ruiter, D.J. and M. Herlyn. *Melanoma-stroma interactions and melanoma progression*. in *19th European Congress of Pathology*. 2003. Ljubljana, SLOVENIA.
25. Tammi, R.H., et al., *Hyaluronan in human tumors: Pathobiological and prognostic messages from cell-associated and stromal hyaluronan.* Seminars in Cancer Biology, 2008. **18**(4): p. 288-295.
26. Chrenek, M.A., P. Wong, and V.M. Weaver, *Tumour-stromal interactions - Integrins and cell adhesions as modulators of mammary cell survival and transformation.* Breast Cancer Research, 2001. **3**(4): p. 224-229.
27. Lorusso, G. and C. Rugg, *The tumor microenvironment and its contribution to tumor evolution toward metastasis.* Histochemistry and Cell Biology, 2008. **130**(6): p. 1091-1103.
28. Boudreau, N. and C. Myers, *Breast cancer-induced angiogenesis: multiple mechanisms and the role of the microenvironment.* Breast Cancer Research, 2003. **5**(3): p. 140-146.
29. Franken, P.A., et al., *Generation of Optical Harmonics.* Physical Review Letters 1961. **7**: p. 118 - 119.
30. Freund, I. and M. Deutsch, *2ND-HARMONIC MICROSCOPY OF BIOLOGICAL TISSUE.* Optics Letters, 1986. **11**(2): p. 94-96.
31. Brown, E., et al., *Dynamic imaging of collagen and its modulation in tumors in vivo using second-harmonic generation.* Nature Medicine, 2003. **9**(6): p. 796-800.
32. Hompland, T., et al., *Second-harmonic generation in collagen as a potential cancer diagnostic parameter.* Journal of Biomedical Optics, 2008. **13**(5).
33. Tu, S.M., S.H. Lin, and C.J. Logothetis, *Stem-cell origin of metastasis and heterogeneity in solid tumours.* Lancet Oncology, 2002. **3**(8): p. 508-513.
34. Wolf, K., et al., *Compensation mechanism in tumor cell migration: mesenchymal-amoeboid transition after blocking of pericellular proteolysis.* Journal of Cell Biology, 2003. **160**(2): p. 267-277.
35. Wang, W.G., et al., *Single cell behavior in metastatic primary mammary tumors correlated with gene expression patterns revealed by molecular profiling.* Cancer Research, 2002. **62**(21): p. 6278-6288.
36. Sternlicht, M.D. and Z. Werb, *How matrix metalloproteinases regulate cell behavior.* Annual Review of Cell and Developmental Biology, 2001. **17**: p. 463-516.
37. Mettler, F.A., et al., *Benefits versus risks from mammography - A critical reassessment.* Cancer, 1996. **77**(5): p. 903-909.
38. Hanahan, D. and R.A. Weinberg, *The hallmarks of cancer.* Cell, 2000. **100**(1): p. 57-70.
39. Visvader, J.E., *Keeping abreast of the mammary epithelial hierarchy and breast tumorigenesis.* Genes & Development, 2009. **23**(22): p. 2563-2577.
40. Pinder, S.E. and I.O. Ellis, *The diagnosis and management of pre-invasive breast disease - Ductal carcinoma in situ (DCIS) and atypical ductal hyperplasia (ADH) - current definitions and classification.* Breast Cancer Research, 2003. **5**(5): p. 254-257.
41. Frykberg, E.R., et al., *DUCTAL CARCINOMA IN-SITU OF THE BREAST.* Surgery Gynecology & Obstetrics, 1993. **177**(4): p. 425-440.
42. Bombonati, A. and D.C. Sgroi, *The molecular pathology of breast cancer progression.* Journal of Pathology, 2011. **223**(2): p. 307-317.

43. Gupta, G.P. and J. Massague, *Cancer metastasis: Building a framework.* Cell, 2006. **127**(4): p. 679-695.
44. Sporn, M.B. *The war on cancer: A review*. in *Conference on Genetics and the Environment*. 1996. New York, New York.
45. Donnenberg, V.S. and A.D. Donnenberg, *Multiple drug resistance in cancer revisited: The cancer stem cell hypothesis.* Journal of Clinical Pharmacology, 2005. **45**(8): p. 872-877.
46. Dontu, G., et al., *In vitro propagation and transcriptional profiling of human mammary stem/progenitor cells.* Genes & Development, 2003. **17**(10): p. 1253-1270.
47. Sheridan, C., et al., *CD44(+)/CD24(-) breast cancer cells exhibit enhanced invasive properties: an early step necessary for metastasis.* Breast Cancer Research, 2006. **8**(5).
48. Bonnet, D. and J.E. Dick, *Human acute myeloid leukemia is organized as a hierarchy that originates from a primitive hematopoietic cell.* Nature Medicine, 1997. **3**(7): p. 730-737.
49. Miyamoto, T., I.L. Weissman, and K. Akashi, *AML1/ETO-expressing nonleukemic stem cells in acute myelogenous leukemia with 8;21 chromosomal translocation.* Proceedings of the National Academy of Sciences of the United States of America, 2000. **97**(13): p. 7521-7526.
50. Singh, S.K., et al., *Identification of a cancer stem cell in human brain tumors.* Cancer Research, 2003. **63**(18): p. 5821-5828.
51. Singh, S.K., et al., *Identification of human brain tumour initiating cells.* Nature, 2004. **432**(7015): p. 396-401.
52. Hemmati, H.D., et al., *Cancerous stem cells can arise from pediatric brain tumors.* Proceedings of the National Academy of Sciences of the United States of America, 2003. **100**(25): p. 15178-15183.
53. Kim, C.F.B., et al., *Identification of bronchioalveolar stem cells in normal lung and lung cancer.* Cell, 2005. **121**(6): p. 823-835.
54. Ho, M.M., et al. *Side population in human lung cancer cell lines and tumors is enriched with stem-like cancer cells*. in *97th Annual Meeting of the American-Association-for-Cancer-Research (AACR)*. 2006. Washington, DC.
55. Fang, D., et al., *A tumorigenic subpopulation with stem cell properties in melanomas.* Cancer Research, 2005. **65**(20): p. 9328-9337.
56. Collins, A.T., et al., *Prospective identification of tumorigenic prostate cancer stem cells.* Cancer Research, 2005. **65**(23): p. 10946-10951.
57. Ricci-Vitiani, L., et al., *Identification and expansion of human colon-cancer-initiating cells.* Nature, 2007. **445**(7123): p. 111-115.
58. Li, C.W., et al., *Identification of pancreatic cancer stem cells.* Cancer Research, 2007. **67**(3): p. 1030-1037.
59. Prince, M.E., et al., *Identification of a subpopulation of cells with cancer stem cell properties in head and neck squamous cell carcinoma.* Proceedings of the National Academy of Sciences of the United States of America, 2007. **104**(3): p. 973-978.
60. Abbott, B.L., et al., *Low levels of ABCG2 expression in adult AML blast samples.* Blood, 2002. **100**(13): p. 4594-4601.
61. Kondo, T., T. Setoguchi, and T. Taga, *Persistence of a small subpopulation of cancer stem-like cells in the C6 glioma cell line.* Proceedings of the National Academy of Sciences of the United States of America, 2004. **101**(3): p. 781-786.
62. Patrawala, L., et al., *Side population is enriched in tumorigenic, stem-like cancer cells, whereas ABCG2(+) and ABCG2(-) cancer cells are similarly tumorigenic.* Cancer Research, 2005. **65**(14): p. 6207-6219.

63. Szotek, P.P., et al., *Ovarian cancer side population defines cells with stem cell-like characteristics and Mullerian Inhibiting Substance responsiveness.* Proceedings of the National Academy of Sciences of the United States of America, 2006. **103**(30): p. 11154-11159.
64. Haraguchi, N., et al., *Characterization of a side population of cancer cells from human gastrointestinal system.* Stem Cells, 2006. **24**(3): p. 506-513.
65. Clarke, R.B., *Isolation and characterization of human mammary stem cells.* Cell Proliferation, 2005. **38**: p. 375–386.
66. Dontu, G., et al., *Stem cells in normal breast development and breast cancer.* Cell Proliferation, 2003 **36**(Suppl. 1): p. 59–72.
67. Lapidot, T., et al., *A CELL INITIATING HUMAN ACUTE MYELOID-LEUKEMIA AFTER TRANSPLANTATION INTO SCID MICE.* Nature, 1994. **367**(6464): p. 645-648.
68. Wang JC and Dick JE, *Cancer stem cells: lessons from leukemia.* Trends in Cell Biology , , 2005. **15**(9): p. 494-501.
69. Dick JE and Lapidot T, *Biology of normal and acute myeloid leukemia stem cells.* International Journal of Hematology . , 2005. **82**(5): p. 389-396.
70. Dick, J.E., *Acute myeloid leukemia stem cells.* Annals of New York Academy of Sciences, 2005 **1044**: p. 1-5.
71. Pohl A, L.G., Kahn M, Lenz HJ, *Stem cells in colon cancer.* Clinical Colorectal Cancer, 2008. **7**(2): p. 92-98.
72. Molyneux, G., J. Regan, and M.J. Smalley, *Mammary stem cells and breast cancer.* Cellular and Molecular Life Sciences, 2007. **64**(24): p. 3248-3260.
73. Eyler, C.E. and J.N. Rich, *Survival of the fittest: Cancer stem cells in therapeutic resistance and angiogenesis.* Journal of Clinical Oncology, 2008. **26**(17): p. 2839-2845.
74. Tang, C., B.T. Ang, and S. Pervaiz, *Cancer stem cell: target for anti-cancer therapy.* Faseb Journal, 2007. **21**(14): p. 3777-3785.
75. *Cancer Staging Manual*, American Joint Committee on Cancer, Editor. 2002, Springer: New York.
76. Hannen, E.J.M. and D. Riediger, *The quantification of angiogenesis in relation to metastasis in oral cancer: a review.* International Journal of Oral and Maxillofacial Surgery, 2004. **33**(1): p. 2-7.
77. Eble, J.A. and J. Haier, *Integrins in cancer treatment.* Current Cancer Drug Targets, 2006. **6**(2): p. 89-105.
78. Alberts, B., et al., *Molecular biology of the cell*. 2002, New York: Garland Science.
79. R Roy, B.Z., M A. Moses, *Making the cut: Protease-mediated regulation of angiogenesis.* Experimental Cell Research 2006. **312**: p. 608 – 622.
80. Kalluri, R. and M. Zeisberg, *Fibroblasts in cancer.* Nature Reviews Cancer, 2006. **6**(5): p. 392-401.
81. Dvorak, H.F., J. Flier, and H. Frank, *Tumors - Wounds that do not heal - Similarities between Tumor Stroma Generation and wound healing.* New England Journal of Medicine, 1986. **315**(26): p. 1650-1659.
82. Mueller, M.M. and N.E. Fusenig, *Friends or foes - Bipolar effects of the tumour stroma in cancer.* Nature Reviews Cancer, 2004. **4**(11): p. 839-849.
83. Serini, G., D. Valdembri, and F. Bussolino, *Integrins and angiogenesis: A sticky business.* Experimental Cell Research, 2006. **312**: p. 651 – 658.
84. Jodele, S., et al., *Modifying the soil to affect the seed: role of stromal-derived matrix metalloproteinases in cancer progression.* Cancer and Metastasis Reviews, 2006. **25**(1): p. 35-43.
85. Jiang, Y.F., I.D. Goldberg, and Y.E. Shi, *Complex roles of tissue inhibitors of metalloproteinases in cancer.* Oncogene, 2002. **21**(14): p. 2245-2252.

86. Mitsiades, N., et al., *Induction of tumour cell apoptosis by matrix metalloproteinase inhibitors: new tricks from a (not so) old drug.* Expert Opinion on Investigational Drugs, 2001. **10**(6): p. 1075-1084.
87. Wernert, N., *The multiple roles of tumour stroma.* Virchows Archive: An international journal of pathology., 1997. **430**(6): p. 433-443.
88. Karnoub, A.E., et al., *Mesenchymal stem cells within tumour stroma promote breast cancer metastasis.* Nature, 2007. **449**(7162): p. 557-U4.
89. Bussard, K.M. and A.M. Mastro, *Osteoblasts naturally produce cytokines that influence the tumor microenvironment in bone metastastic breast cancer.* Clinical & Experimental Metastasis, 2008. **25**: p. 32-32.
90. Senger, D.R., et al., *The alpha(1)beta(1) and alpha(2)beta(1) Integrins provide critical support for vascular endothelial growth factor signaling, endothelial cell migration, and tumor angiogenesis.* American Journal of Pathology, 2002. **160**(1): p. 195-204.
91. Van Lint, P. and C. Libert, *Matrix metalloproteinase-8: Cleavage can be decisive.* Cytokine & Growth Factor Reviews, 2006. **17**(4): p. 217-223.
92. Allinen, M., et al., *Molecular characterization of the tumor microenvironment in breast cancer.* Cancer Cell, 2004. **6**(1): p. 17-32.
93. Ghajar, C.M. and M.J. Bissell, *Extracellular matrix control of mammary gland morphogenesis and tumorigenesis: insights from imaging.* Histochemistry and Cell Biology, 2008. **130**(6): p. 1105-1118.
94. Baker, S.G. and B.S. Kramer, *Using microarrays to study the microenvironment in tumor biology: The crucial role of statistics.* Seminars in Cancer Biology, 2008. **18**(5): p. 305-310.
95. Ingber, D.E., *Can cancer be reversed by engineering the tumor microenvironment?* Seminars in Cancer Biology, 2008. **18**(5): p. 356-364.
96. Ilan, N., M. Elkin, and I. Vlodavsky, *Regulation, function and clinical significance of heparanase in cancer metastasis and angiogenesis.* International Journal of Biochemistry and Cell Biology, 2006.
97. Chechowska-Pasko M, Palka J, and Wojtukiewicz MZ, *Enhanced prolidase activity and decreased collagen content in breast cancer tissue.* International Journal of Experimental Pathology, 2006. **87**(4): p. 289-296.
98. Chabottaux, V. and A. Noel, *Breast cancer progression: insights into multifaceted matrix metalloproteinases.* Clinical & Experimental Metastasis, 2007. **24**(8): p. 647-656.
99. Padua, D. and J. Massague, *Roles of TGF beta in metastasis.* Cell Research, 2009. **19**(1): p. 89-102.
100. Wilson, T.J. and R.K. Singh, *Proteases as modulators of tumor-stromal interaction: Primary tumors to bone metastases.* Biochimica Et Biophysica Acta-Reviews on Cancer, 2008. **1785**(2): p. 85-95.
101. Barr, S., et al., *Bypassing cellular EGF receptor dependence through epithelial-to-mesenchymal-like transitions.* Clinical & Experimental Metastasis, 2008. **25**(6): p. 685-693.
102. Fritz, G. and B. Kaina, *Rho GTPases: promising cellular targets for novel anticancer drugs.* Current cancer drug targets, 2006. **6**(1): p. 1-14.
103. Roomi MW, I.V., Netke S, Kalinovsky T, Niedzwiecki A, Rath M, , *In vivo and in vitro antitumor effect of ascorbic acid, lysine, proline and green tea extract on human melanoma cell line A2058.* In vivo (Athens, Greece), 2006 **20**(1): p. 25-32.
104. Wolf, K. and P. Friedl, *Functional imaging of pericellular proteolysis in cancer cell invasion.* Biochimie 2005. **87** p. 315–320.

105. Stoller, P., et al. *Imaging collagen orientation using polarization-modulated second harmonic generation*. in *Conference on Multiphoton Microscopy in the Biomedical Sciences II*. 2002. San Jose, Ca.
106. Zoumi, A., A. Yeh, and B.J. Tromberg, *Imaging cells and extracellular matrix in vivo by using second-harmonic generation and two-photon excited fluorescence.* Proceedings of the National Academy of Sciences of the United States of America, 2002. **99**(17): p. 11014-11019.
107. Zipfel, W.R., et al., *Live tissue intrinsic emission microscopy using multiphoton-excited native fluorescence and second harmonic generation.* Proceedings of the National Academy of Sciences of the United States of America, 2003. **100**(12): p. 7075-7080.
108. Wilder-Smith, P., et al. *Noninvasive imaging of oral premalignancy and malignancy*. in *4th Inter Workshop on Optical Imaging from Bench to Bedside*. 2004. Bethesda, MD.
109. Campagnola, P.J., et al., *High-resolution nonlinear optical imaging of live cells by second harmonic generation.* Biophysical Journal, 1999. **77**(6): p. 3341-3349.
110. Le, T., et al., *Hollow fiber for flexible sub-20-fs pulse delivery.* Optics Letters, 2011. **36**(4): p. 442-444.
111. Nielsen, H.M., et al., *Study of failure pattern among high-risk breast cancer patients with or without postmastectomy radiotherapy in addition to adjuvant systemic therapy: Long-term results from the Danish Breast Cancer Cooperative Group DBCG 82 b and c randomized studies.* Journal of Clinical Oncology, 2006. **24**(15): p. 2268-2275.
112. Christgen, M., et al., *Identification of a distinct side population of cancer cells in the Cal-51 human breast carcinoma cell line.* Molecular and Cellular Biochemistry, 2007. **306**(1-2): p. 201-212.
113. Shi, G.M., et al., *Identification of side population cells in human hepatocellular carcinoma cell lines with stepwise metastatic potentials.* Journal of Cancer Research and Clinical Oncology, 2008. **134**(11): p. 1155-1163.
114. Goodell, M.A., et al., *Isolation and functional properties of murine hematopoietic stem cells that are replicating in vivo.* Journal of Experimental Medicine, 1996. **183**(4): p. 1797-1806.
115. Wang, J., et al., *Identification of cancer stem cell-like side population cells in human nasopharyngeal carcinoma cell line.* Cancer Research, 2007. **67**(8): p. 3716-3724.
116. Li, X.X., et al., *Intrinsic resistance of tumorigenic breast cancer cells to chemotherapy.* Journal of the National Cancer Institute, 2008. **100**(9): p. 672-679.
117. Rottenberg, S., et al., *Selective induction of chemotherapy resistance of mammary tumors in a conditional mouse model for hereditary breast cancer.* Proceedings of the National Academy of Sciences of the United States of America, 2007. **104**(29): p. 12117-12122.
118. Phillips, T.M., W.H. McBride, and F. Pajonk, *The response of CD24(-/low)/CD44(+) breast cancer-initiating cells to radiation.* Journal of the National Cancer Institute, 2006. **98**(24): p. 1777-1785.
119. Phillips, T.M., et al., *Effects of recombinant erythropoietin on breast cancer-initiating cells.* Neoplasia, 2007. **9**(12): p. 1122-1129.
120. Eriksson, M., et al., *Oncolytic adenoviruses kill breast cancer initiating CD44(+)CD24(-/Low) cells.* Molecular Therapy, 2007. **15**(12): p. 2088-2093.
121. Noel, A. and J.M. Foidart, *The role of stroma in breast carcinoma growth in vivo.* Journal of Mammary Gland Biology and Neoplasia, 1998. **3**(2): p. 215-225.

122. Shekhar, M.P.V., R. Pauley, and G. Heppner, *Host microenvironment in breast cancer development - Extracellular matrix-stromal cell contribution to neoplastic phenotype of epithelial cells in the breast.* Breast Cancer Research, 2003. **5**(3): p. 130-135.
123. Pupa, S.M., et al., *New insights into the role of extracellular matrix during tumor onset and progression.* Journal of Cellular Physiology, 2002. **192**(3): p. 259-267.
124. Campagnola, P.J., et al., *Three-dimensional high-resolution second-harmonic generation imaging of endogenous structural proteins in biological tissues.* Biophysical Journal, 2002. **82**(1): p. 493-508.
125. Williams, R.M., D.W. Piston, and W.W. Webb, *2-PHOTON MOLECULAR-EXCITATION PROVIDES INTRINSIC 3-DIMENSIONAL RESOLUTION FOR LASER-BASED MICROSCOPY AND MICROPHOTOCHEMISTRY.* Faseb Journal, 1994. **8**(11): p. 804-813.
126. Lin SJ, J.S., Kuo CJ, Wu RJ, Lin WC, Chen JS, Liao YH, Hsu CJ, Tsai TF, Chen and D.C. YF, *Discrimination of basal cell carcinoma from normal dermal stroma by quantitative multiphoton imaging.* Optics Letters, 2006. **31**(18): p. 2756-8.
127. Wilder-Smith P, K.T., Jung WG, Zhang J, Chen Z, Osann K, Tromberg B., *Noninvasive imaging of oral premalignancy and malignancy.* Journal of Biomedical Optics, 2005. **10**(5).
128. Lyubovitsky, J.G., et al., *In situ multiphoton optical tomography of hair follicles in mice.* Journal of Biomedical Optics, 2007. **12**(4).
129. Piston, D.W., *Imaging living cells and tissues by two-photon excitation microscopy.* Trends in Cell Biology, 1999. **9**(2): p. 66-69.
130. Soeller, C. and M.B. Cannell, *Construction of a two-photon microscope and optimisation of illumination pulse duration.* Pflugers Archiv-European Journal of Physiology, 1996. **432**(3): p. 555-561.
131. Ragan, T., et al., *High-resolution whole organ imaging using two-photon tissue cytometry.* Journal of Biomedical Optics, 2007. **12**(1).
132. Wu, Q.F. and A.T. Yeh, *Rabbit cornea microstructure response to changes intraocular pressure visualized by using nonlinear optical microscopy.* Cornea, 2008. **27**(2): p. 202-208.
133. Strupler, M., et al., *Second harmonic imaging and scoring of collagen in fibrotic tissues.* Optics Express, 2007. **15**(7): p. 4054-4065.
134. Kirkpatrick, N.D., et al., *Live imaging of collagen remodeling during angiogenesis.* American Journal of Physiology-Heart and Circulatory Physiology, 2007. **292**(6): p. H3198-H3206.
135. Chen, M.H., et al., *Multiphoton autofluorescence and second-harmonic generation imaging of the tooth.* Journal of Biomedical Optics, 2007. **12**(6).
136. Provenzano, P.P., et al., *Nonlinear optical imaging and spectral-lifetime computational analysis of endogenous and exogenous fluorophores in breast cancer.* Journal of Biomedical Optics, 2008. **13**(3).
137. Provenzano, P.P., et al., *Nonlinear Optical Imaging of Cellular Processes in Breast Cancer.* Microscopy and Microanalysis, 2008. **14**(6): p. 532-548.
138. Zhuo S, C.J., Luo T, Jiang X, Xie S, Chen R, *Two-layered multiphoton microscopic imaging of cervical tissue.* Lasers in medical science, 2008.
139. Kirkpatrick, N.D., M.A. Brewer, and U. Utzinger, *Endogenous optical biomarkers of ovarian cancer evaluated with multiphoton microscopy.* Cancer Epidemiology Biomarkers & Prevention, 2007. **16**(10): p. 2048-2057.
140. Provenzano, P.P., et al., *Collagen reorganization at the tumor-stromal interface facilitates local invasion.* Bmc Medicine, 2006. **4**.
141. Muller, M., et al., *Dispersion pre-compensation of 15 femtosecond optical pulses for high-numerical-aperture objectives.* Journal of Microscopy-Oxford, 1998. **191**: p. 141-150.

142. Fork, R.L., O.E. Martinez, and J.P. Gordon, *NEGATIVE DISPERSION USING PAIRS OF PRISMS.* Optics Letters, 1984. **9**(5): p. 150-152.
143. Iyer, V., B.E. Losavio, and P. Saggau, *Compensation of spatial and temporal dispersion for acousto-optic multiphoton laser-scanning microscopy.* Journal of Biomedical Optics, 2003. **8**(3): p. 460-471.
144. Tang, S., et al., *Effect of pulse duration on two-photon excited fluorescence and second harmonic generation in nonlinear optical microscopy.* Journal of Biomedical Optics, 2006. **11**(2).
145. Schelhas LT, S.J., Dantus M, *Advantages of ultrashort phase-shaped pulses for selective two-photon activation and biomedical imaging.* Nanomedicine, 2006. **2**(3): p. 177-81.
146. Horning, J.L., et al., *3-D tumor model for in vitro evaluation of anticancer drugs.* Molecular Pharmaceutics, 2008. **5**(5): p. 849-862.
147. Kim, J.H., et al., *Relaxin expression from tumor-targeting adenoviruses and its intratumoral spread, apoptosis induction, and efficacy.* Journal of the National Cancer Institute, 2006. **98**(20): p. 1482-1493.
148. McKee, T.D., et al., *Degradation of fibrillar collagen in a human melanoma xenograft improves the efficacy of an oncolytic herpes simplex virus vector.* Cancer Research, 2006. **66**(5): p. 2509-2513.
149. Chen, F.L., W.L. Xia, and N.L. Spector, *Acquired Resistance to Small Molecule ErbB2 Tyrosine Kinase Inhibitors.* Clinical Cancer Research, 2008. **14**(21): p. 6730-6734.
150. Symmans, W.F., *Breast cancer response to paclitaxel in vivo.* Drug Resistance Updates, 2001. **4**(5): p. 297-302.
151. StCroix, B., et al., *Reversal by hyaluronidase of adhesion-dependent multicellular drug resistance in mammary carcinoma cells.* Journal of the National Cancer Institute, 1996. **88**(18): p. 1285-1296.
152. Chang, H.Y., et al., *Robustness, scalability, and integration of a wound-response gene expression signature in predicting breast cancer survival.* Proceedings of the National Academy of Sciences of the United States of America, 2005. **102**(10): p. 3738-3743.
153. Finak, G., et al., *Stromal gene expression predicts clinical outcome in breast cancer.* Nature Medicine, 2008. **14**(5): p. 518-527.
154. Mills, P.J., et al., *Predictors of inflammation in response to anthracycline-based chemotherapy for breast cancer.* Brain Behavior and Immunity, 2008. **22**(1): p. 98-104.
155. Farmer, P., et al., *A stroma-related gene signature predicts resistance to neoadjuvant chemotherapy in breast cancer (vol 15, pg 68, 2009).* Nature Medicine, 2009. **15**(2): p. 220-220.
156. Shankar, D.B., et al., *ABT-869, a multitargeted receptor tyrosine kinase inhibitor: inhibition of FLT3 phosphorylation and signaling in acute myeloid leukemia.* Blood, 2007. **109**(8): p. 3400-3408.
157. Zhou, J., et al., *Synergistic antileukemic effects between ABT-869 and chemotherapy involve downregulation of cell cycle-regulated genes and c-Mos-mediated MAPK pathway.* Leukemia, 2008. **22**(1): p. 138-146.
158. Baroni, S.S., et al., *Stimulatory autoantibodies to the PDGF receptor in systemic sclerosis.* New England Journal of Medicine, 2006. **354**(25): p. 2667-2676.
159. Green, H., G.J. Todaro, and B. Goldberg, *Collagen synthesis in fibroblasts transformed by oncogenic viruses.* Nature, 1966. **209**(5026): p. 916-&.
160. Smolle, J., et al., *Quantitative morphology of collagen fibers in cutaneous malignant melanoma and melanocytic nevus.* American Journal of Dermatopathology, 1996. **18**(4): p. 358-363.

161. Lester, B.R. and J.B. McCarthy, *Tumor-cell adhesion to the extracellular-matrix and signal transduction mechanisms implicated in tumor-cell motility, invasion and metastasis.* Cancer and Metastasis Reviews, 1992. **11**(1): p. 31-44.
162. Misra, S., S. Ghatak, and B.P. Toole, *Regulation of MDR1 expression and drug resistance by a positive feedback loop involving hyaluronan, phosphoinositide 3-kinase, and ErbB2.* Journal of Biological Chemistry, 2005. **280**(21): p. 20310-20315.
163. Weaver, V.M., et al., *beta 4 integrin-dependent formation of polarized three-dimensional architecture confers resistance to apoptosis in normal and malignant mammary epithelium.* Cancer Cell, 2002. **2**(3): p. 205-216.
164. Hazlehurst, L.A., et al., *Reduction in drug-induced DNA double-strand breaks associated with beta 1 integrin-mediated adhesion correlates with drug resistance in U937 cells.* Blood, 2001. **98**(6): p. 1897-1903.
165. Newman, M.J., *Transforming growth-factor-Beta and the cell surface in tumor progression.* Cancer and Metastasis Reviews, 1993. **12**(3-4): p. 239-254.
166. Purps, O., et al., *Loss of TGF-beta dependent growth control during HSC transdifferentiation.* Biochemical and Biophysical Research Communications, 2007. **353**(3): p. 841-847.
167. Provenzano, P.P., et al., *Matrix density-induced mechanoregulation of breast cell phenotype, signaling and gene expression through a FAK-ERK linkage.* Oncogene, 2009. **28**(49): p. 4326-4343.
168. Ranieri, G. and G. Gasparini, *Angiogenesis and angiogenesis inhibitors: a new potential anticancer therapeutic strategy.* Current Drug Targets. Immune, Endocrine and Metabolic Disorders, 2001. **1**(3): p. 241-53.
169. Wiseman, B.S. and Z. Werb, *Development - Stromal effects on mammary gland development and breast cancer.* Science, 2002. **296**(5570): p. 1046-1049.
170. McSherry, E.A., et al., *Molecular basis of invasion in breast cancer.* Cellular and Molecular Life Sciences, 2007. **64**(24): p. 3201-3218.
171. Sleeman, J.P. and N. Cremers, *New concepts in breast cancer metastasis: tumor initiating cells and the microenvironment.* Clinical & Experimental Metastasis, 2007. **24**(8): p. 707-715.
172. Dempster, A.P., N.M. Laird, and D.B. Rubin, *Maximum Likelihood from Incomplete Data via the EM algorithm.* Journal of the Royal Statistical Society, Series B, 1977. **39**(1): p. 1 - 38.
173. Xia, Y. and K. Elder, *Quantification of the graphical details of collagen fibrils in transmission electron micrographs.* Journal of Microscopy-Oxford, 2001. **204**: p. 3-16.
174. Reiser, K.M., et al., *Quantitative analysis of structural disorder in intervertebral disks using second harmonic generation imaging: comparison with morphometric analysis.* Journal of Biomedical Optics, 2007. **12**(6).
175. Stein, A.M., et al., *An algorithm for extracting the network geometry of 3d collagen gels.* Journal of Microscopy, 2008. **232**(3).
176. Chernyavskiy, O., et al., *Imaging of Mouse Experimental Melanoma In Vivo and Ex Vivo by Combination of Confocal and Nonlinear Microscopy.* Microscopy Research and Technique, 2009. **72**(6): p. 411-423.
177. Han, X., et al., *Second harmonic properties of tumor collagen: determining the structural relationship between reactive stroma and healthy stroma.* Optics Express, 2008. **16**(3): p. 1846-1859.
178. Provenzano, P.P., K.W. Eliceiri, and P.J. Keely, *Multiphoton microscopy and fluorescence lifetime imaging microscopy (FLIM) to monitor metastasis and the tumor microenvironment.* Clinical & Experimental Metastasis, 2009. **26**(4): p. 357-370.

179. Wang, C.C., et al., *Differentiation of normal and cancerous lung tissues by multiphoton imaging.* Journal of Biomedical Optics, 2009. **14**(4).
180. Zhuo, S.M., et al., *Extracting diagnostic stromal organization features based on intrinsic two-photon excited fluorescence and second-harmonic generation signals.* Journal of Biomedical Optics, 2009. **14**(2).
181. Williams, R.M., et al., *Strategies for High-Resolution Imaging of Epithelial Ovarian Cancer by Laparoscopic Nonlinear Microscopy.* Translational Oncology, 2010. **3**(3): p. 181-194.
182. Provenzano, P.P., et al., *Collagen density promotes mammary tumor initiation and progression.* Bmc Medicine, 2008. **6**.